INFORMATION TO USERS

The most advanced technology has been used to photograph and reproduce this manuscript from the microfilm master. UMI films the text directly from the original or copy submitted. Thus, some thesis and dissertation copies are in typewriter face, while others may be from any type of computer printer.

The quality of this reproduction is dependent upon the quality of the copy submitted. Broken or indistinct print, colored or poor quality illustrations and photographs, print bleedthrough, substandard margins, and improper alignment can adversely affect reproduction.

In the unlikely event that the author did not send UMI a complete manuscript and there are missing pages, these will be noted. Also, if unauthorized copyright material had to be removed, a note will indicate the deletion.

Oversize materials (e.g., maps, drawings, charts) are reproduced by sectioning the original, beginning at the upper left-hand corner and continuing from left to right in equal sections with small overlaps. Each original is also photographed in one exposure and is included in reduced form at the back of the book. These are also available as one exposure on a standard 35mm slide or as a 17" x 23" black and white photographic print for an additional charge.

Photographs included in the original manuscript have been reproduced xerographically in this copy. Higher quality 6" x 9" black and white photographic prints are available for any photographs or illustrations appearing in this copy for an additional charge. Contact UMI directly to order.

U·M·I

University Microfilms International
A Bell & Howell Information Company
300 North Zeeb Road, Ann Arbor, MI 48106-1346 USA
313/761-4700 800/521-0600

Order Number 8905793

Transient response of laminated composites with subsurface cracks

Karim, Md. Rezaul, Ph.D.

The University of Arizona, 1988

U·M·I
300 N. Zeeb Rd.
Ann Arbor, MI 48106

TRANSIENT RESPONSE OF LAMINATED COMPOSITES WITH SUBSURFACE CRACKS

by

Md. Rezaul Karim

A Dissertation Submitted to the Faculty of the

DEPARTMENT OF CIVIL ENGINEERING

&

ENGINEERING MECHANICS

In Partial Fulfillment of the Requirements

For the Degree of

DOCTOR OF PHILOSOPHY

WITH A MAJOR IN ENGINEERING MECHANICS

In the Graduate College

THE UNIVERSITY OF ARIZONA

1 9 8 8

THE UNIVERSITY OF ARIZONA
GRADUATE COLLEGE

As members of the Final Examination Committee, we certify that we have read the dissertation prepared by Md. Rezaul Karim

entitled TRANSIENT RESPONSE OF LAMINATED COMPOSITES WITH SUBSURFACE CRACKS

and recommend that it be accepted as fulfilling the dissertation requirement for the Degree of Doctor of Philosophy.

Tribikram Kundu	9/30/88
Dr. Tribikram Kundu	Date
D.C. DaDeppo	9/30/88
Dr. Donald DaDeppo	Date
Ralph M. Richard	9/30/88
Dr. Ralph M. Richard	Date
Panos D. Kiousis	9/30/88
Dr. Panos D. Kiousis	Date
Bruce R. Simon	9/30/88
Dr. Bruce R. Simon	Date

Final approval and acceptance of this dissertation is contingent upon the candidate's submission of the final copy of the dissertation to the Graduate College.

I hereby certify that I have read this dissertation prepared under my direction and recommend that it be accepted as fulfilling the dissertation requirement.

Tribikram Kundu	9/30/88
Dissertation Director Dr. T. Kundu	Date

STATEMENT BY AUTHOR

This dissertation has been submitted in partial fulfillment of requirements for an advanced degree at The University of Arizona and is deposited in the University Library to be made available to borrowers under rules of the library.

Brief quotations from this dissertation are allowable without special permission, provided that accurate acknowledgement of source is made. Requests for permission for extended quotation from or reproduction of this manuscript in whole or in part may be granted by the head of the major department or the Dean of the Graduate College when in his or her judgment the proposed use of the material is in the interests of scholarship. In all other instances, however, permission must be obtained from the author.

SIGNED: 

ACKNOWLEDGMENT

Professor Tribikram Kundu had been a vigilant and enthusiastic supervisor from the embryonic stage of this dissertation. The author expresses his deep sense of gratitude and profound indebtedness to Dr. Kundu for his sincere and untiring effort in this regard.

The author is also grateful to Prof. D. DaDeppo, Prof. R. Richard, Prof. P. Kiousis and Prof. B. Simon for their willingness to serve on his dissertation committee.

TABLE OF CONTENTS

page

TABLE OF CONTENTS—continued

page

TABLE OF CONTENTS—continued

page

ABSTRACT

The dynamic response of subsurface cracks in fiber reinforced composites is analytically studied. The response of layered half-space and three-layered plate with two interface cracks excited by a plane SH-wave and line load respectively are studied by formulating the problem as integral equations in the frequency domain. The governing equations along with boundary, regularity and continuity conditions across the interface are reduced to a coupled set of singular integral equations by using Betti's reciprocal theorem along with the Green's functions. In addition, the transient response of an orthotropic half-space with a subsurface crack subjected to inplane line load at an arbitrary angle is analyzed. Two new Green's functions for the uncracked medium are developed and used along with the representation theorem to derive the scattered field. Satisfaction of the traction free condition at the crack surfaces gives rise to a system of singular integral equations.

Singular integrals involved in the analysis are computed numerically by removing the poles. Part of the integrals containing the poles are then obtained analytically by using residue theorem. The solution of singular integral equations are obtained by expanding the unknown crack opening displacements (COD) in terms of a complete set of Chebychev polynomials. The problem is first solved in the frequency domain, the time histories are then obtained numerically by inverting the spectra via Fast Fourier Transform (FFT) routine.

Numerical results are presented for isotropic and anisotropic materials for several different crack geometries. The results show significant influence of crack geometries and material properties on the COD and surface response of composites.

CHAPTER–1
INTRODUCTION

1.1 MOTIVATION

In the recent years laminated composites have been used increasingly because of their high strength and modulus of elasticity combined with their light weight. These laminated composites are formed by combining very thin laminae (known as preimpregnated tape or prepeg) of a two phase material composed of randomly distributed parallel fiber embedded in a matrix. A number of laminae are bonded together by a matrix material, usually the same matrix material as in the laminae. It is well known that laminated fiber reinforced composites often suffer significant internal damage due to cooling during the manufacturing process, dynamic loads associated with impact or thermal shock during its service life or due to high stresses induced in any other way. The damage may involve matrix cracking, fiber breakage and debonding as well as delamination between the two adjacent laminae. Such damage causes severe loss in load carrying capacity of the structure. For quality control and for assuring safety during the service life of composites internal damages must be detected. One of the most practical methods for accomplishing this, in the case of engineering interest, utilizes the scattering of elastic waves and the subsequent detection of these scattered waves by an appropriate transducer. The goal of the present work is to contribute to the theoretical basis of detecting subsurface cracks by these means. In this study, attention is restricted to the subsurface cracks only.

The central issue that needs to be addressed here is the determination of wave fields within reasonably realistic models of the composites when they are

subjected to given dynamic loads which are representative of the impact or non-destructive evaluation (NDE) tests. For laminated composites if the rate of loading is slow so that the generated waves are long compared to its overall dimensions, then quasi-static and thin plate approximation (Joshi and Sun, 1985) may be used with reasonably good results. In the case of NDE applications, one is required to use elastic waves of wavelengths comparable to or much smaller than the thickness of individual laminae. It is clear that neither quasi-static approximations nor thin plate theories are adequate for such problems. A more realistic approach would be to model the laminated solid as a multilayered medium in which each lamina has certain directional (anisotropic) properties and formulate the resulting mathematical problem on the basis of linear elasto-dynamic fracture theories. This model is still approximate since the individual fibers in the lamina and matrix layers between the lamina are not explicitly modelled. However, in most applications the wave lengths are much larger than the fiber diameters and each lamina can be adequately modelled as orthotropic materials

1.2 A REVIEW OF ANALYTICAL FRACTURE MECHANICS

The fundamental investigations concerning the behaviour of cracks in materials were initiated by Griffith (1921, 1924) in the early part of this century. In particular, Griffith considered the thermodynamics of brittle fracture, treating the crack as a closed system and evaluating the free energy change involved in its formation. The valuable contributions of Griffith in understanding brittle crack behaviour are extremely general, mainly due to the power of the energy formulation approach. In the following three decades not much attention was paid to the crack problems until Williams (1957, 1959) first examined the singular character of the stresses at the crack tips. An analysis leading to the stress field expressions about an elastic

crack subjected to three modes of deformation, namely the opening, sliding and tearing modes led Irwin (1957, 1960) to formulate stress intensity factors (K_I, K_{II}, K_{III}) for each of these modes. Barenblatt (1962) proposed an analytical model where the crack tip singularity could be eliminated by a superposition of cohesive forces on the elastic stress field at the tip.

Meanwhile, the development of elasticity theory to include various distortions showed that dislocations are fundamental elastic entities characterized by the geometry of the surrounding medium as well as the nature of the stress singularity (Volterra, 1907; Love, 1944). The equivalence between the continuum mechanics and those of dislocation theory as applied to the study of cracks has been proved by the development of a very rigorous theory which utilizes the energy-momentum tensor (Eshelby, 1956). The force acting on a singularity in terms of the energy momentum tensor represents a more general approach than that developed from the linear elastic methods applied specifically to cracks. In fact, the realization that cracks are only a special case of more generalized distortions becomes clear from a more extensive study which utilizes the method of differential geometry (Marcinkowski 1979a, b).

Although earlier theoretical developments were aimed at understanding brittle crack behaviour, it has become evident from experiments that most materials, with few exceptions, are ductile and therefore linear elastic analysis should be modified accordingly. A model for plane stress yielding proposed by Dugdale (1960) is similar to the cohesive force model of Barenblatt (1962). The result derived from the energy-momentun tensor concept applied to elastic cracks (Eshelby, 1956) has been extended to include plastic cracks by Rice (1968) by defining a path independent integral known as the J-integral.

In all the work mentioned so far, analyses of cracks were based on the assumption that there is no contact between the crack surfaces. Comninou (Comninou, 1977a, b, Comninou and Schemueser, 1978) introduced the idea of a small zone of non-linear material response coming from the mechanical contact of the crack surfaces near the crack tip to take care of the physical unrealities of the oscillatory singularity in the stress field near the tip of an interface crack.

Microcracking in a process zone near macrocrack tips has been observed in many brittle materials (Hoagland et al., 1973). Interaction of the microcrack array with the main crack can significantly alter the stress concentration at the main crack tip. Depending on the geometry of the microcrack array, it can either increase the effective stress intensity factor (SIF) (stress amplification) or decrease it (stress shielding or 'toughening by microcracking'). In the recent years much effort has been made to study the behavior of such multiple cracks. Chudnovosky et al. (Chudnovosky and Kachanov, 1983; Chudnovosky, Dolgopolsky and Kachanov, 1987) solved the problem by relating tractions on individual cracks to self consistancy conditions. Tractions on microcracks were approximated by Taylor's polynomials and polynomial coefficients for different cracks were related through potential representations (applicable for both 2-D and 3-D configurations). Similar polynomial approximations for 2-D array of cracks and holes was used by Horii and Nemat-Nasser (1985). The same approach but with a different set of polynomials were used by Chen (1983). Kachanov (1985, 1987) and Kachanov and Montagut (1986) analyzed the problem of multiple cracks based on the superposition technique and the idea of self consistancy applied to the average tractions on the individual cracks. All these methods for the multiple crack problems are approximate. Rose (1986) and Rubinstein (1985,1986) obtained exact solutions for the problem of two cracks using linear elasticity theories.

In addition to the works already mentioned, the plane and axisymmetric problems for a medium which consists of two or three different materials and which contains a crack parallel to or located at a bimaterial interface were considered by Erdogan and Gupta (1971a, b), Arin and Erdogan (1971), Erdogan and Arin (1971). The problem of a crack perpendicular to the interface may be found in Lu and Erdogan (1983), Cook and Erdogan (1972), Erdogan and Biricikoglu (1973), Bogy (1973), Gupta (1973) and Arin (1975). The problem of a T-shaped crack located on and perpendicular to the interface of two bonded half planes was discussed by Goree and Venezia (1977). The layered composite which consists of a periodical arrangement of two dissimilar bonded layers with cracks perpendicular to the interface was considered by Erdogan and Bakioglu (1976, 1977).

The analysis of dynamic crack problems goes back to Mott (1948) who showed that for a dynamic crack analysis, the energy balance should contain not only the elastic and surface energies, but also terms due to the kinetic energy of the materials. Flitman (1962) and Kostrov (1963) established the use of Wiener-Hopf technique to dynamic fracture problems when they obtained the response of a strip of finite width but infinite length lying on and inside an elastic medium respectively due to a plane P-wave incidence.

Because of the complexities of the dynamic crack problems of laminated composites only a few idealized cases are amenable to mathematical treatment. The complexities arise from the interaction of waves scattered by the crack with those reflected by the material interfaces and free surfaces. A popular approach to the diffraction of waves from obstacles has been that of separation of variables, where the formal solution of the wave equation is given by an infinite series of orthogonal functions (Pao, 1962; Pao and Mow, 1962; Thau and Pao, 1967). Such an approach, however, is effective only for obstacle shapes adapted to those co-ordinate

systems in which the wave equation is separable. For this reason, the dynamic stress concentrations around circular and parabolic obstacles have received considerable attention in the past. Problems involving diffraction of plane harmonic, horizontally polarized shear waves (SH-waves) by a semi-infinite crack can be formulated in terms of integral equations by the Wiener-Hopf technique (Noble, 1958). However, as pointed out by Sih (1968), since the static limit of a semi-infinite crack solution is unbounded, it is not possible to estimate precisely the magnification of stresses due to dynamic effects. To overcome this shortcomings Loeber and Sih (1968) proposed to add another barometer into the problem, namely the crack width and managed to obtain the exact behaviour of the crack front displacement and the stress fields for the case of SH-waves diffracted by a finite internal crack. Ang and Knopoff (1964) attempted to solve the internal crack problem earlier by the Wiener-Hopf technique, but their method yielded results which are restricted to low frequencies and to distances far away from the crack.

Miles (1960) and Papadopoulus (1963) have investigated crack problems concerning the diffraction of plane harmonic compression waves (P-waves) and vertically polarized shear waves (SV-waves) by a line crack. Their work discusses only the qualitative character of the displacement potential without any explicit information given on the local stress distributions. Sih and Loeber (1969) used an integral transform method for handling steady state wave propagation problems of elastic waves impinging on cracks. Mal (1971) also solved the same problem independently by using a slightly different method. Ravera and Sih (1969) and Sih et al.(1972) have used the same technique to solve for the transient response of a finite crack in an infinite medium for antiplane and inplane problems, respectively. Sih and Chen (1980) used a similar technique to study the scattering of waves by a crack embedded in the middle layer, in a three layered medium, due to impact load applied at

the crack surface. Thau and Lu (1970, 1971) employed the so called generalized Wiener-Hopf method which yields an iterative series solution to the problem of a finite crack in an infinite medium when subjected to a plane SH-wave. This solution is exact for a finite period of time, which increases with increasing iteration. Representation theorem developed by Knopoff (1956) and de Hoop (1958) to obtain a representation of motion at a general point in the medium in terms of body forces and informations on boundaries, were used by Mal (1972) to obtain surface motion due to a moving fault in a homogeneous half space. Neerhoff (1979) used the familier Betti's reciprocal theorem along with the Green's function to solve the problem of an interface crack in a layered half space for antiplane dynamic loading. Van der Hijden and Neerhoff (1984) later extended this technique to inplane problems by studying the response of a Griffith crack at the interface of two isotropic half spaces. Subsequently this technique was used by several investigators (Ryan and Mall, 1982; Zhang, 1984; Kundu, 1986; Boström, 1987) to solve antiplane problems. Achenbach and his group (Achenbach and Brind, 1981a, b; Achenbach, Lin and Keer, 1983; Keer, Lin and Achenbach, 1984a; Lin, Keer and Achenbach, 1984b) extensively studied the problem of a subsurface crack in a homogeneous, isotropic half space at different orientations by using a techique similar to the Neerhoff's technique. The response of interface Griffith and penny shaped cracks between two dissimilar isotropic infinite half spaces subjected to inplane loading was studied by Srivastava, Palaiya and Gupta (1979a, b) by an integral transform method using Hankel transform. The problem of an interface crack in a layered half-space was the subject of study by Yang and Bogy (1985) and Gracewski and Bogy (1986a, b). Corresponding problems of surface breaking cracks also received due attention (Datta, 1979; Stone et al., 1980; Mendelson et al., 1980; Kundu and Mal, 1981).

All these studies involving dynamic cracks mentioned so far have been restricted to a single crack. This is because of the severe mathematical complexities in finding a solution for geometries involving multiple cracks. Jain and Kanwal (1972) overcame some of these difficulties and presented a solution of the diffraction problem of normally incident longitudinal and anti-plane shear waves by symmetrical coplaner Griffith cracks located in an infinite isotropic and homogeneous elastic medium. Their solution was found to be valid only at low frequencies. Itou (1978) determined the stresses in an infinite elastic body with two coplaner Griffith cracks using a series expansion in the frequency domain. Angel and Achenbach (1985) used a similar technique to solve the problem of a periodic array of Griffith cracks in an infinite medium. More recently Gross and Zhang (1988) used the representation theorem to obtain the response of arbitrarily oriented multiple cracks subjected to plane SH-wave in an infinite medium. Kundu (1987a, b) obtained the response of two Griffith cracks at the interface of a layered half-space and a three layered plate, respectively. There the layers were made of isotropic materials and applied loads were continuous surface loads. Kundu's technique is an extension of Neerhoff's technique. In his work attention was restricted to finding crack opening displacements only. Achenbach and Zhang (1988) recently solved the problem of multiple cracks subjected to inplane loading using Boundary Element Methods.

Although almost all the attention of the investigators is devoted to the solution of two dimensional problems, it should be kept in mind that most of the physical problems are three dimensional. This realization lead Achenbach and Gautensen (1977) and Itou (1978) to solve three dimensonal steady state and transient problems of a Griffith cracks in a homogeneous medium using the Wiener-Hopf technique and integral equation methods, respectively.

Although many investigators have limited the scope of their studies to the isotropic materials, recent wide spread use of composite materials warrants the investigation of the response of orthotropic or anisotropic materials with cracks. Helmholtz' decomposition which simplifies the two dimensional problems for isotropic materials is not valid for composite materials. Although for static problems involving orthotropic materials a parallel decomposition was developed [Georgiadis and Papadopaulos (1987)], no such simplifying decomposition has been developed for dynamic problems yet. So these problems have to be solved in terms of displacements in the frequency domain. Kassir and Bandyopadhyay (1983), studied the response of a central crack in an infinite orthotropic medium. Kuo (1984a, b) studied the response of cracks at the interface of two dissimilar orthotropic or anisotropic half-spaces. Ang (1988) solved the problem of a crack in an orthotropic layer sandwiched between two orthotropic half-spaces. In all these studies external loads were applied only at the crack surfaces. A number of symmetry and anti symmetry conditions were used to reduce the problem to a set of singular integral equations in the frequency domain.

Traditionally, internal cracks are considered to be open and do not transmit any traction. Achenbach and Norris (1982) have proposed a set of nonlinear flaw plane conditions to account for the separation and friction effects. Other conditions of linear type, have been discussed by Thompson and Fiedler (1984). Another approach has been persued by Comninou and Dunders (1977, 1979); they have considered the interaction of elastic waves with an interface crack between two half-spaces that cannot transmit tensile tractions and where frictional slip may or may not be significant. The possible zones of separation are not known beforehand. A paper by Miller and Tran (1981) has extended the results of Comninou and Dunders (1977, 1979) to a broader class of friction laws, under the condition of no separation.

1.3 DESCRIPTION OF THE WORK

To the author's knowledge no attempt has been made yet to study analytically, the dynamic behavior of laminated composites made of anisotropic materials with subsurface cracks in a medium that has a finite boundary. In the present study three different problems involving interface and/or subsurface cracks in a half-space and a layered plate are considered. Although some progress has been made in modelling the response of cracks under dynamic loads that incorporate slip and contact force at the crack surfaces, finding such forces experimentally for a particular problem can be very difficult or even impossible with our present state of knowledge. In the current study crack surfaces are considered to be smooth and stress free, in other words contact and transmission of stresses across the crack are neglected.

Both the representation theorem (Knopoff, 1956; de Hoop, 1958) and Betti's reciprocal theorem in combination with appropriate Green's functions (Neerhoff, 1979), are used in the present study. In both techniques governing equations along with boundary, regularity and continuity conditions across the interface are reduced to a coupled set of singular integral equations. Solutions of these equations are obtained by expanding unknown crack opening displacements (COD) in terms of a complete set of Chebychev polynomials. The problem is first solved in the frequency domain, then the transient response is obtained by Fourier inversion of the spectrum using Fast Fourier Transform (FFT) routines.

The transient surface response of layered isotropic and anisotropic half-spaces with two interface cracks under the action of a plane SH-wave is studied in chapter 2. Neerhoff's technique (Neerhoff, 1979) is used to formulate the problem as a set of singular integral equations. The main difficulty encountered in solving this problem is the evaluation of the singular integrals. A technique developed by Kundu (Kundu

1983, Kundu and Mal, 1985) has been used with proper modification to overcome this problem. Details of the numerical method to compute the singular integrals are also discussed in chapter 2.

The transient response of a three layered plate with both isotropic and anisotropic layers containing two interface cracks is studied in chapter 3 by using Neerhoff's (Neerhoff, 1979) method. Loading is considered as an antiplane line load. Attention is restricted to obtaining the crack opening displacement (COD) and the surface response of the plate. Since COD is directly proportional to tearing mode stress intensity factor (K_{III}), the same behavior would have been observed for K_{III}, if it were plotted instead of COD.

Although the antiplane problem (SH-case) is much easier to solve mathematically and it gives valuable insight about the physical problems, in real world not many problems fall into this catagory. In plane problems are far more complex but useful. Keeping this in mind the transient response of a subsurface crack in an orthotropic half-space due to a line load incident at an arbitrary angle at the surface is computed in chapter 4 using the representation theorem. The line load solution can be considered as a fundamental solution from which all other solutions can be derived by appropriate integration. Attention is restricted to the calculation of the surface response at different points.

Several interesting conclusions are drawn from the analytical results. The conclusions and recommendations for further research are presented in chapter 5.

CHAPTER–2

RESPONSE OF LAYERED HALF-SPACE WITH INTERFACE CRACKS

The transient response of the surface of a layered isotropic or anisotropic half-space, with two interface cracks, excited by a plane SH-wave is investigated. The incident field is taken as a bulk wave. As sample problems, the surface response of isotropic as well as anisotropic layered half-spaces with and without crack interactions are computed.

2.1 PROBLEM FORMULATION

An elastic layer of thickness h is bonded to an elastic half-space as shown in Fig. 2.1. Two Griffith cracks of length $2a_1$ and $2a_2$ are located at the interface at $y = h$ with a distance d between the crack centers. The incident field is chosen as a plane SH-wave with an angle of incidence θ with the y-axis as shown in the figure. The problem geometry is independent of the z-direction.

To solve this problem, first one needs to solve two canonical problems. The two problems are then combined by Betti's reciprocal theorem.

2.1.1 Canonical Problem 1: Flawless Layered Half-Space Subjected to an Antiplane Stress Field

The geometry of this problem is very similar to Fig. 2.1, the only difference is that there is no crack at the interface. The time harmonic antiplane stress field of time dependence $e^{-i\omega t}$ acts as a bulk wave. Solutions of the wave equations for this problem are given below.

2.1.1.1 Isotropic Material

For the isotropic case, let us assume that ρ_1, ρ_2 and μ_1, μ_2 are material

densities and shear moduli for the layer and the substrate, respectively. The governing equation in the frequency domain is given by

$$\frac{\partial^2 U_j}{\partial x^2} + \frac{\partial^2 U_j}{\partial y^2} = -\frac{\rho_j \omega^2 U_j}{\mu_j} \tag{2.1}$$

where U_j is the transformed displacement in the j-th medium in z-direction ($j = 1$ for the layer and 2 for the substrate). Repeated index j does not imply summation.

Solution of this equation gives

$$U_j = A_j e^{i(kx+\eta_j(y-y_{j-1}))} + B_j e^{i(kx-\eta_j(y-y_{j-1}))} \tag{2.2}$$

where

$$\eta_j = (k_{sj}^2 - k^2)^{\frac{1}{2}}$$

$$k = k_{sj} \sin\theta$$

$k_{sj}(j = 1, 2)$ is the S-wave number for the j-th medium. The time dependence $e^{-i\omega t}$ in equation (2.2) and in all subsequent equations is implied. The expressions for unknown coefficients A_j and B_j can be obtained by using boundary and continuity conditions given below

$$\begin{aligned} \sigma_4^1 &= 0 \quad \text{at} \quad y = 0 \\ \sigma_4^1 &= \sigma_4^2 \quad \text{at} \quad y = h \\ U_1 &= U_2 \quad \text{at} \quad y = h \end{aligned} \tag{2.3}$$

where σ_4^α, $\alpha = 1$ and 2 are the shearing stresses related to yz-directions in the frequency domain for the layer and substrate respectively. Expressions for A_j, B_j are given in Appendix-A.

2.1.1.2 Anisotropic Material

For anistropic materials, it is assumed that in each medium, layer as well as substrate, planes normal to the y-axis are the planes of symmetry. In composites,

this is known as monoclinic symmetry. C_{44}^j and C_{55}^j are shear moduli related to the yz and zx-directions in the j-th medium (refer to Appendix-B). In composite materials these are related to principal elastic and shear moduli. Such relations can be found in a standard text book on composites (Vinson and Sierakowski, 1986). The governing equation in the frequency domain for this material is given by

$$C_{44}^j \frac{\partial^2 U_j}{\partial y^2} + C_{55}^j \frac{\partial^2 U_j}{\partial x^2} = -\rho_j \omega^2 U_j \tag{2.4}$$

Solution of this equation gives exactly the same equation as (2.2) with the following redefinition of values of k and η_j (see Appendix-B)

$$\begin{aligned} k &= \left\{ \frac{\rho_2 \omega^2 \sin^2\theta}{(C_{44}^j)^2 - (C_{44}^j)^2 \sin^2\theta + (C_{55}^j)^2 \sin^2\theta} \right\}^{\frac{1}{2}} \\ \eta_j &= \left\{ \frac{\rho_j \omega^2 - C_{55}^j k^2}{C_{44}^j} \right\}^{\frac{1}{2}} \end{aligned} \tag{2.5}$$

2.1.2 Canonical Problem 2: A Line Load in a Layered Flawless Half-Space

The geometry of this problem is shown in Fig. 2.2. A time harmonic line load is acting at a point $P(x_p, y_p)$ as shown in the figure. The solution of this problem is available in the literature on wave propagations in multilayered solids (Kundu, 1986). The displacement field in the j-th medium ($j = 1$ for the layer, 2 for the half-space) generated by this line load is given by

$$U_j^G = \frac{i}{4\pi\mu_x^j} \int_{-\infty}^{\infty} \left\{ \delta_{1j} \frac{e^{i\eta_1 |y-y_p|}}{\eta_1} + C_j e^{i\eta_j y} + \delta_{1j} D_1 e^{-i\eta_1 y} \right\} e^{ik(x-x_p)} dk \tag{2.6}$$

where, for isotropic materials

$$\eta_j = (k_{sj}^2 - k^2)^{\frac{1}{2}}$$

$$\mu_x^j = \mu_j, \qquad j = 1, 2$$

and for anisotropic materials

$$\eta_j = \left\{ \frac{\rho_j \omega^2 - k^2 C_{55}^j}{C_{44}^j} \right\}^{\frac{1}{2}}$$
$$\mu_x^j = C_{44}^j, \quad j = 1, 2$$

and δ_{1j} is the Kronecker delta function which is 1 for j equal to 1 and 0 for j not equal to 1.

The unknown coefficients C_1, C_2 and D_1 can be obtained from stress-free boundary conditions and continuity conditions across the interface. Expressions of these coefficients are given in the Appendix-A. The superscripts G of U_j indicate displacements corresponding to the Green's elastodynamic state.

2.2 APPLICATION OF BETTI'S RECIPROCAL THEOREM

Let us consider two solution states S and G. State S corresponds to the scattered field of the original problem. So when S is added to the displacement field of the canonical problem 1, the solution state of the problem of our interest is obtained. The canonical problem 2, the Green's elastodynamic state, is referred as state G. Using Betti's reciprocal theorem these two states can be related in the following manner

$$\int_V F_i^S U_i^G dV + \int_S T_i^S U_i^G dS = \int_V F_i^G U_i^S dV + \int_S T_i^G U_i^S dS \quad \texttt{(summation implied)} \tag{2.7}$$

where F_i is the body force per unit volume acting in the x_i direction, T_i is the surface traction per unit area acting in the x_i direction, and U_i is the displacement in the x_i direction. Superscripts S and G represent states S and G respectively. However, the body force for state S is zero and for state G it is equal to $\delta(\bar{r} - \bar{r_p})$ acting in the z-direction. $\bar{r_p}$ is the position vector of point P and $\bar{r}$ is the position

vector of any point of interest. For an antiplane problem all non zero forces and displacements act in the z-direction. So for our problem the general equation (2.7) takes the form,

$$\int_S T^S U^G dS = U^S(\bar{r_p}) + \int_S T^G U^S dS \tag{2.8}$$

where U is the particle displacement and T is the surface traction per unit area, both are in the z-direction. Since the problem is invariant in the z-direction, surface integrals may be reduced to line integrals. This line integral is carried out along a contour, shown in Fig.2.3.

The integral of the left-hand side of equation (2.8) vanishes because T^S is zero on C_1, C_2, C_3 and integrals of $T^S U^G$ on Σ_j^+ and Σ_j^- cancel each other for $j = 1$ and 2. The only nonzero term comes from the integral of the right-hand side of equation (2.8) along the integration paths Σ_j^+ and Σ_j^-. After some simplification, equation (2.8) is reduced to

$$U^S(r_p) = \int_{-a_1}^{a_1} \phi(x) T_{yz}^G dx + \int_{d-a_2}^{d+a_2} \psi(x-d) T_{yz}^G dx \tag{2.9}$$

where $\phi(x)$ and $\psi(x-d)$ are crack opening displacements (COD) of the two cracks and are defined as

$$\begin{aligned} \phi(x) &= U^S(x, h^+) - U^S(x, h^-) \\ \psi(x-d) &= U^S(x-d, h^+) - U^S(x-d, h^-) \end{aligned} \tag{2.10}$$

and $\bar{r}_p$ is the position vector of the point P. The expression for T_{yz}^G at $y = h$ may be obtained from

$$T_{yz}^G(x,h) = T_1^G(x,h^-) = T_2^G(x,h^+) = \mu_x^1 \left\{ \frac{\partial U_1^G}{\partial y} \right\}_{y=h} \tag{2.11}$$

where U_1^G is given in equation (2.6).

If point P is now moved to the crack surface, the displacement of that point can be obtained from equation (2.9) if T_{yz}^G, $\phi(x)$ and $\psi(x-d)$ are known. Combining equations (2.9) and (2.11) the displacement field at (x_p, y_p) is obtained as,

$$U_1^S(x_p,y_p) = -\frac{1}{4\pi}\int_{-a_1}^{a_1}\phi(x)\int_{-\infty}^{\infty}\left\{e^{i\eta_1(h-y_p)}+\eta_1(C_1Q_1-D_1Q_1^{-1})\right\} e^{ik(x-x_p)}dkdx - \frac{1}{4\pi}\int_{d-a_2}^{d+a_2}\psi(x-d) \int_{-\infty}^{\infty}\left\{e^{i\eta_1(h-y_p)}+\eta_1(C_1Q_1-D_1Q_1^{-1})\right\} e^{ik(x-x_p)}dkdx \tag{2.13}$$

where

$$Q_1 = e^{i\eta_1 h}$$

The scattered stress field can be obtained from the displacement field of equation (2.13). Then it is equated to the negative of the incident stress field along the crack surfaces ($y = h$ and $|x| < a_1$ or $|X| < a_2$ where $X = x - d$) to obtain

$$\eta_2(1-B_2)e^{ikx_p} = \frac{\mu_x^1}{4\pi}\int_{-a_1}^{a_1}\phi(x)\int_{-\infty}^{\infty}F(k)e^{ik(x-x_p)}dkdx + \frac{\mu_x^1}{4\pi}\int_{-a_2}^{a_2}\psi(X)\int_{-\infty}^{\infty}F(k)e^{ik(X-x_p)+ikd}dkdX \qquad for \quad -a_1 < x_p < a_1 \tag{2.14a}$$

and

$$\eta_2(1-B_2)e^{ikX_p+ikd} = \frac{\mu_x^1}{4\pi}\int_{-a_1}^{a_1}\phi(x)\int_{-\infty}^{\infty}F(k)e^{ik(x-X_p)-ikd}dkdx + \frac{\mu_x^1}{4\pi}\int_{-a_2}^{a_2}\psi(X)\int_{-\infty}^{\infty}F(k)e^{ik(X-X_p)}dkdX \qquad for \quad -a_2 < X_p < a_2 \tag{2.14b}$$

where

$$F(k) = \frac{2\eta_1\eta_2(Q_1^2-1)}{\mu_x^1\eta_1(Q_1^2-1)-\mu_x^2\eta_2(Q_1^2+1)} \tag{2.15}$$

B_2 in equations (2.14) is defined in equation (2.2).

2.2.1 Computation of the Crack Opening Displacement Functions

In order to evaluate the crack opening displacements, $\phi(x)$ and $\psi(x)$ are expanded in a complete set of Chebyshev polynomials, so that it gives square root singularity in the stress field in front of the crack tip and satisfy the boundary conditions at the crack tip (Neerhoff, 1979),

$$\begin{aligned}\phi(x) &= \sum_{n=0}^{\infty}\left[\frac{\alpha_{2n}}{2n}\phi_{2n}(x) + i\frac{\alpha_{2n+1}}{2n+1}\phi_{2n+1}(x)\right] \\ \psi(x) &= \sum_{n=0}^{\infty}\left[\frac{\gamma_{2n}}{2n}\psi_{2n}(x) + i\frac{\gamma_{2n+1}}{2n+1}\psi_{2n+1}(x)\right]\end{aligned} \tag{2.16}$$

where

$$\begin{aligned}\phi_{2n}(x) &= \sin\{2n\arcsin(x/a_1)\} \\ \psi_{2n}(x) &= \sin\{2n\arcsin(x/a_2)\} \\ \phi_{2n+1}(x) &= \cos\{(2n+1)\arcsin(x/a_1)\} \\ \psi_{2n+1}(x) &= \cos\{(2n+1)\arcsin(x/a_2)\}\end{aligned} \tag{2.17}$$

To obtain the unknown coefficients α_n and γ_n, both sides of equation (2.14a) are multiplied by $\phi_m(x_p)$, then integrated from $x_p = -a_1$ to $x_p = a_1$ and both sides of equation (2.14b) are multiplied by $\psi_m(X_p)$, then integrated from $X_p = -a_2$ to $X_p = a_2$. After some algebraic manipulation an infinite set of linear equations is obtained to solve for α_n and γ_n,

$$\begin{aligned}\sum_{n=1}^{\infty}(K_{mn}\alpha_n + L_{mn}\gamma_n) &= \frac{4\eta_2(1-B_2)J_m(ka_1)l_m}{\mu_x^1 k} \\ \sum_{n=1}^{\infty}(M_{mn}\alpha_n + N_{mn}\gamma_n) &= \frac{4\eta_2(1-B_2)J_m(ka_2)l_m}{\mu_x^1 k}\end{aligned} \tag{2.18}$$

where J_m is the Bessel function of first kind of order m, and

$$\begin{aligned}l_m &= -i, \quad \text{for odd } m \\ &= i, \quad \text{for even } m\end{aligned}$$

when $(m+n)$ is even,

$$
\begin{aligned}
K_{mn} &= 2\int_0^\infty \left\{\frac{F(k)}{k^2} - \frac{2i}{k(\mu_x^1+\mu_x^2)}\right\} J_m(ka_1)J_n(ka_1)dk \quad + \frac{2i}{\mu_x^1+\mu_x^2}\frac{\delta_{mn}}{m} \\
L_{mn} &= 2\int_0^\infty \frac{F(k)}{k^2} J_m(ka_1)J_n(ka_2)\cos(kd)dk \\
M_{mn} &= 2\int_0^\infty \frac{F(k)}{k^2} J_m(ka_2)J_n(ka_1)\cos(kd)dk \\
N_{mn} &= 2\int_0^\infty \left\{\frac{F(k)}{k^2} - \frac{2i}{k(\mu_x^1+\mu_x^2)}\right\} J_m(ka_2)J_n(ka_2)dk \quad + \frac{2i}{\mu_x^1+\mu_x^2}\frac{\delta_{mn}}{m}
\end{aligned}
\tag{2.19}
$$

and when $(m+n)$ is odd,

$$
\begin{aligned}
K_{mn} &= N_{mn} = 0 \\
L_{mn} &= 2i\int_0^\infty \frac{F(k)}{k^2} J_m(ka_1)J_n(ka_2)\sin(kd)dk \\
M_{mn} &= -2i\int_0^\infty \frac{F(k)}{k^2} J_m(ka_2)J_n(ka_1)\sin(kd)dk
\end{aligned}
\tag{2.20}
$$

From equations (2.19) and (2.20) it can be clearly seen that K and N matrices are symmetric but L and M matrices are not. However L and M satisfy the following relations

$$
L_{mn} = \begin{cases} M_{nm}, & for \quad m+n=\text{even} \\ -M_{nm} & for \quad m+n=\text{odd} \end{cases}
$$

When this technique is applied to the case of continuous surface load (Kundu, 1987a, b) only two entries occur in the right hand side of equation (2.18) but for the case of plane wave incident at an arbitrary angle the right hand side becomes fully populated. Equations (2.18) have infinite series in their expressions, however, they can be terminated after a finite number of terms without introducing any significant error (Kundu, 1986). Then α_n, γ_n can be obtained from a finite set of linear equations.

2.2.2 Computation of Surface Displacement

The total displacement U is given by

$$U = U^i + U^s \tag{2.21}$$

in which U^i is the total field in the absence of any crack given by equation (2.2), where as the scattered field U^s, represents the change in U^i due to the presence of cracks. U^s is given by equation (2.13) for the layer. At any point on the surface $P(x_p, 0)$

$$U^i(x_p, 0) = (A_1 + B_1)e^{ikx_p} \tag{2.22}$$

and

$$\begin{aligned} U^s(x_p,0) = &-\frac{1}{4\pi}\int_{-a_1}^{a_1}\phi(x)\int_{-\infty}^{\infty} f(k)e^{ik(x-x_p)}dkdx \\ &-\frac{1}{4\pi}\int_{d-a_2}^{d+a_2}\psi(x-d)\int_{-\infty}^{\infty} f(k)e^{ik(x-x_p)}dkdx \end{aligned} \tag{2.23}$$

where

$$f(k) = -\frac{4\mu_x^2\eta_2 Q_1}{\mu_x^1\eta_1(Q_1^2-1) - \mu_x^2\eta_2(Q_1^2+1)} \tag{2.24}$$

after some simplification (see Appendix-B) this equation can be written as

$$\begin{aligned} U^s(x_p,0) = &-\frac{i}{2}\int_0^{\infty}\frac{f(k)}{k}\cos(kx_p)\sum_{n=odd}^{\infty}\{\alpha_n J_n(ka_1)\}\,dk \\ &-\frac{1}{2}\int_0^{\infty}\frac{f(k)}{k}\sin(kx_p)\sum_{n=even}^{\infty}\{\alpha_n J_n(ka_1)\}\,dk \\ &-\frac{i}{2}\int_0^{\infty}\frac{f(k)}{k}\cos(kd-kx_p)\sum_{n=odd}^{\infty}\{\gamma_n J_n(ka_2)\}\,dk \\ &+\frac{1}{2}\int_0^{\infty}\frac{f(k)}{k}\sin(kd-kx_p)\sum_{n=even}^{\infty}\{\gamma_n J_n(ka_2)\}\,dk \end{aligned} \tag{2.25}$$

then equations (2.22) and (2.23) are added to obtain the total surface displacement.

2.3 COMPUTATIONAL ASPECTS

The main task involved in obtaining the solution of this problem is the computation of the integral expressions of K_{mn}, L_{mn}, M_{mn}, N_{mn} and U^s. The major difficulty in computing these integrals comes from the fact that a finite number of poles or singular points, which are the roots of the denominator of $f(k)$ in equation (2.24) or $F(k)$ in equation (2.15), lie on the real path of integration. A number of techniques are available in literature (Muskhelishvili, 1953; Copson, 1960; Erdogen and Gupta, 1972) to obtain singular integarals. All these techniques are suitable when there is only one pole. For multiple pole on the real axes two different techniques were used by the previous investigators. The technique used by Neerhoff (1979) and Keer et al. (1984), merely deforms the contour of integration below the real k-axis as shown in Fig. 2.4, so that no poles appear on the path of integration. In order to optimize accuracy and computation time, a juditious choice of the two parameters k_1 and k_2, that determine the deformed path, is required.

Kundu (Kundu, 1983; Kundu and Mal, 1985) introduced a technique for removing poles from the singular integrals. This technique is adopted in the present work with appropriate modification because of the avialability of the software and vast amount of supporting literature.

All the singular integrals involved can be expressed in the following form

$$I = \int_0^\infty \frac{G(k)}{D(k)} H(J_m) dk \tag{2.26}$$

where G and D are tanscendental functions of k and H is a function of Bessel functions. D is the Love wave denominator.

Let p_1, p_2, ...p_M be the M roots of D(k) at a given frequency ω; then

$$D(k) = Y(k)(k^2 - p_1^2)(k^2 - p_2^2).....(k^2 - p_M^2) \tag{2.27}$$

so that

$$\frac{G(k)}{D(k)} = \frac{G(k)}{Y(k)(k^2-p_1^2)(k^2-p_2^2).....(k^2-p_M^2)} = \frac{G(k)}{Y(k)}\sum_{i=1}^{M}\frac{A_i}{(k^2-p_i^2)} \tag{2.28}$$

where

$$A_i = \prod_{j=1}^{M}\frac{1}{(p_i^2-p_j^2)} \quad i \neq j \tag{2.29}$$

and $\prod$ is the multiplication symbol. Thus I in (2.26) may be rewritten in the form

$$\begin{aligned} I &= \sum_{i=1}^{M} A_i \int_0^\infty \frac{G(k)H(J_m)}{Y(k)(k^2-p_i^2)}dk \\ &= \sum_{i=1}^{M}\left\{A_i\int_0^\infty\left[\frac{G(k)}{Y(k)}-\frac{G(p_i)}{Y(p_i)}\right]\frac{H(J_m)}{(k^2-p_i^2)}dk + \frac{A_iG(p_i)}{Y(p_i)}\int_0^\infty\frac{H(J_m)}{(k^2-p_i^2)}dk\right\} \end{aligned} \tag{2.30}$$

In equation (2.30) the first integral inside the square braket does not have any singularity for real k. Both the numerator and dinominator vanish at $k = p_i$, but the integrand has a limit which can be obtained by applying L'Hospital's rule numerically. The second integral contains a simple pole at $k = p_i$, but can be evaluated analytically by contour integration (Kundu and Mal, 1985; Kundu, 1986; Kundu, 1987a, b). The following integrals are involved in the second integral

$$I_1 = \int_0^\infty \frac{J_m(ka_i)J_n(ka_i)}{k^2-p^2}dk, \quad i = 1 \text{ or } 2 \tag{2.31}$$

$$I_2 = \int_0^\infty \frac{J_m(ka_i)J_n(ka_j)\cos(kd)}{k^2-p^2}dk, \quad i,j = 1{,}2 \text{ or } 2{,}1; \quad i \neq j \tag{2.32}$$

$$I_3 = \int_0^\infty \frac{J_m(ka_i)J_n(ka_j)\sin(kd)}{k^2-p^2}dk, \quad i,j = 1{,}2 \text{ or } 2{,}1; \quad i \neq j \tag{2.33}$$

$$I_4 = \int_0^\infty \frac{kJ_0(ka_i)}{k^2-p^2}dk, \quad i = 1{,}2 \tag{2.34}$$

$$I_5 = \int_0^\infty \frac{J_1(ka_i)}{k^2-p^2}dk, \quad i = 1{,}2 \tag{2.35}$$

$$I_6 = \int_0^\infty \frac{kJ_2(ka_i)}{k^2 - p^2} dk, \quad i = 1,2 \tag{2.36}$$

where p is a pole of the integrand on the real k-axis. Integrals in equation (2.31) through (2.36) can be found in Kundu and Mal (1985), Kundu (1986) and Kundu (1987a).

In addition to the above integrals, we also encounter the following integral in trying to compute U^s

$$I = \int_0^\infty \frac{f_1(k)J_n(ka_i)}{k} dk, \quad i = 1,2 \tag{2.37}$$

where $f_1(k)$ is an even function of k.

Kundu's technique (Kundu, 1983) requires that the integrand be even. However, in this case n can take any integer value odd or even. The integrand of equation (2.37) is first decomposed into integrands containing J_0, J_1 and J_2 only by using the well-known recurrance relation (Abramowitz and Stegun, 1970)

$$J_{n-1}(ka) + J_{n+1}(ka) = \frac{2n}{ka} J_n(ka) \tag{2.38}$$

Then the integrand is further manipulated to get integral expression of the form given in equations (2.31) through (2.36). Thus integral in equation (2.37) is computed.

A second difficulty in numerically computing the semi-infinite integrals such as those shown in equation (2.19) comes from the fact that any integral of the form

$$\int_0^\infty \frac{F(k)J_m(ka_i)J_n(ka_j)}{k^2} dk, \quad i,j = 1,2 \tag{2.39}$$

is a very slowly converging integral. To get a better convergence the asymptotic expression of $\frac{F(k)}{k^2}$ is subtracted from it. Thus one obtains the term

$$\left\{ \frac{F(k)}{k^2} - \frac{2i}{k(\mu_x^1 + \mu_x^2)} \right\}$$

in the expressions of K_{mn} and N_{mn} in equation (2.19). This term decays at a faster rate with k. The asymptotic part is then integrated analytically to obtain the additional term

$$\frac{2i}{\mu_x^1 + \mu_x^2} \frac{\delta_{mn}}{m}$$

Similar treatment could reduce the computation time of L_{mn} and M_{mn} but asymptotic parts of L_{mn} and M_{mn} could not be integrated analytically. However, it does not cause much numerical difficulty since L and M matrices essentially contain the interaction effects where as K and N contain the direct effects, thus numerically L and M are much smaller than K and N matrices. So even if we allow some error in the computation of L and M matrices, due to their slow convergence property its effect on the final result become even smaller.

In all our computations the integrand has been truncated when its value has been reduced by three orders of magnitude. It is numerically observed that a further reduction in the truncation value does not improve the results any more.

2.4 RESULTS

The method discussed above has been implemented in a FORTRAN program. For isotropic materials, the results are given for a copper-plated quartz specimen which is often used in electronic industries. Material properties for these materials are given in table 2.1. For anisotropic case, same material properties are used with direction dependent properties $C_{44}^j = 1.2C_{55}^j = 1.2\mu^j$.

Table 2.1: Material Properties and Dimensions of the Specimen

Layer/ Half-Space	Material Type	Thickness h in mm	Density $\rho(gm/cc)$	Shear modulus $\mu(GPa)$
Layer	Copper	1.0	8.9	47.90
Half-Space	Quartz	∞	2.2	31.26

Two sample problems are solved to study the interaction between two cracks. In the first problem, two cracks of length 7 mm and 9 mm are located at the interface. The distance between the crack centers is 10 mm. Second problem is same as the first problem but the distance between the crack centers is 16 mm. Displacements at three surface points, P_1 ($x_1 = 3.0\ mm$), P_2 ($x_2 = 5.5\ mm$) and P_3 ($x_3 = 16\ mm$) are computed for an SH-wave pulse propagating at an angle $\theta = 30^0$ with a plane wave front (see Fig. 2.1). The pulse has the following time dependence,

$$f(t) = \begin{cases} 16Pt^2(t-\tau)^2\tau^{-4} & 0 \le t \le \tau \\ 0 & t \ge \tau \end{cases} \tag{2.40}$$

whose Fourier transform is given by

$$F(\omega) = \frac{32P}{\tau^4\omega^3}\left[\left\{-\frac{6\tau}{\omega} + i\left(\tau^2 - \frac{12}{\omega^2}\right)\right\}e^{i\omega\tau} - \left\{\frac{6\tau}{\omega} + i\left(\tau^2 - \frac{12}{\omega^2}\right)\right\}\right] \tag{2.41}$$

Variation of excitation load with time is shown in Fig. 2.5. In the above equation P defines the peak value of the pulse. In subsequent calculations P is set equal to 1 KN/mm^2. τ is the duration of the pulse. Results are given for $\tau = 2.0$ and $0.5\ \mu sec$. In the results presented in Figs. 2.6 through 2.12, length, time and frequency units are in mm, μsec and MHz respectively.

Displacements at P_1 for the two different problems mentioned above, for an incident SH-wave pulse with $\tau = 0.5\ \mu sec$, are shown in Fig. 2.6. In this case the

specimen has isotropic materials only. The left column shows response spectra and the right column gives time histories. The top row shows the surface displacement in absence of any crack. The second row gives the displacement at the same point when the two interface cracks have a tip to tip distance of 2.0 mm (or a center to center distance of 10.0 mm, problem 1), where as for the third row the tip to tip distance is 8.0 mm (problem 2). In both second and third rows, two curves are drawn in each plot. Thicker curves are the actual plots and the thin curves are obtained when the interaction effect between the two cracks is not considered properly. Thin curves are obtained by setting L and M matrices equal to zero in equation (2.18). In other words with L and M equal to zero, the presence of two cracks are considered separately, i.e. it is assumed that there is no interaction between them, and their individual contributions are added to get the thin curves. It can be concluded from this figure that a significant difference in surface displacements occurs if the interaction effect is ignored. There is also a big difference between the surface response of uncracked and cracked bodies. The surface movement sustains for a longer period of time, when interface cracks exist. It is due to the fact that because of the presence of crack surfaces at the interface, the energy of the top layer cannot easily transmit into the half space through the interface, instead part of it reflects back into the layer after being reflected by the crack surfaces.

Fig. 2.7 is the same as Fig. 2.6, the only difference here is that the duration time τ is increased to 2.0 μsec. In this case also a significant difference is observed between responses computed by considering (thick line) and neglecting (thin line) the interaction effect.

The surface response at P_1 when the layer and the substrate are made of anisotropic materials is shown in Fig. 2.8. The time duration (τ) of the pulse is 0.5 μsec. The top row shows the response in absence of any crack and the bottom

row shows it in presence of two interface cracks with a tip to tip distance of 2.0 mm (problem 1). The main difference between the isotropic (Fig. 2.6) and anisotropic (Fig. 2.8) cases is that for the isotropic case the surface motion decays at a slower rate than the anisotropic case. Fig. 2.9 is same as Fig. 2.8, but here τ is increased to 2.0 μsec.

Surface displacements at P_2 and P_3 are given in Figs. 2.10 and 2.11. For both these figures $\tau = 2.0$ μsec and the layered half space is made of isotropic layers and substrates. From Figs. 2.10 and 2.11 it can be seen that the crack interaction effect is slightly reduced as the distance between crack centers is increased. The difference between the thick and thin curves is smaller in Fig. 2.10 in comparison to Fig. 2.7.

In Figs. 2.6 and 2.8 time history plots may have some error, introduced by numerical inversion of the spectra. Ideally the entire spectrum should be considered during FFT inversion. However to save some computational time it was decided to truncate the spectra at 2.4 MHz. But for $\tau = 0.5$ μsec, the spectra do not go to zero at that frequency [Figs. 2.6 and 2.8] so some truncation error is introduced in the time history plots. To examine the order of this error, a typical spectrum (top row of Fig. 2.6) is inverted after truncating it at 2.4 MHz and 4.8 MHz respectively and corresponding time histories are plotted in top and bottom rows of Fig. 2.12. It can be seen from this figure that, the overall nature of the plot doesn't change but sharp peaks become slightly blunt, when the spectrum is truncated at 2.4 MHz. In this case the sharp peak lengths are reduced by about two percent due to early truncation and small oscillations occur before and after the main motion in the time history plot. Since none of these errors are serious enough to alter the overall nature of the time histories we can have confidence in these results.

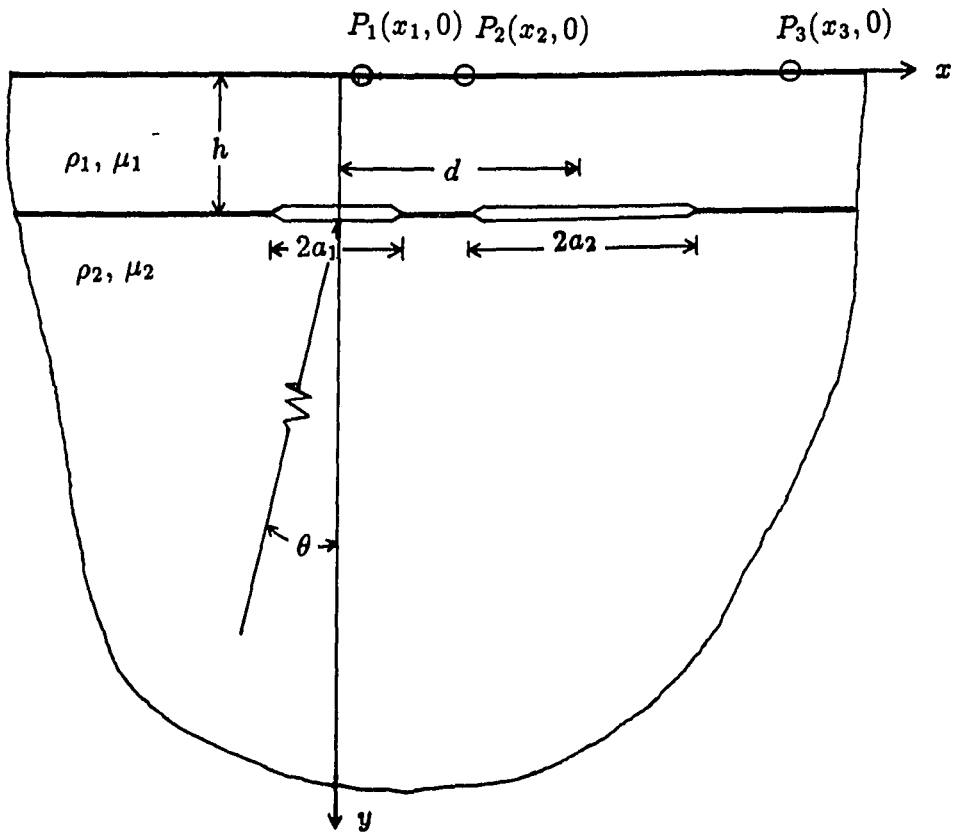

FIG. 2.1: Geometry of the problem. A layered half-space containing two interface cracks is subjected to a plane SH-wave. Surace motion is computed at three surface points P_1, P_2 and P_3.

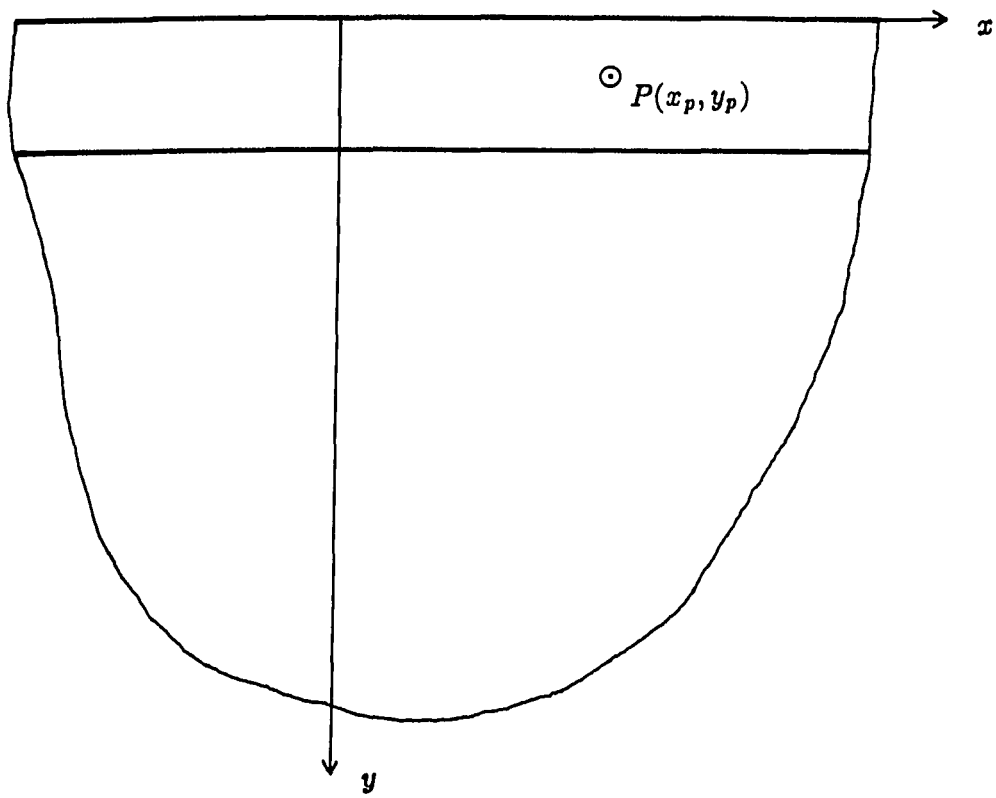

Fig. 2.2: A point load in a layered half space.

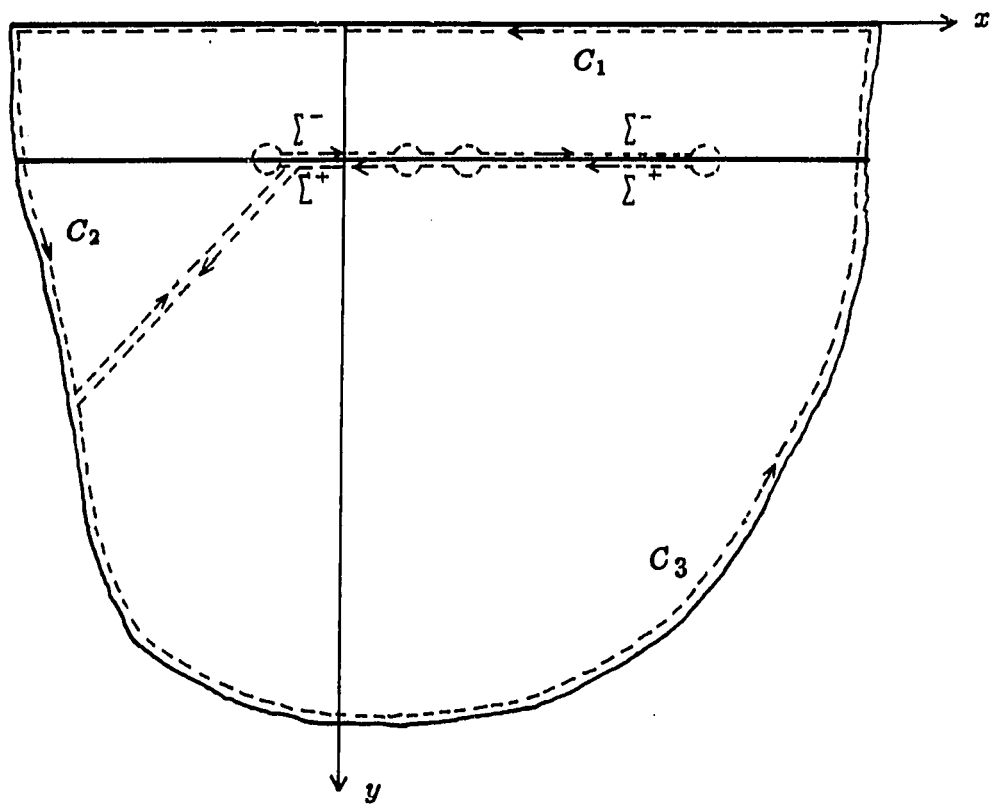

Fig. 2.3: Contour of integration (Equation 2.5).

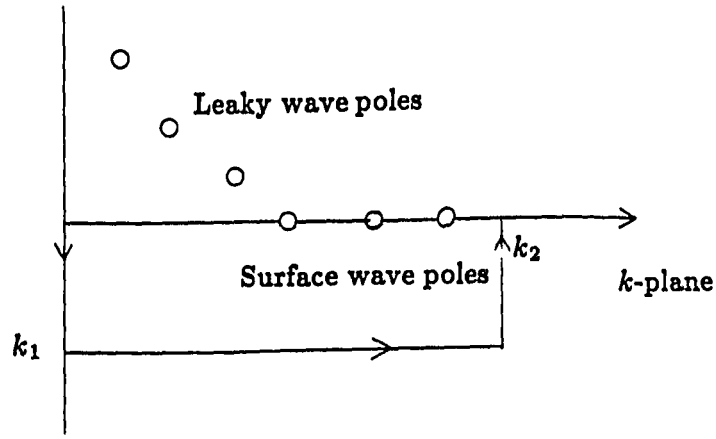

Fig. 2.4: Contour of integration for Neerhoff's (1979) method.

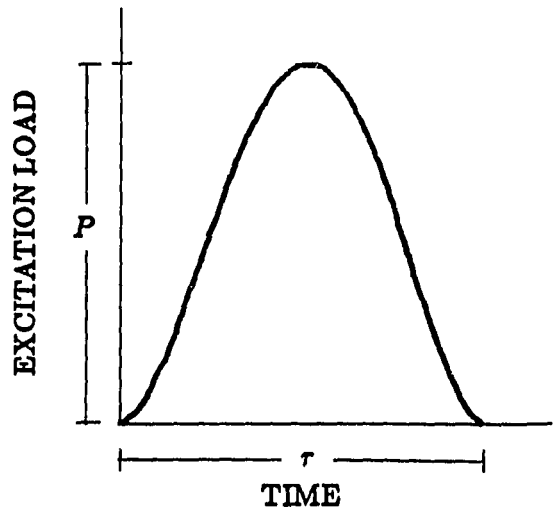

FIG. 2.5: Variation of excitation load with times.

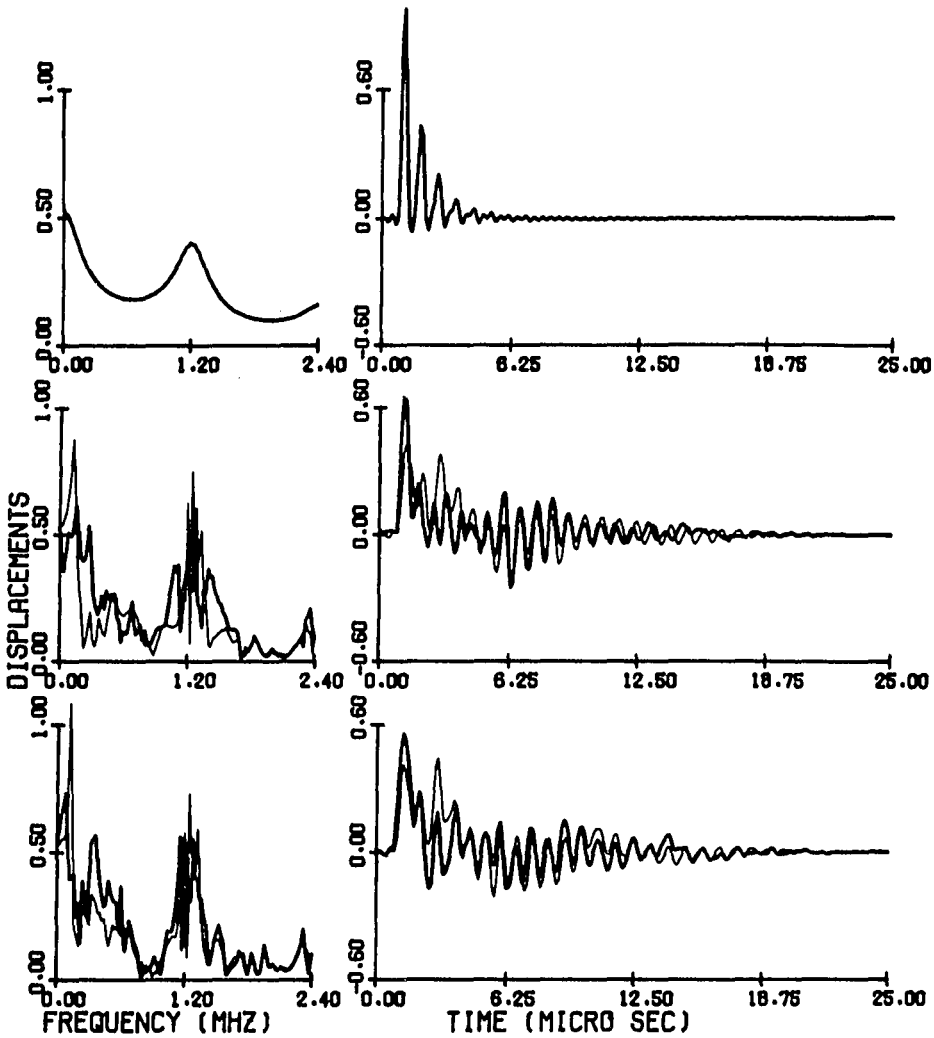

Fig. 2.6: Surface displacements in a layered isotropic half space at $x = 3$ *mm*. The half space is excited by a SH-wave pulse propagating at thirty degree angle, with pulse duration time $\tau = 0.5$ μsec. The top row shows the surface displacement without any crack. The middle row gives the surface displacement when two interface cracks have center to center distance of 10 *mm* (problem 1) and the bottom row is same as the middle row but here the distance between the crack centers is 16 *mm* (problem 2). In middle and bottom rows bold curves give actual displacements and thin curves give uncoupled displacements (neglecting interaction effect). Left column: Spectral amplitude of displacement in *mm*-μsec. Right column: Time histories in mm.

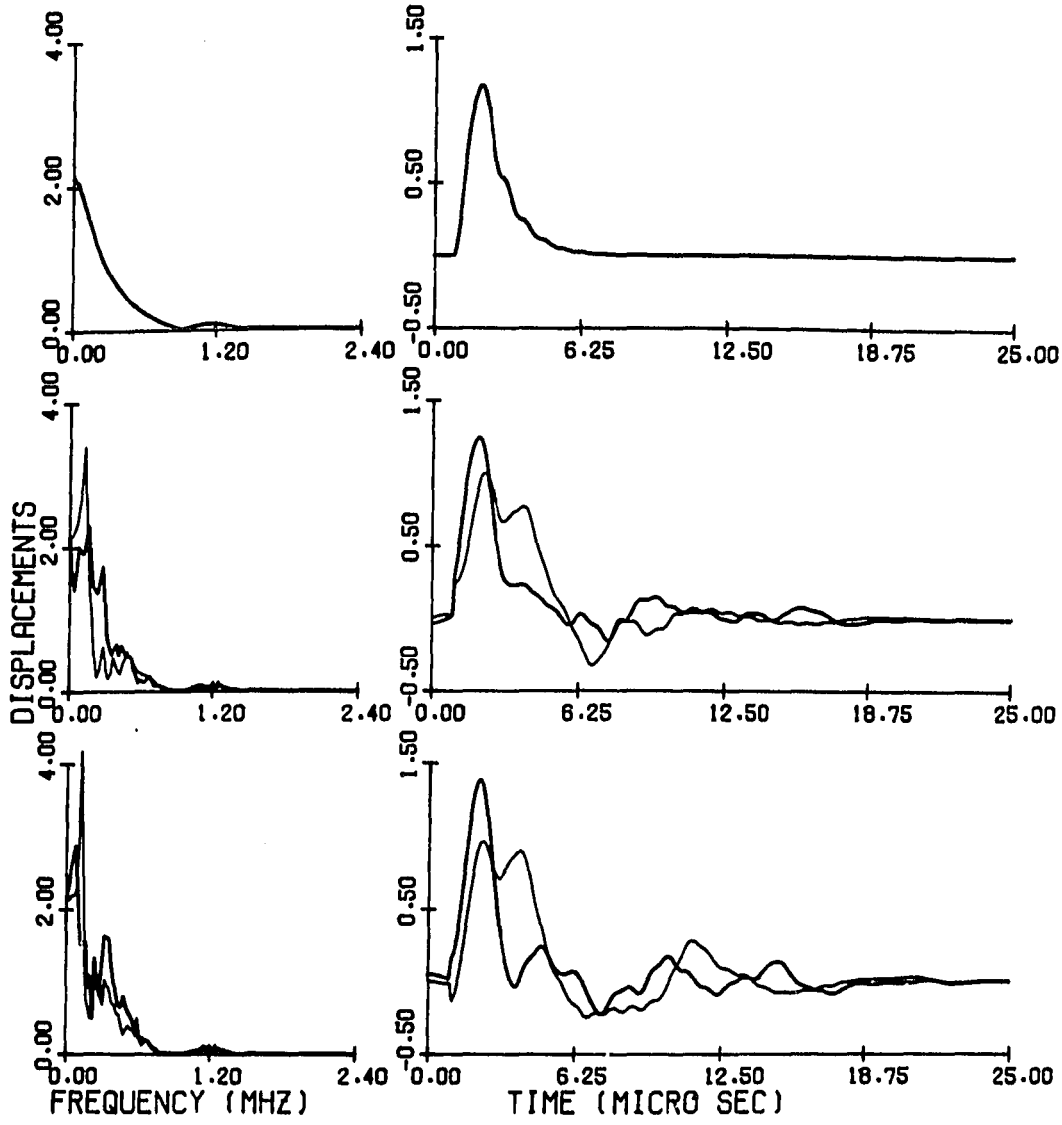

Fig. 2.7: Same as Fig. 3 but $\tau = 2.0\ \mu sec.$

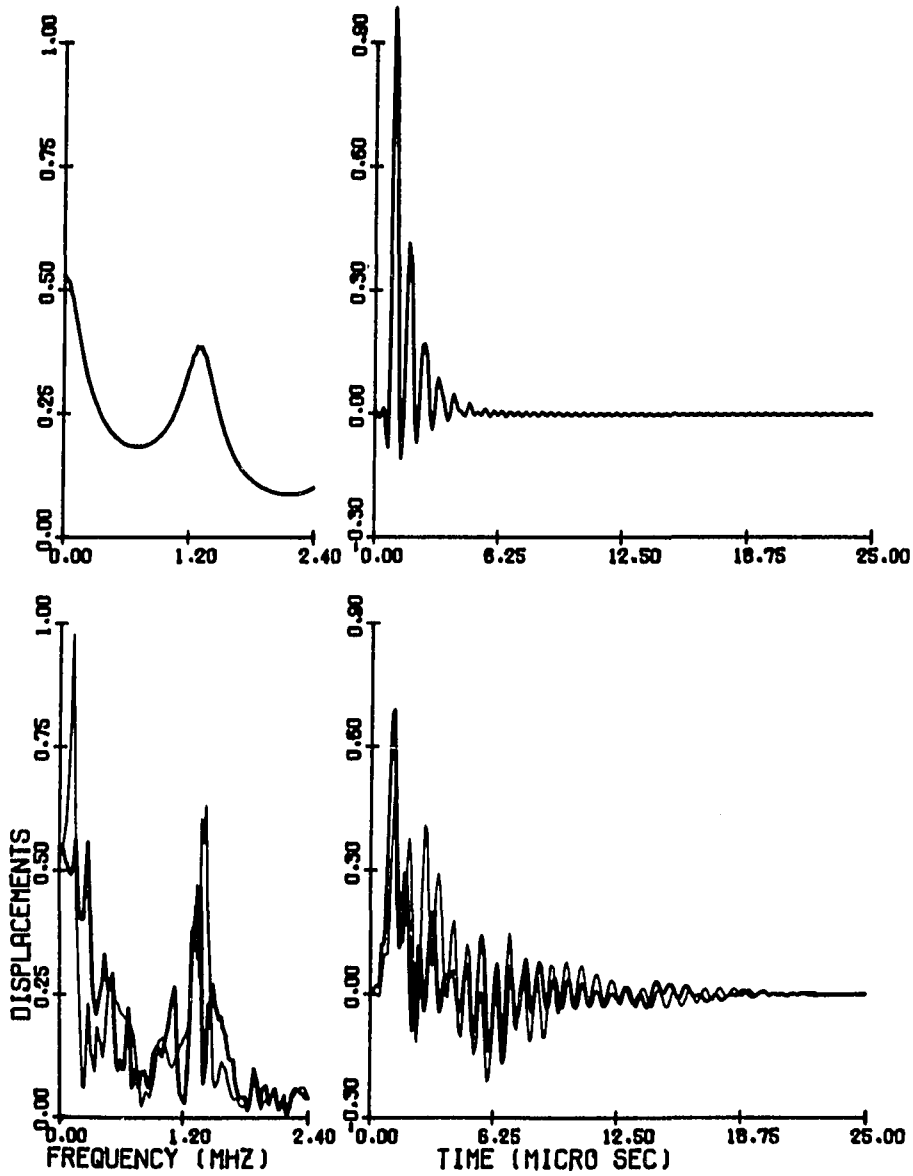

Fig. 2.8: Same as top and middle rows of Fig. 2.6 but layer and substate are made of anisotropic materials.

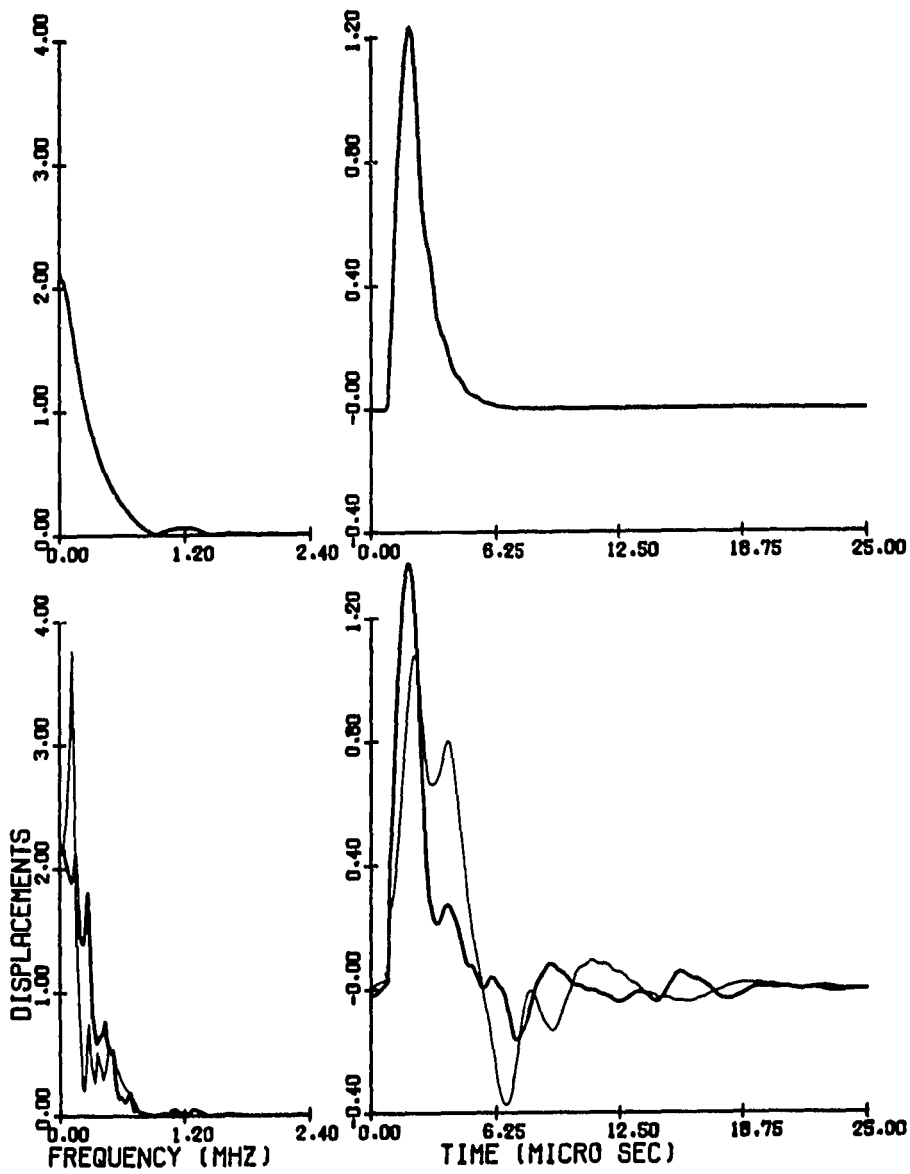

Fig. 2.9: Same as Fig. 2.8 but $\tau = 2.0$ $\mu sec.$

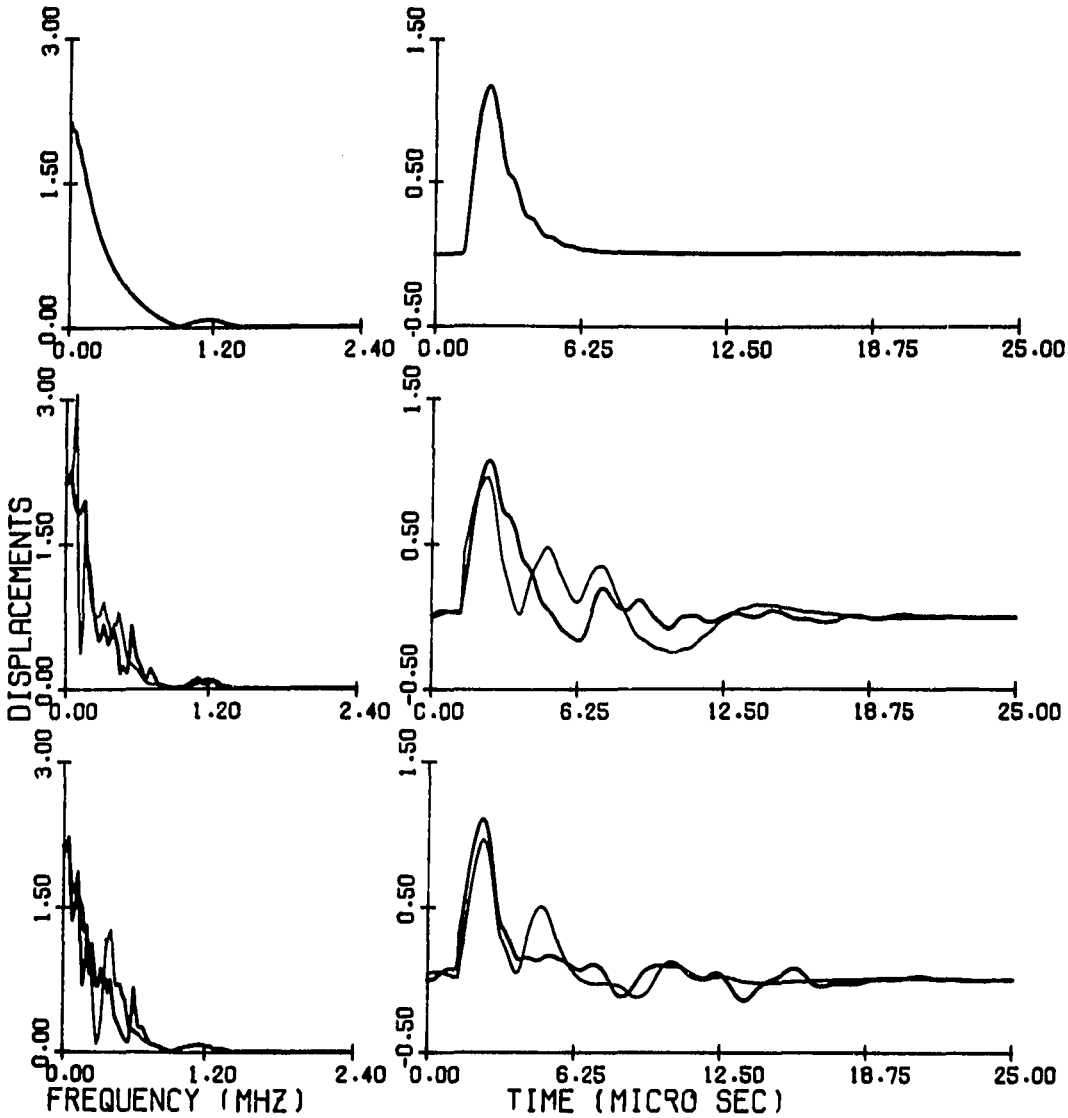

Fig. 2.10: Same as Fig. 2.7 but $x = 5.5\ mm$.

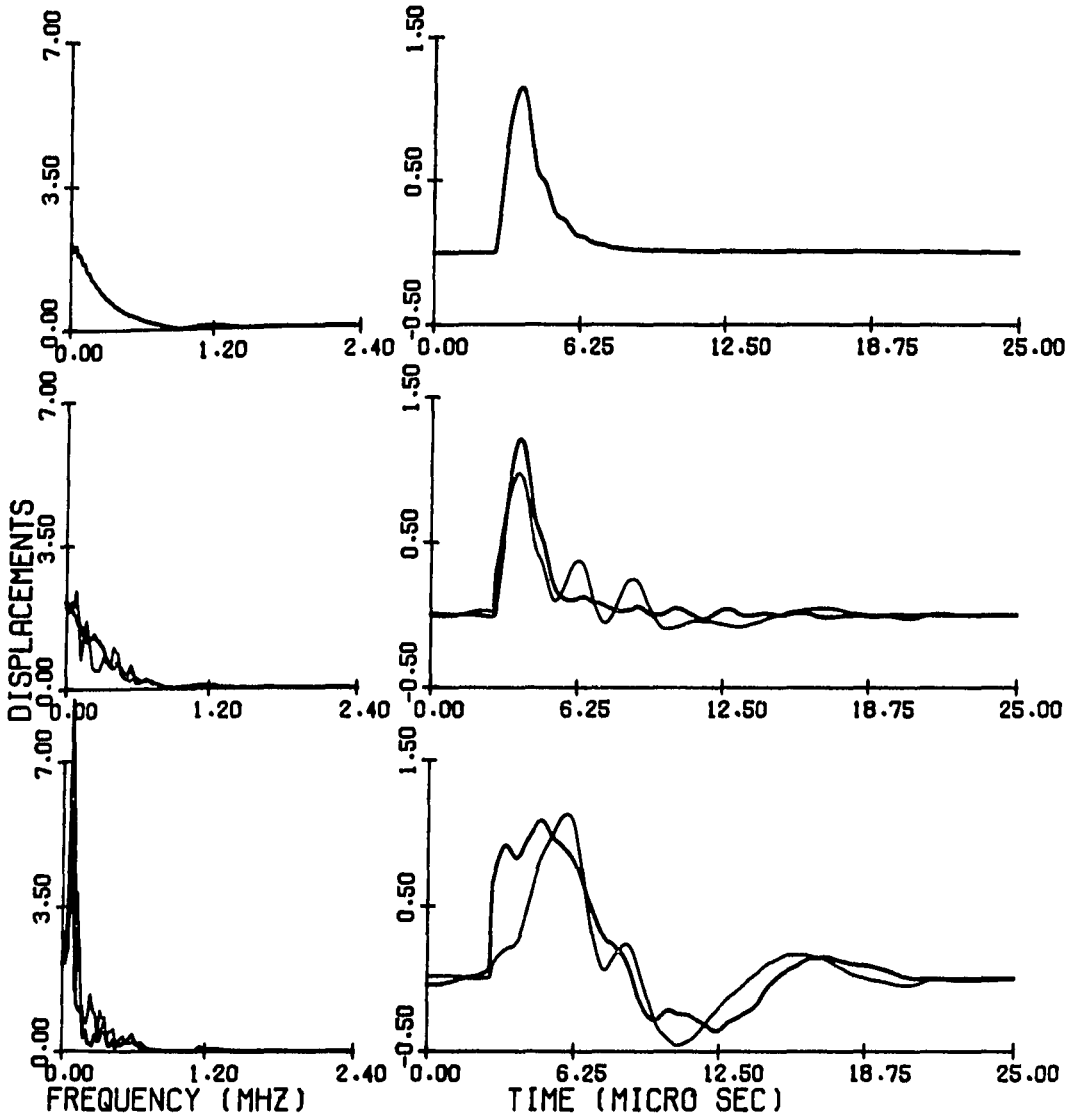

Fig. 2.11: Same as Fig. 2.7 but $x = 16.0\ mm$.

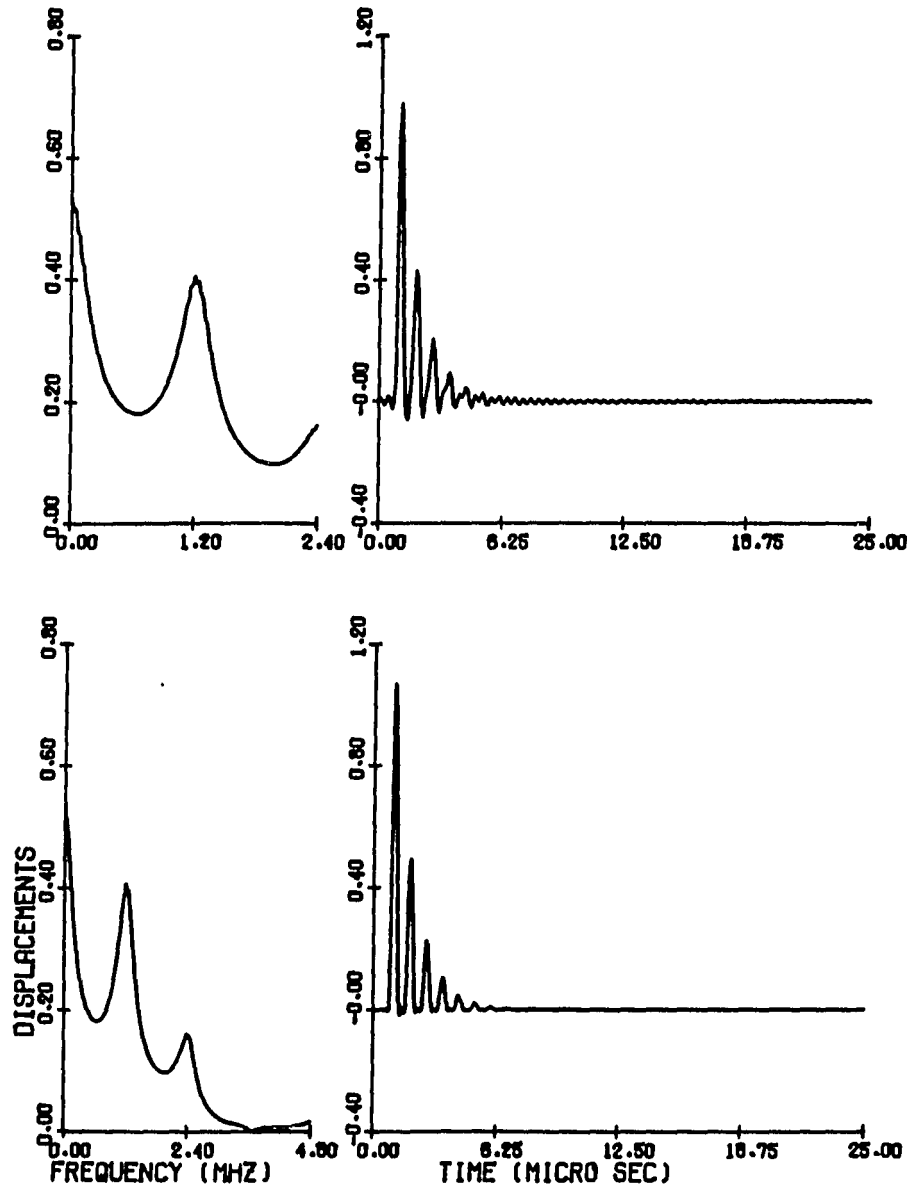

Fig. 2.12: Effect of premature truncation of spectra on time history plots. Top figure is truncated at 2.4 MHz, bottom figure is truncated at 4.8 MHz.

CHAPTER–3

DYNAMIC RESPONSE OF A THREE LAYERED COMPOSITE PLATE WITH INTERFACE CRACKS

The dynamic response of three layered composite plate, with two interface cracks, subjected to an antiplane line load is analyzed in this chapter. Green's function for the uncracked medium is used with the appropriate form of Betti's reciprocal theorem to derive the scattred field. Numerical results for two sample problems are presented, for both isotropic and anisotropic materials.

3.1 PROBLEM FORMULATION

A plate is made of three elastic layers, 1, 2 and 3, of thickness h_1, h_2, h_3 as shown in Fig. 3.1. Plate dimensions along x and z-directions are infinite. Two Griffith cracks of lengths $2a_1$ and $2a_2$ are located at the two interfaces at $y = y_1(= h_1)$ and $y = y_2(= h_1 + h_2)$ with a distance d between the crack centers. An antiplane line load, $\tau_{yz} = \delta(x)f(t)$, is applied at the origin as shown in Fig. 3.1. The plate, crack geomerties and loadings are invariant in the z-direction.

To solve this problem, we need to solve two canonical problems as discussed in the previous chapter. The two problems are then combined with the aid of Betti's reciprocal theorem.

3.1.1 Canonical Problem 1: Flawless Layered Plate Subjected to a Line Load at the Boundary

The geometry of this problem is similar to Fig. 3.1, the only difference is that there is no crack at the interface. The time harmonic antiplane stress field of

time dependence $e^{-i\omega t}$ acts as a line load. Solutions of the wave equations for this problem are given below.

3.1.1.1 Isotropic Material

For the isotropic case let us assume that ρ_j and μ_j are the material density and shear modulus of the j-th layer ($j = 1, 2, 3$). The governing equation in the frequency domain is identical to that given in equation (2.1). The solution of equation (2.1) for a line load can be written as

$$U_j = \frac{1}{2\pi} \int_{-\infty}^{\infty} \left\{ A_j e^{i\eta_j y} + B_j e^{-i\eta_j y} \right\} e^{ikx} dk \qquad (3.1a)$$

where

$$\begin{aligned} \eta_j &= (k_{sj} - k^2)^{\frac{1}{2}} \qquad for \qquad k < k_{sj} \\ &= i(k^2 - k_{sj})^{\frac{1}{2}} \quad for \qquad k > k_{sj} \end{aligned} \qquad (3.1b)$$

$k_{sj} (j = 1, 2, 3)$ is the S-wave number of the $j\text{-}th$ medium. The time dependence $e^{-i\omega t}$ in equation (3.1a) and in all subsequent equations is implied. The expressions for unknown coefficients A_j and B_j can be obtained from known boundary and interface conditions and are given in the Appendix-C. The integral expression in equation (3.1a) is required to account for the point load at the boundary.

3.1.1.2 Anisotropic Material

For anisotropic materials, it is assumed that in each layer, planes normal to the y-axis are planes of symmetry. C_{44}^j and C_{55}^j are shear moduli related to yz and zx-directions in the $j\text{-}th$ medium. The governing equation in the frequency domain

for this material is identical to that in equation (2.4). The solution of this equation gives exactly the same equation as (3.1a) with the following redefinition of η_j

$$\begin{aligned} \eta_j &= \left\{ \frac{\rho_j \omega^2 - k^2 C_{55}^j}{C_{44}^j} \right\}^{\frac{1}{2}} \quad \text{for} \quad k < \omega(\frac{\rho_j}{C_{55}})^{\frac{1}{2}} \\ &= i \left\{ \frac{k^2 C_{55}^j - \rho_j \omega^2}{C_{44}^j} \right\}^{\frac{1}{2}} \quad \text{for} \quad k > \omega(\frac{\rho_j}{C_{55}})^{\frac{1}{2}} \end{aligned} \tag{3.2}$$

3.1.2 Canonical Problem 2: A Line Load in a Layered Flawless Plate

The geometry of this problem is shown in Fig. 3.2. A time harmonic line load is acting at a point $P(x_p, y_p)$ as shown in the figure. The displacement field in the $j\text{-}th$ layer generated by a line load in layer α is given by

$$U_j^\alpha = \frac{i}{4\pi\mu_x^1} \int_{-\infty}^{\infty} \left\{ \delta_{\alpha j} \frac{e^{i\eta_2|y-y_p|}}{\eta_2} + C_j^\alpha e^{i\eta_j y} + D_j^\alpha e^{-i\eta_j y} \right\} e^{ik(x-x_p)} dk \tag{3.3}$$

where, $\alpha = 1, 2$ and $j = 1, 2, 3$ and for isotropic materials

$$\mu_x^j = \mu_j$$

and for anisotropic materials

$$\mu_x^j = C_{44}^j$$

and $\delta_{\alpha j}$ is the Kronecker delta function which is 1 for j equal to α and 0 for j not equal to α.

The unknown coefficients C_j^α and D_j^α can be obtained from stress-free boundary conditions and continuity conditions across the interface. Expressions of these coefficients are given in the Appendix-C. The superscript G of U_j indicates displacements corresponding to the Green's elastodynamic state.

3.2 APPLICATION OF BETTI'S RECIPROCAL THEOREM

Let us consider two solution states S and G. State S corresponds to the scattered field of the original problem. So when S is added to the displacement field of the canonical problem 1 the solution state of the problem of our interest is obtained. The canonical problem 2, the Green's elastodynamic state, is referred as state G. Using Betti's reciprocal theorem these two states can be related in the following manner

$$\int_V F_i^S U_i^G dV + \int_S T_i^S U_i^G dS = \int_V F_i^G U_i^S dV + \int_S T_i^G U_i^S dS \quad \text{(summation implied)} \tag{3.4}$$

where F_i is the body force per unit volume acting in the x_i direction, T_i is the surface traction per unit area acting in the x_i direction, and U_i is the displacement in the x_i direction. Superscripts S and G represent states S and G respectively.

Equation (3.4) can be reduced to a very simple form by contour integration. For a very similar problem Kundu (1987b) has discussed the procedure, we repeat it here again for completeness. The body force for state S is zero and for state G it is equal to $\delta(\bar{r} - \bar{r_p})$ acting in the z-direction. $\bar{r_p}$ is the position vector of point P and $\bar{r}$ is the position vector of any point of interest. For an antiplane problem all nonzero forces and displacements act in the z-direction. So for our problem the general equation (3.4) takes the form,

$$\int_S T^S U^G dS = U^S(\bar{r_p}) + \int_S T^G U^S dS \tag{3.5}$$

where U is the particle displacement and T is the shear stress. Since the problem is invariant in the z-direction, surface integrals may be reduced to line integrals. This line integral is carried out along a contour, as shown in Fig.3.3.

The integral of the left-hand side of equation (3.5) vanishes because T^S is zero on C_1, C_2, C_3, C_4 and integrals of $T^S U^G$ on Σ_j^+ and Σ_j^- cancel each other for $j = 1$ and 2. The only nonzero term comes from the integral of the right-hand side of equation (3.5) along the intgration paths Σ_j^+ and Σ_j^-. After some simplification, equation (3.5) is reduced to

$$U^S(\bar{r}_p) = \int_{d_1-a_1}^{d_1+a_1} \phi(x-d_1) T_{yz}^G dx + \int_{d_2-a_2}^{d_2+a_2} \psi(x-d_2) T_{yz}^G dx \tag{3.6}$$

where $\phi(x-d_1)$ and $\psi(x-d_2)$ are crack opening displacements (COD) of the two cracks and are defined as

$$\begin{aligned} \phi(x-d_1) &= U^S(x-d_1, y_1^+) - U^S(x-d_1, y_1^-) \\ \psi(x-d_2) &= U^S(x-d_2, y_2^+) - U^S(x-d_2, y_2^-) \end{aligned} \tag{3.7}$$

and $\bar{r}_p$ is the position vector of the point P. The expression for T_{yz}^G at $y = y_1$ and y_2 may be obtained from

$$T_{yz}(x, y_1) = T_1^2(x, y_1^-) = T_2^2(x, y_1^+) = C_{44}^2 \left\{ \frac{\partial U_2^2}{\partial y} \right\}_{y=y_1} \tag{3.8a}$$

and

$$T_{yz}(x, y_2) = T_2^2(x, y_2^-) = T_3^2(x, y_2^+) = C_{44}^2 \left\{ \frac{\partial U_2^2}{\partial y} \right\}_{y=y_2} \tag{3.8b}$$

where U_2^2 is given in equation (3.3).

If point P is now taken on the crack surface, the displacement of that point can be obtained from equation (3.6) if T_{yz}^G, $\phi(x-d_1)$ and $\psi(x-d_2)$ are known. Combining equations (3.6) and (3.8) the displacement field at x_p, y_p ($y_p = y_1$ or y_2) is obtained:

$$\begin{aligned} U_2^S(x_p, y_p) = \frac{1}{4\pi} \int_{d_1-a_1}^{d_1+a_1} \phi(x-d_1) \int_{-\infty}^{\infty} \left\{ e^{i\eta_2(y_p-y_1)} - \eta_2(C_2^2 - D_2^2) \right\} \\ e^{ik(x-x_p)} dk dx - \frac{1}{4\pi} \int_{d_2-a_2}^{d_2+a_2} \psi(x-d_2) \\ \int_{-\infty}^{\infty} \left\{ e^{i\eta_2(y_2-y_p)} + \eta_2(C_2^2 Q_2 - D_2^2 Q_2^{-1}) \right\} e^{ik(x-x_p)} dk dx \end{aligned} \tag{3.9}$$

where

$$Q_2 = e^{i\eta_2 h_2}$$

The scatterd stress field can be obtained from the displacement field of equation (3.9). Then it is equated to the negative of the incident stress field along the crack surfaces ($y = y_1$, $|X_1| < a_1$ and $y = y_2$, $|X_2| < a_2$, when $X_1 = x - d_1, X_2 = x - d_2$) to obtain

$$\int_{-\infty}^{\infty} \{A_2 - B_2\}\, \eta_2 e^{ikX_{1p}+ikd_1} dk = \frac{1}{2}\int_{-a_1}^{a_1} \phi(X_1) \int_{-\infty}^{\infty} F_1(k) e^{ik(X_1 - X_{1p})} dk dX_1 + \frac{1}{2}\int_{-a_2}^{a_2} \psi(X_2) \int_{-\infty}^{\infty} F_2(k) e^{ik(X_2 - X_{1p})+ikd} dk dX_2 \quad for \quad -a_1 < X_{1p}(= x_p - d_1) < a_1 \tag{3.10a}$$

and

$$\int_{-\infty}^{\infty} \left\{A_2 Q_2 - B_2 Q_2^{-1}\right\} \eta_2 e^{ikX_{2p}+ikd_2} dk = \frac{1}{4\pi}\int_{-a_1}^{a_1} \phi(X_1) \int_{-\infty}^{\infty} F_3(k)\, e^{ik(X_1 - X_{2p})-ikd} dk dX_1 + \frac{1}{4\pi}\int_{-a_2}^{a_2} \psi(X_2) \int_{-\infty}^{\infty} F_4(k) e^{ik(X_2 - X_{2p})} dk dX_2 \quad for \quad -a_2 < X_{2p}(= x_p - d_2) < a_2 \tag{3.10b}$$

where

$$\begin{aligned} F_1(k) &= -\eta_2 \left\{1 + i\frac{\partial}{\partial y_p}(C_2^2 - D_2^2)\right\}_{y_p = y_1} \\ F_2(k) &= -\eta_2 \left\{Q_2 + i\frac{\partial}{\partial y_p}(C_2^2 Q_2 - D_2^2 Q_2^{-1})\right\}_{y_p = y_1} \\ F_3(k) &= -\eta_2 \left\{Q_2 + i\frac{\partial}{\partial y_p}(C_2^2 - D_2^2)\right\}_{y_p = y_2} \\ F_4(k) &= -\eta_2 \left\{1 + i\frac{\partial}{\partial y_p}(C_2^2 Q_2 - D_2^2 Q_2^{-1})\right\}_{y_p = y_2} \end{aligned} \tag{3.11}$$

A_2, B_2 in equations (3.10) and C_2^2, D_2^2 in equations (3.11) are defined in equations (3.1) and (3.3) respectively. Partial derivatives of C_2^2 and D_2^2 with respect to y_p at $y_p = y_1$ and y_2 are given in the Appendix-C.

3.2.1 Computation of the Crack Opening Displacement Functions

In order to evaluate the crack opening displacements, $\phi(x)$ and $\psi(x)$ are expanded in a complete set of Chebyshev polynomials, as in equation (2.16). To obtain the unknown coefficients α_n and γ_n, both sides of equation (3.10a) are multiplied by $\phi_m(X_{1p})$, then integrated from $X_{1p} = -a_1$ to $X_{1p} = a_1$ and both sides of equation (3.10b) are multiplied by $\psi_m(X_{2p})$, then integrated from $X_{2p} = -a_2$ to $X_{2p} = a_2$. After some algebraic manipulation an infinite set of linear equations is obtained to solve for α_n and γ_n,

$$\begin{aligned}
\sum_{n=1}^{\infty}(K_{mn}\alpha_n + L_{mn}\gamma_n) &= -\frac{4l_m}{\pi}\int_0^{\infty} f_1(k)\eta_2\frac{J_m(ka_1)}{k}dk \\
\sum_{n=1}^{\infty}(M_{mn}\alpha_n + N_{mn}\gamma_n) &= -\frac{4l_m}{\pi}\int_0^{\infty} f_2(k)\eta_2\frac{J_m(ka_2)}{k}dk
\end{aligned} \tag{3.12}$$

where for odd m

$$\begin{aligned}
f_1(k) &= (A_2 - B_2)\cos(kd_1) \\
f_2(k) &= (A_2Q_2 - A_2Q_2^{-1})\cos(kd_2) \\
l_m &= i
\end{aligned} \tag{3.13a}$$

for even m

$$\begin{aligned}
f_1(k) &= (A_2 - B_2)\sin(kd_1) \\
f_2(k) &= (A_2Q_2 - A_2Q_2^{-1})\sin(kd_2) \\
l_m &= 1
\end{aligned} \tag{3.13b}$$

and $J_m$is the Bessel functions of first kind of order m. K, L, M and N matrices are defined in the following manner for even $(m+n)$

$$
\begin{aligned}
K_{mn} &= 2\int_0^\infty \left\{\frac{F_1(k)}{k^2} - \frac{2i\mu_x^1}{k(\mu_x^1+\mu_x^2)}\right\} J_m(ka_1)J_n(ka_1)dk \quad + \frac{2i\mu_x^1}{\mu_x^1+\mu_x^2}\frac{\delta_{mn}}{m} \\
L_{mn} &= 2\int_0^\infty \frac{F_2(k)}{k^2} J_m(ka_1)J_n(ka_2)\cos(kd)dk \\
M_{mn} &= 2\int_0^\infty \frac{F_2(k)}{k^2} J_m(ka_2)J_n(ka_1)\cos(kd)dk \\
N_{mn} &= 2\int_0^\infty \left\{\frac{F_4(k)}{k^2} - \frac{2i\mu_x^3}{k(\mu_x^2+\mu_x^3)}\right\} J_m(ka_2)J_n(ka_2)dk \quad + \frac{2i\mu_x^3}{\mu_x^2+\mu_x^3}\frac{\delta_{mn}}{m}
\end{aligned}
\tag{3.14}
$$

and for odd $(m+n)$,

$$
\begin{aligned}
K_{mn} &= N_{mn} = 0 \\
L_{mn} &= 2i\int_0^\infty \frac{F_2(k)}{k^2} J_m(ka_1)J_n(ka_2)\sin(kd)dk \\
M_{mn} &= -2i\int_0^\infty \frac{F_2(k)}{k^2} J_m(ka_2)J_n(ka_1)\sin(kd)dk
\end{aligned}
\tag{3.15}
$$

From equations (3.14) and (3.15) it can be clearly seen that K and N matrices are symmetric but L and M matrices are not. However L and M satisfy the following relations

$$
L_{mn} = \begin{cases} M_{nm}, & for \quad m+n\text{=even} \\ -M_{nm} & for \quad m+n\text{=odd} \end{cases}
$$

Equations (3.12) have infinite series in their expressions, however, they can be terminated after a finite number of terms without introducing any significant error (Kundu, 1986). Then α_n and γ_n can be obtained from a finite set of linear equations and finally $\phi(x)$ and $\psi(x)$ can be computed from equation (2.16) without any difficulty.

After obtaining ϕ and ψ the tearing mode stress intensity factor K_{III} can be easily obtained from the following relation (Hassan, 1985; Kundu and Hassan, 1987),

$$
K_{III} = \frac{\mu_x^1\mu_x^2}{\mu_x^1+\mu_x^2}\sqrt{\frac{\pi}{2r}}\phi(r) \tag{3.16}
$$

where μ_x^1, μ_x^2 are shear moduli of the two layers adjacent to the crack, $\phi(r)$ is the crack opening displacement at a distance r from the crack tip ($r << 1$).

3.2.2 Computation of Surface Displacement

The total displacement U is given by

$$U = U^i + U^s \tag{3.17}$$

in which U^i is the total field in the absence of any crack given by equation (3.1), whereas the scattered field U^s, represents the change in U^i due to the presence of cracks. U_1^s, the scattered field in layer 1, can be obtained by repeating the procedure used to obtain the equation (3.9). At any point on the surface $A(x_p, 0)$ after some simplification we can write

$$U^i(x_p, 0) = \frac{1}{2\pi} \int_{\infty}^{\infty} (A_1 + B_1) e^{ikx_p} dk \tag{3.18}$$

and

$$\begin{aligned} U_1^s(x_p, 0) = & -2i \int_0^{\infty} \frac{f^1(k)}{k} \cos(kd_1 - kx_p) \sum_{n=odd}^{\infty} \{\alpha_n J_n(ka_1)\}\, dk \\ & +2 \int_0^{\infty} \frac{f^1(k)}{k} \sin(kd_1 - kx_p) \sum_{n=even}^{\infty} \{\alpha_n J_n(ka_1)\}\, dk \\ & -2i \int_0^{\infty} \frac{f^2(k)}{k} \cos(kd_2 - kx_p) \sum_{n=odd}^{\infty} \{\gamma_n J_n(ka_2)\}\, dk \\ & +2 \int_0^{\infty} \frac{f^2(k)}{k} \sin(kd_2 - kx_p) \sum_{n=even}^{\infty} \{\gamma_n J_n(ka_2)\}\, dk \end{aligned} \tag{3.19}$$

where

$$\begin{aligned} f^1(k) &= \frac{\{F_2(F_3 + F_4) + F_2 Q_2^2 (F_3 - F_4)\}}{(1 + Q_1^2) M} \\ f^2(k) &= \frac{2F_2 F_3 Q_1 Q_2}{(1 + Q_1^2) M} \end{aligned} \tag{3.20}$$

where M, F_1, F_2, F_3, F_4 and Q_j are defined in equation (3.21)

$$
\begin{aligned}
M &= (F_1 + F_2)(F_3 + F_4) - Q_2^2(F_1 - F_2)(F_3 - F_4) \\
F_1 &= \mu_x^1 \eta_1 (1 - Q_1^2) \\
F_2 &= \mu_x^2 \eta_2 (1 + Q_1^2) \\
F_3 &= \mu_x^3 \eta_3 (1 - Q_3^2) \\
F_4 &= \mu_x^2 \eta_2 (1 + Q_3^2) \\
Q_j &= e^{i\eta_j h_j}
\end{aligned}
\tag{3.21}
$$

then equations (3.18) and (3.19) are added to get the total surface displacement.

3.3 RESULTS

The method discussed above has been implemented in a FORTRAN program. Results for some sample problems are presented in this section. For isotropic materials, the plate specimen for which numerical results are given is made of copper, steel and quartz. A crack of length 2 mm is located at the copper-steel interface and a second crack of length 4 mm is located at the quartz-steel interface. For the first problem, the distance between the crack centers is 0.5 mm and load is applied on the surface, at a point located directly below the center of the 2 mm crack, then d_1 in Fig. 3.1 is zero. The second problem is same as the first problem, but in this case the distance between the crack centers is 3 mm and d_1 is 0.5 mm (see Fig. 3.1). Properties of the plate materials are given in Table 3.1.

Table 3.1: Material Properties and Dimensions of the Specimen

Layer Number	layer Material	Thickness h in mm	Density $\rho(gm/cc)$	Shear modulus $\mu(GPa)$
1	Copper	0.5	8.9	47.90
2	Steel	0.5	7.9	80.90
3	Quartz	0.5	2.2	31.27

The same two problem geometries are also considered with anisotropic layers. For each problem two types of material anisotropy are considered. In the first case, $C^j_{55} = 1.5C^j_{44} = 1.5\mu^j$, and in the second case $C^j_{44} = 1.5C^j_{55} = 1.5\mu^j$.

In the results presented in Figs. 3.4 through 3.13, length, time and frequency units are in mm, μsec and MHz respectively. Response of the cracks to impact loadings are shown in Figs. 3.4 through 3.13. The same loading function as in Chapter 2 (equation 2.40) is considered. In Figs. 3.4 through 3.10, P is set to 10. Results are given for $\tau = 2$ and 0.2 micro seconds.

In Figs. 3.4 through 3.9 CODs are plotted. Spectra are plotted in the left column, while the right column shows the time histories. Time histories are obtained numerically by inverting the response spectra using FFT (Fast Fourier Transform) routine. In all these figures two curves are plotted, one with a bold pen and the other with a thin pen. The bold curves are actual plots of COD and the thin curves are the COD plots when the interaction between the two cracks is neglected. In other words thin curves represent the response of one crack when the other crack is absent. They are obtained by setting the coupling matrices L and M equal to a null matrix.

Figs. 3.4 through 3.6 are for the first problem ($d_1 = 0$, $d_2 = 0.5\ mm$) with $\tau = 2.0\ \mu sec$. In Fig. 3.4 the top row shows COD at the right quarter point of the 2 mm crack. The second row shows COD at the left quarter point of the same crack. Third and fourth rows are same as first and second rows respectively for the 4 mm crack. The problem geometry and excitation load for Fig. 3.5 and 3.6 are identical to those in Fig. 3.4. Figs. 3.5 and 3.6 show response of plates made of anisotropic layers. For Fig. 3.5 the relation betweeen C^j_{44} snd C^j_{55} is given by $C^j_{55} = 1.5C^j_{44} = 1.5\mu^j$ and for Fig. 3.6 it is $C^j_{44} = 1.5C^j_{55} = 1.5\mu^j$. From these figures it can be seen that in all cases the interaction effect is more for the 4 mm

crack than that for the 2 mm crack. This is due to the fact that the 2 mm crack is located between the source and the 4 mm crack, hence its presence significantly influences the waves striking the 4 mm crack. Comparing Figs. 3.4 through 3.6, it can be concluded that a change in C^j_{44} affects the results much more than a change in C^j_{55}. It seems logical because of the orientation of the cracks. On the crack surface $\tau_{yz} = 0$, and τ_{yz} is affected more by changing C^j_{44} than C^j_{55}.

Figs. 3.7 through 3.9 show COD at the left quarter point of the 4 mm crack. The top row is for the layered plate with isotropic layers and the other two rows are for plates with anisotropic layers. For the middle row $C^j_{55} = 1.5C^j_{44} = 1.5\mu^j$ and the bottom row is for $C^j_{44} = 1.5C^j_{55} = 1.5\mu^j$. Fig. 3.7 is for $d_1 = 0\ mm$, $d_2 = 0.5\ mm$ and Fig. 3.8 is for $d_1 = 0.5\ mm$, $d_2 = 3.5\ mm$. In both figures $\tau = 0.2\ \mu sec$. Fig. 3.9 is same as Fig. 3.10 but for $\tau = 2.0\ \mu sec$.

The distance between the crack and the source (the point of load application) is greater in Fig. 3.8 than in Fig. 3.7. Hence due to geometric damping COD in Fig. 3.8 is smaller than that in Fig. 3.7.

In all figures, 3.4 through 3.9, it is observed that interaction effect increases COD of the 4 mm crack significantly. This is due to the fact that in presence of the 2 mm crack the stress waves are shifted from their normal path to have higher concentrations near the two ends of this crack, hence more stress waves strike the 4 mm crack and increase its COD when the 2 mm crack is present.

It should be noted here that for the same problem geometry and material properties, Fig. 3.9 shows larger COD than Fig. 3.8. This is because the load duration time τ in Fig. 3.9 is larger, hence the external work done on the plate is more in Fig. 3.9 than in Fig. 3.8. Hence Fig. 3.9 shows greater crack opening displacements.

In Fig. 3.10 the effect of fiber reinforcement direction on the crack opening displacement is shown. In this figure COD at the left quarter point of the 4 mm crack is plotted for the first problem geometry ($d_1 = 0$, $d_2 = 0.5\ mm$) with $\tau = 2.0$ μsec. The top row shows the COD of the 4 mm crack in an anisotropic homogeneous plate with fiber layup in the 0^0 direction. For this plot $C^j_{55} = 1.5C^j_{44} = 121.35\ GPa$. The middle row shows the crack response in a three layer plate with 0^0–90^0–0^0 lay up. Here the top and bottom layers have the same properties, $C^{1,3}_{55} = 1.5C^{1,3}_{44} = 121.35\ GPa$ and for the middle layer shear moduli are $C^2_{44} = 1.5C^2_{55} = 121.35\ GPa$. The layer properties are interchanged in the bottom row of this figure. In these plots the top and bottom layers have the same shear moduli equal to $C^{1,3}_{44} = 1.5C^{1,3}_{55} = 121.35\ GPa$ and for the middle layer they are $C^2_{55} = 1.5C^2_{44} = 121.35\ GPa$. Hence this lay up can be identified as a 90^0–0^0–90^0 lay up. The strong influence of fiber directions on the crack opening displacement should be noted here. Like other figures here also the thin curves are obtained when interaction effects are neglected.

The surface responses to impact loads for different problem geometries are shown in Figs. 3.11 and 3.12. The peak value of the plate surface excitation load, P, is set equal to 100. τ, the duration of the impact load is taken as $\tau = 0.2$ micro seconds.

Displacements at point $A(3,0)$ of Fig. 3.1 for the two different problem geometries mentioned above, for a line load are shown in Fig. 3.11. In this case the multilayered specimen has isotropic elastic layers. The left column shows the response spectra and the right column gives time histories. The top row shows the surface displacement in absence of any crack. The second row gives displacement at the same point when the two interface cracks have a center to center distance of 3.0 mm, (problem 1), where as for the third row the center to center distance is of 6.0 mm (problem 2). In both the second and third rows two curves are drawn

in each plot. Thicker curves are the actual plots and the thin curves are obtained when the interaction effect between the two cracks is not considered properly. Thin curves are obtained by setting L and M matrices equal to zero in equation (3.17). In other words with L and M equal to zero, the presence of two cracks are considered separately, i.e. it is assumed that there is no interaction between them, and their contributions are added to get the thin curves. It can be concluded from this figure that no significant difference in surface displacements occurs if the interaction effect is ignored. This is in contradiction with the previous result for a plane wave front and the line load when the second crack is located on the path of propagation of elastic waves. There is however, a big difference between surface responses of uncracked and cracked bodies. The surface movement of relatively bigger magnitude sustains for a longer period of time, when interface crack exists. It is due to the fact that because of the presence of crack surfaces at the interface, the energy of the bottom layer cannot easily transmit into the adjoining layer, instead part of it reflects back into the layer after being reflected by the crack surfaces.

In Fig. 3.12, the top row is for the layered plate with isotropic layers and other two rows is for plates with anisotropic layers. For the middle row $C^j_{55} = 1.5C^j_{44} = 1.5\mu^j$ and bottom row is for $C^j_{44} = 1.5C^j_{55} = 1.5\mu^j$. From the figure it is evident that material anisotropy can affect the response significantly.

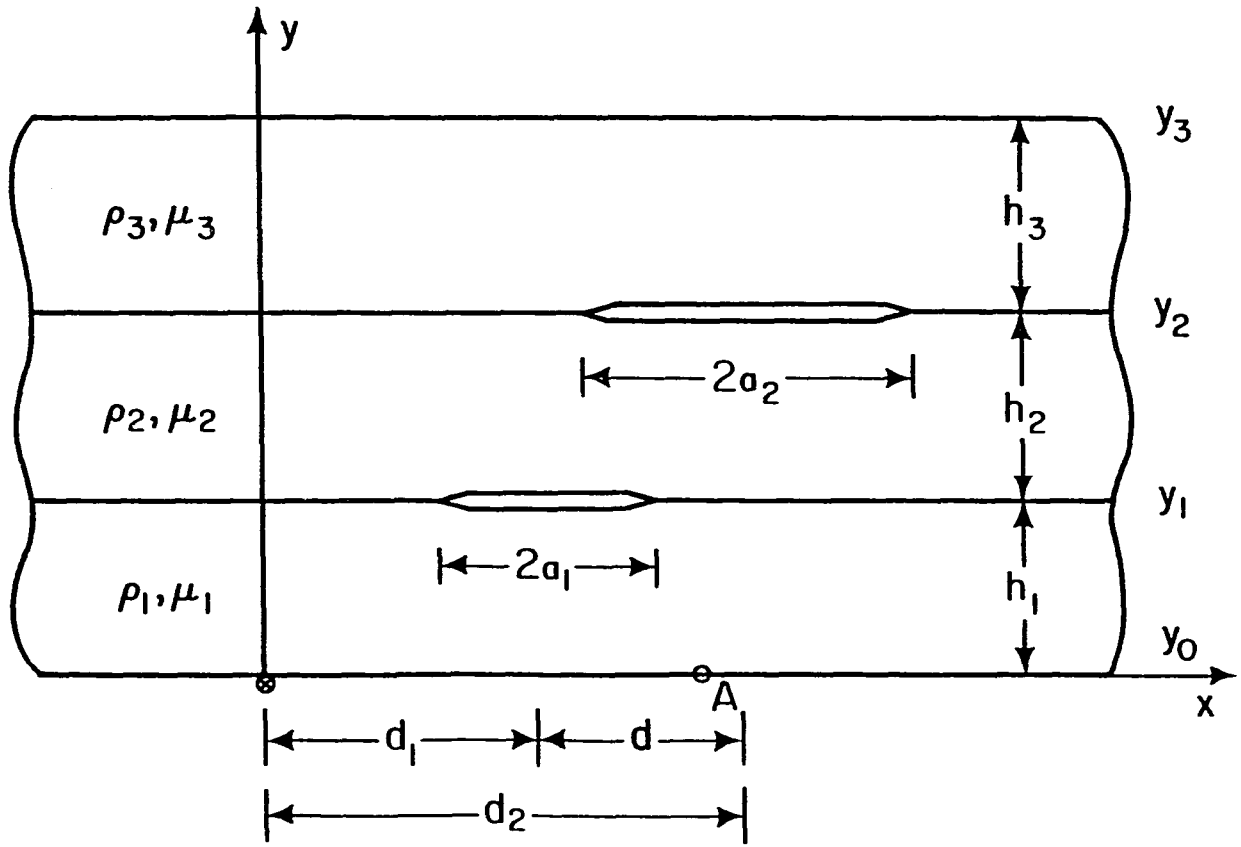

Fig. 3.1: Geometry of the problem. A three layered plate containing two interface cracks is subjected to an antiplane line load.

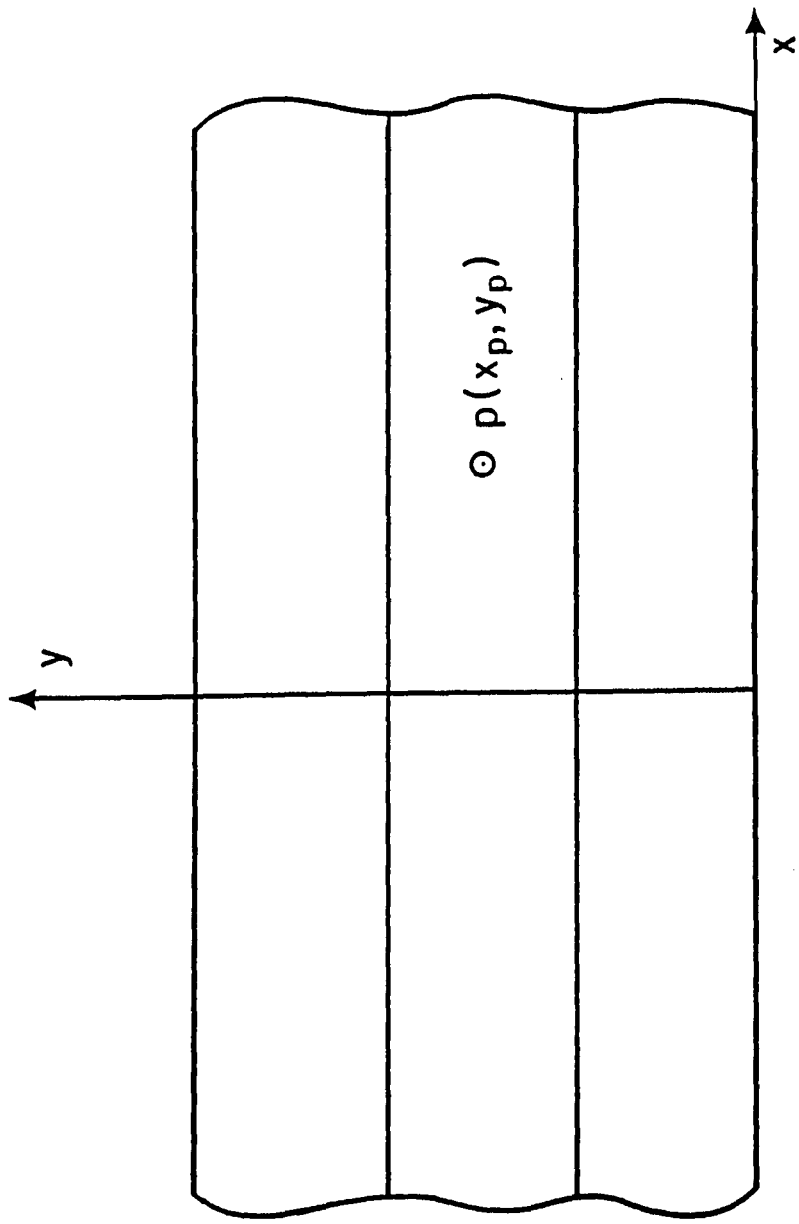

Fig. 3.2: A line load in a three layered plate.

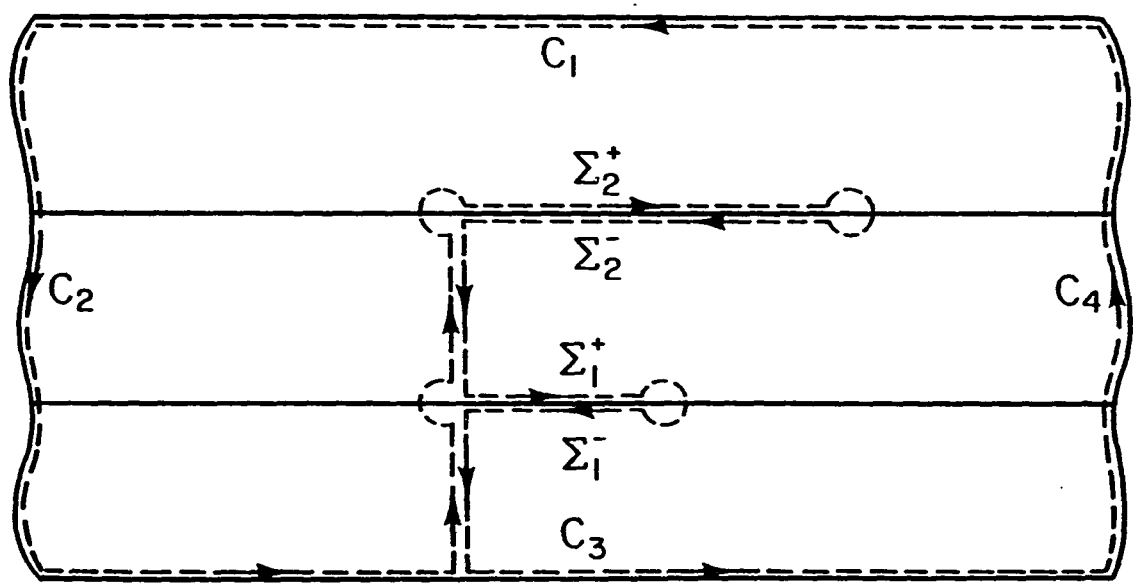

Fig. 3.3: Contour of Integration (equation 3.4).

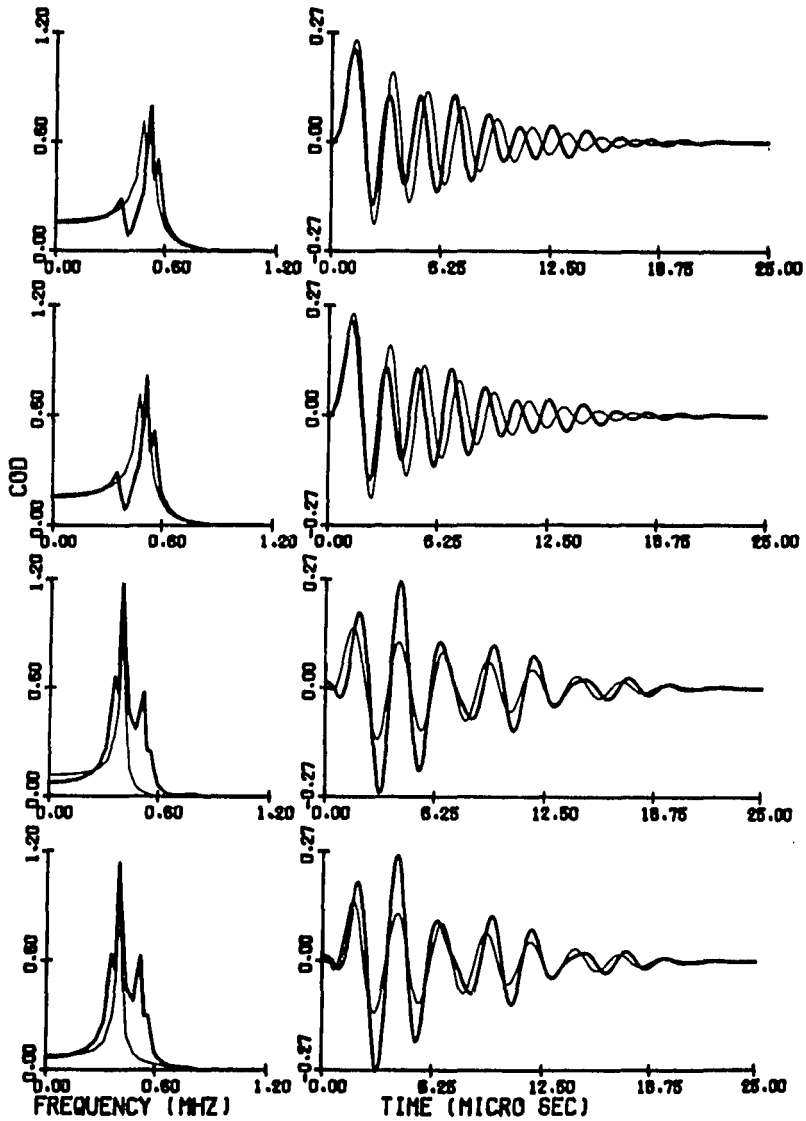

Fig. 3.4: Spectral amplitudes (left column) and time histories (right collumn) of COD in a three layered plate with isotropic layers. $1st$ and $2nd$ rows are COD of 2 mm crack at right and left quarter points respectively. $3rd$ and $4th$ rows are the same for 4 mm crack at right and left quarter points respectively. Load duration time $\tau = 2.0$ μsec.

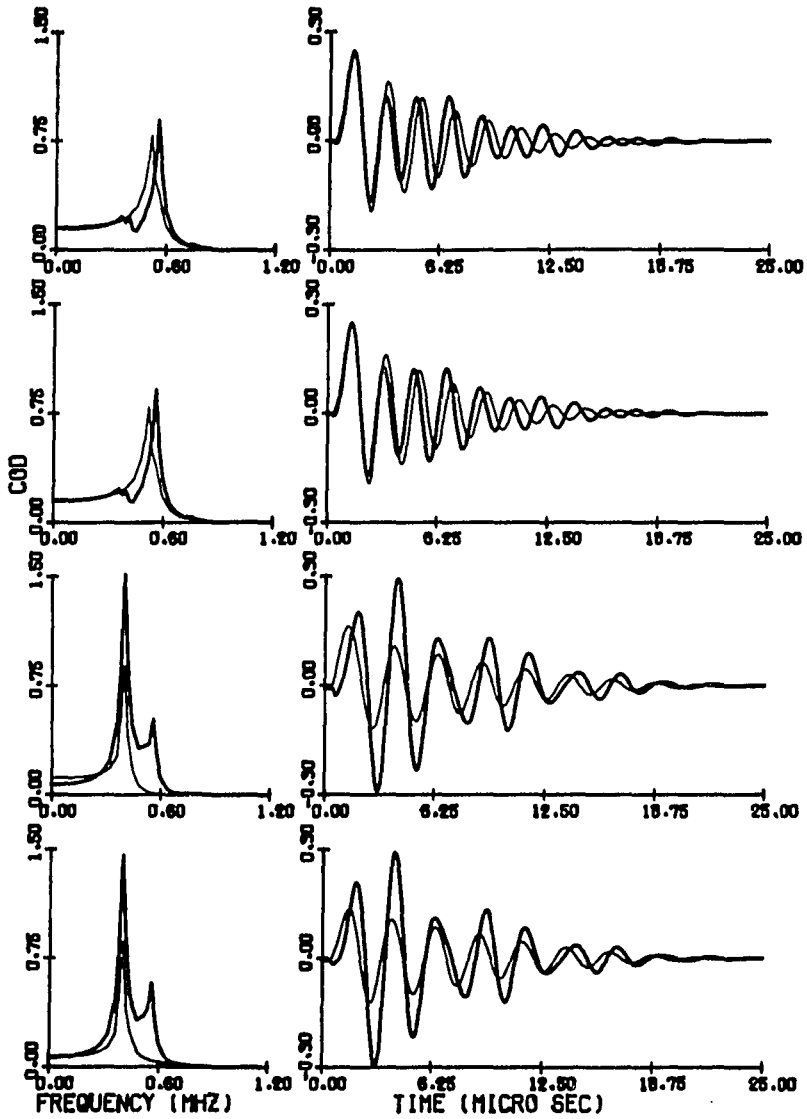

Fig. 3.5: Same as Fig. 3.4 but here layers are made of anisotropic materials for which $C_{55} = 1.5C_{44} = 1.5\mu$.

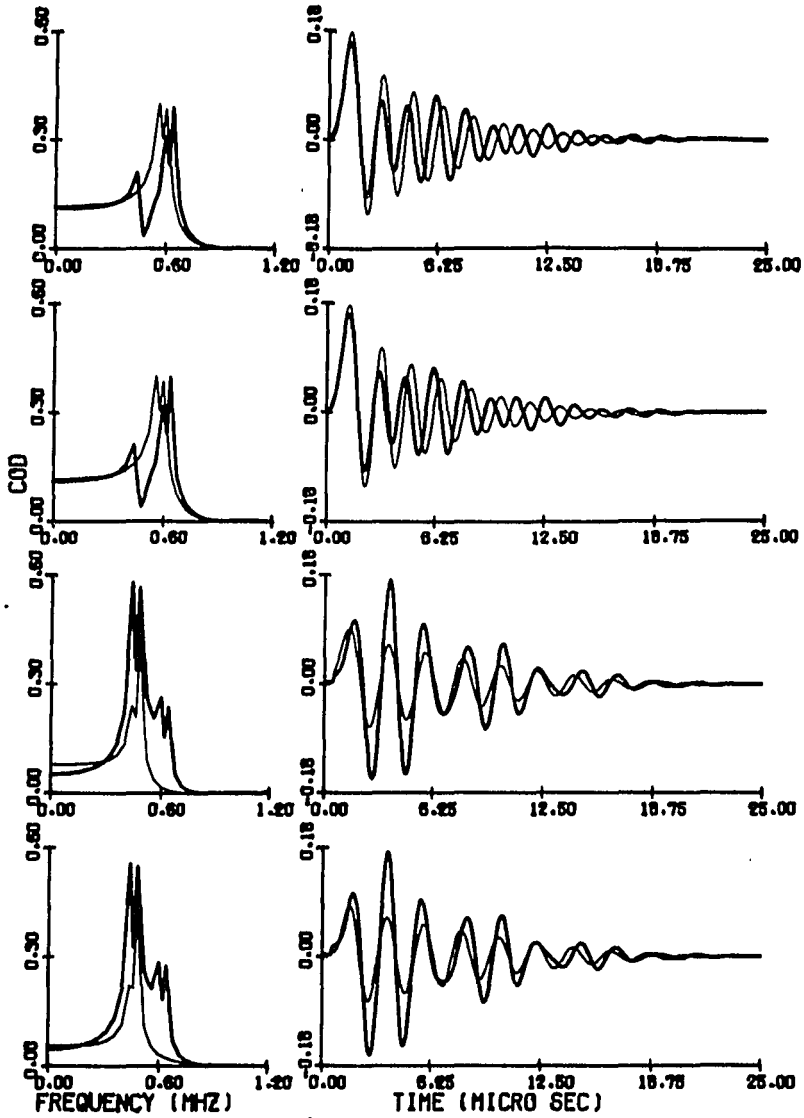

Fig. 3.6: Same as Fig. 3.4 but here $C_{44} = 1.5C_{55} = 1.5\mu$

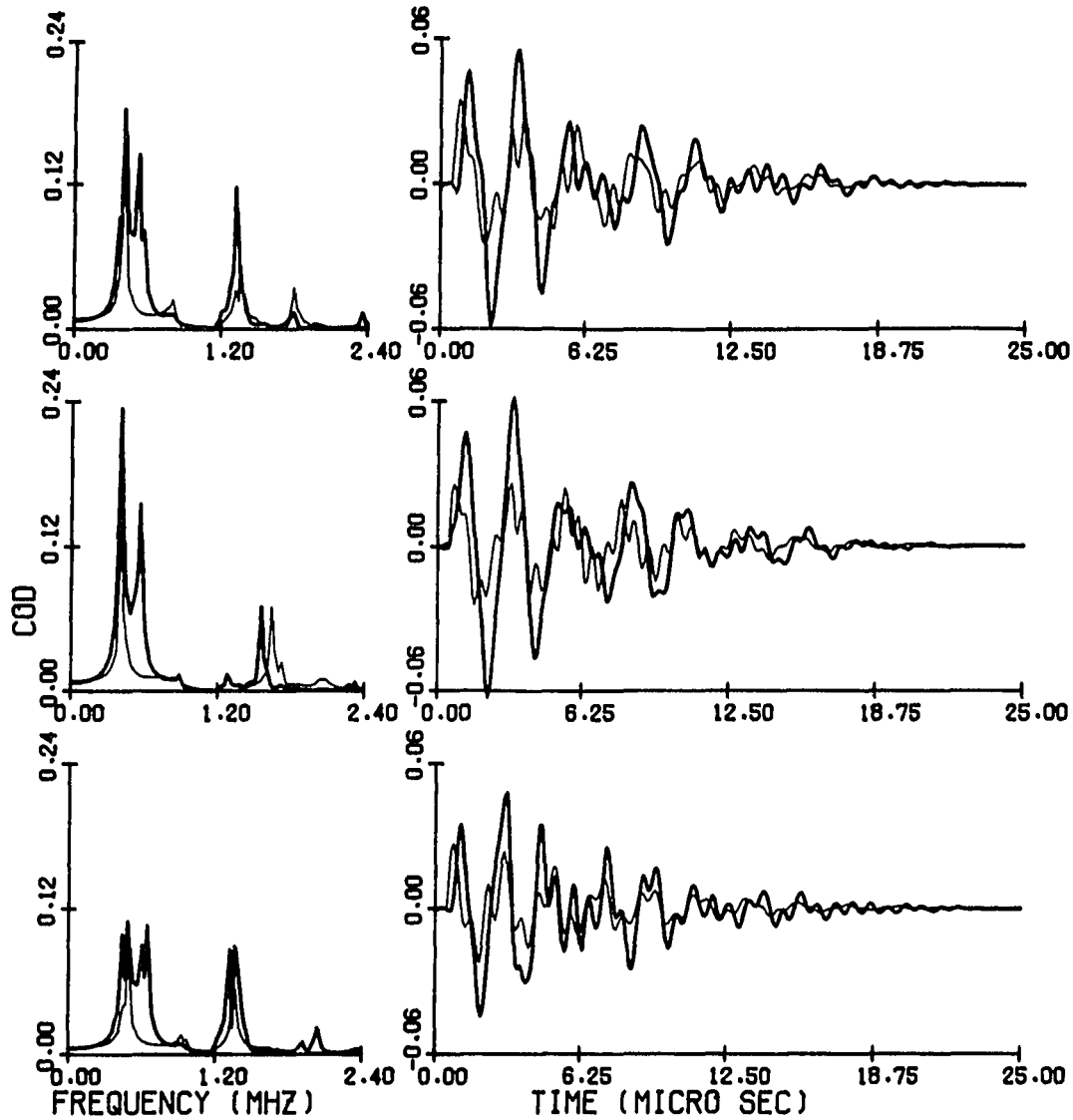

Fig. 3.7: Spectral amplitudes (left column) and time histories (right column) of COD at left quarter point of the 4 mm crack for the first problem ($d_1 = 0$, $d_2 = 0.5\ mm$). Top row is for isotropic layers ($C_{44} = C_{55} = \mu$). Middle row is for anisotropic layers with $C_{55} = 1.5C_{44} = 1.5\mu$ and the bottom row is also for anisotropic layers with $C_{44} = 1.5C_{55} = 1.5\mu$. Load duration time $\tau = 0.2\ \mu sec$.

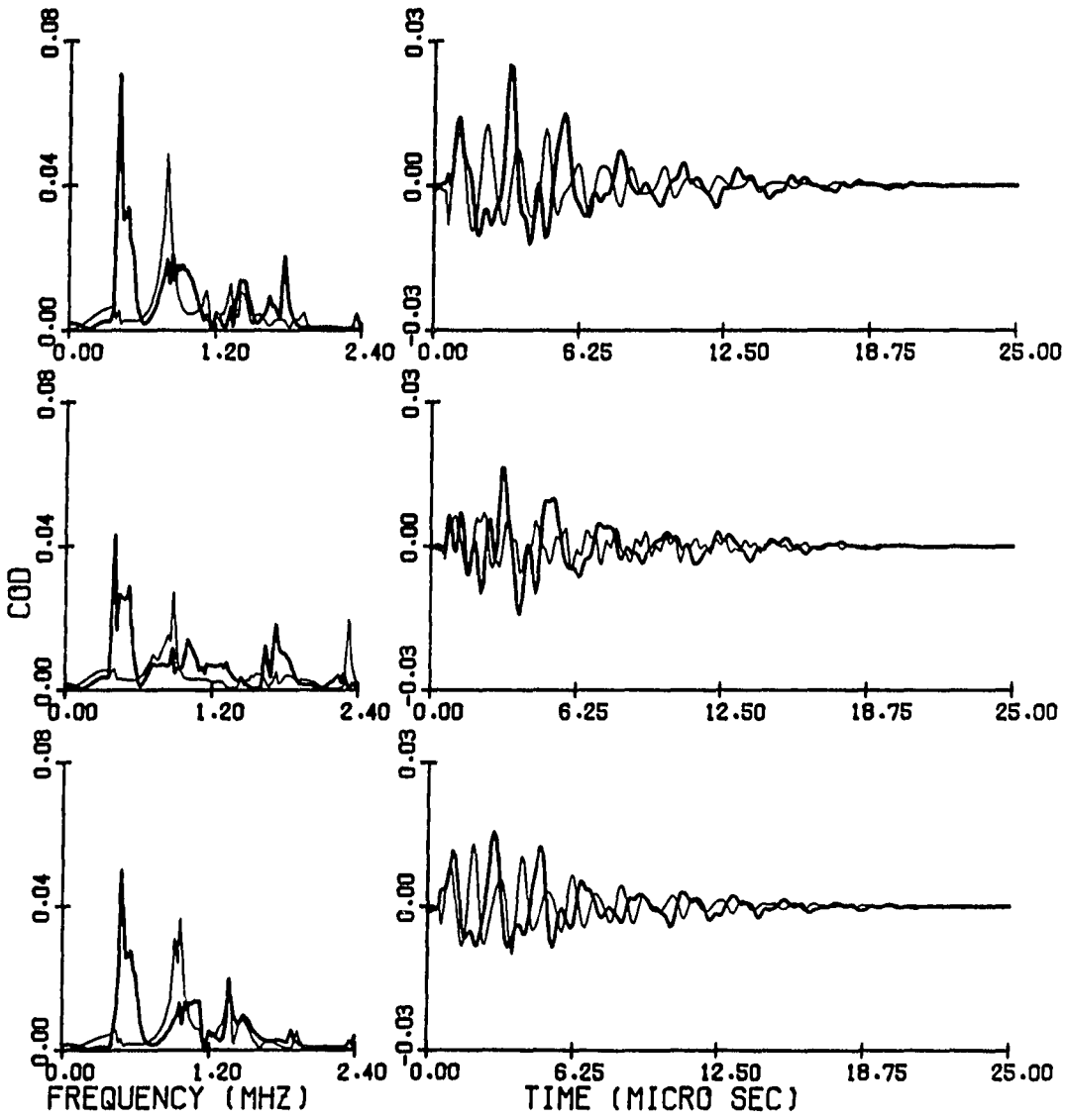

Fig. 3.8: Same as Fig. 3.7 but here $d_1 = 0.5\ mm$, $d_2 = 3.5\ mm$.

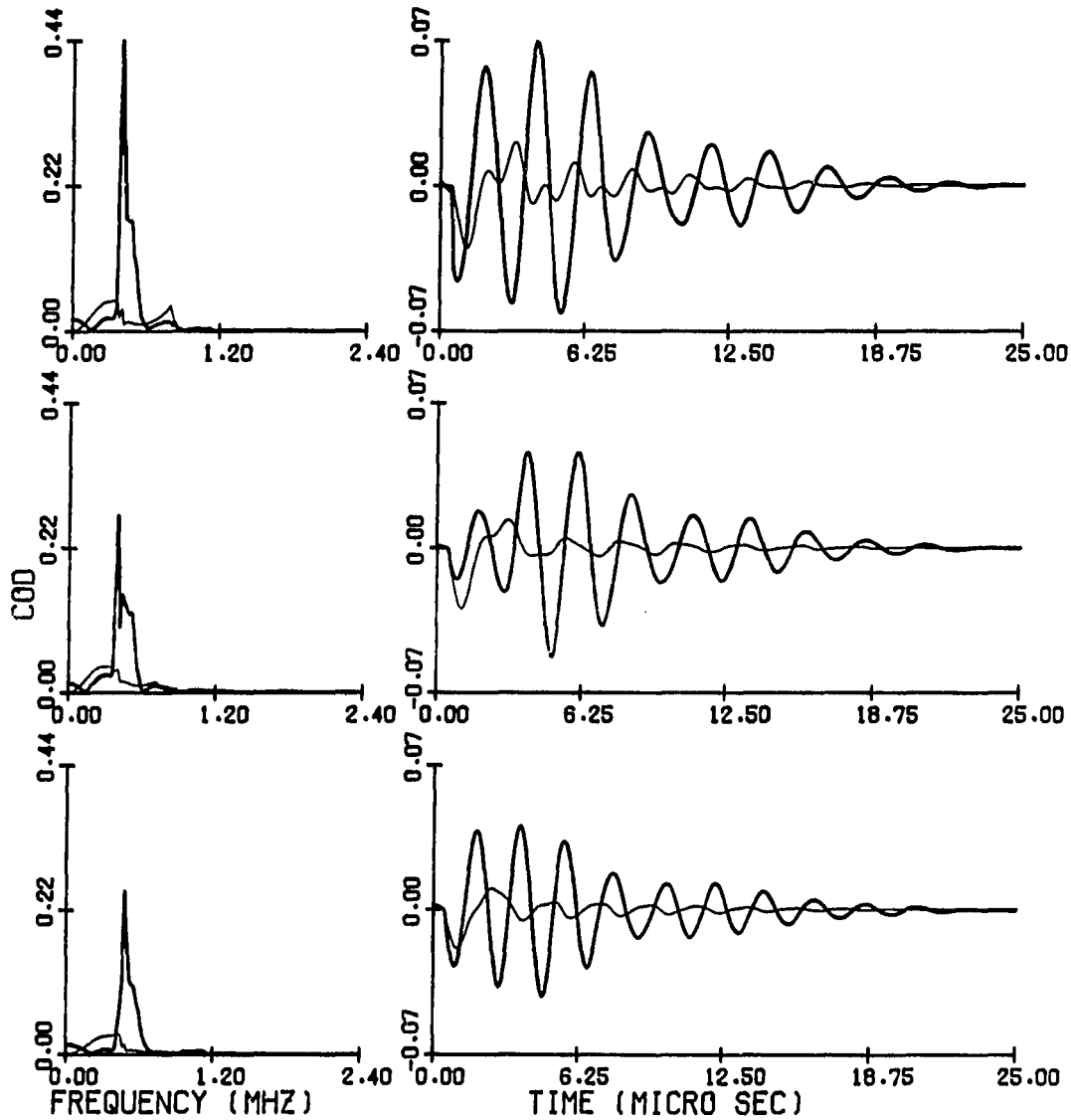

Fig. 3.9: Same as Fig. 3.7 but $\tau = 2.0$ $\mu sec.$

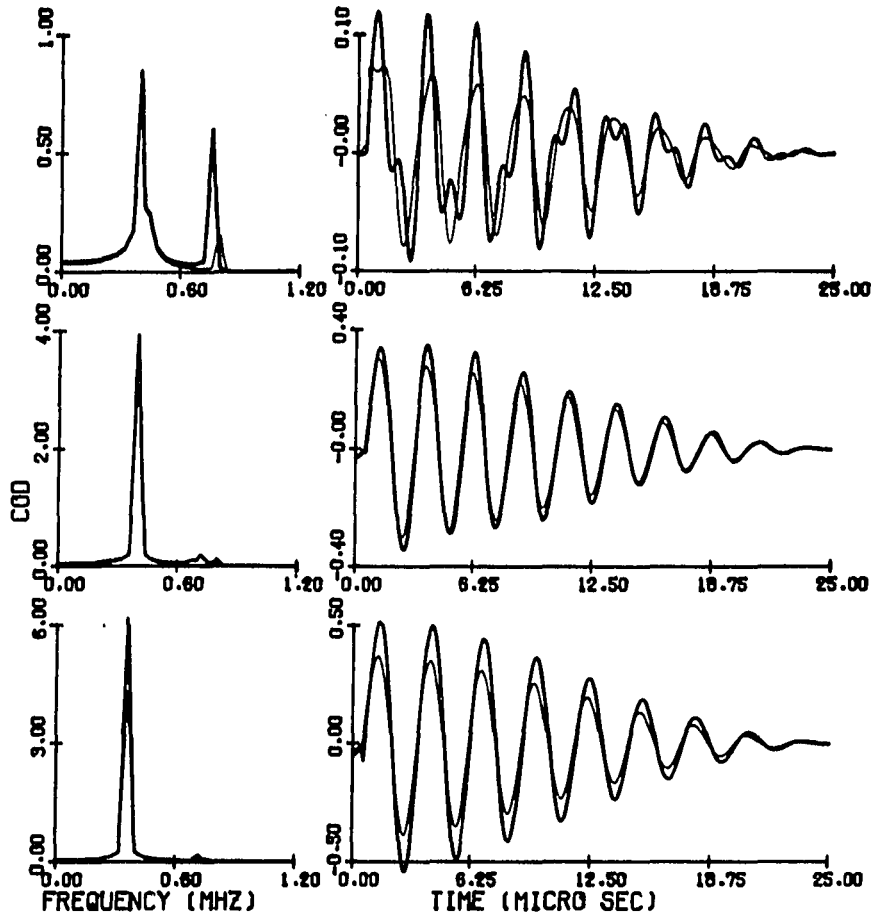

Fig. 3.10: Spectral amplitudes (left column) and time histories (right column) of the COD at the left quarter point of the 4 mm crack for the first problem geometry ($d_1 = 0$ $d_2 = 0.5$ mm) with $\tau = 2.0$ $\mu sec.$ The top row is for a homogeneous anisotropic plate with $C_{55} = 1.5C_{44} = 121.35$ $GPa.$ The middle row is for a 0^0–90^0–0^0 lay up - top and bottom layers have shear moduli equal to $C_{55} = 1.5C_{44} = 121.35$ GPa and for the middle layer they are $C_{44} = 1.5C_{55} = 121.35$ $GPa.$ When the layer properties are interchanged plots of the bottom row are obtained for 90^0–0^0–90^0 lay ups. Thin curves are computed by neglecting the interaction effect.

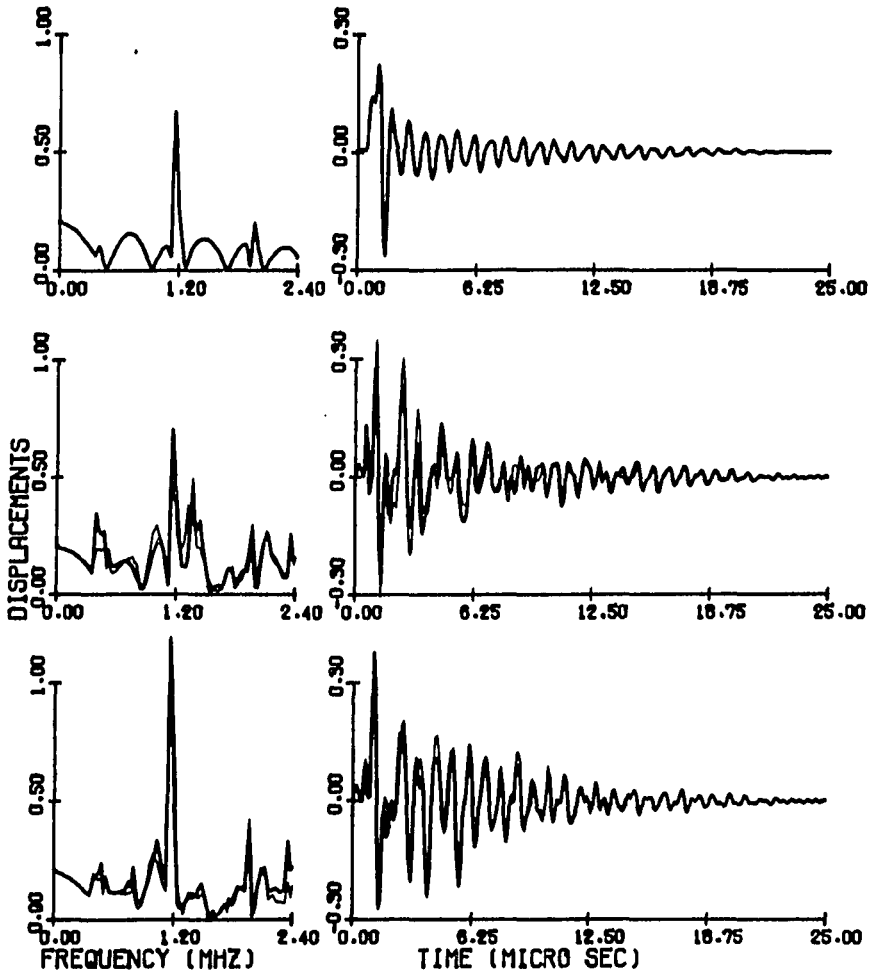

Fig. 3.11: Surface displacement in a three layered orthotropic plate at A(3,0). The plate is excited by a line load with pulse duration $\tau = 0.2\mu sec$. The top row shows the surface displacement without any crack. The middle row gives surface displacement when two interface cracks have center to center distance of 3 mm and the bottom row is same as middle row but here the distance between the crack centers is 6 mm. In middle and bottom rows bold curves give actual displacements and thin curves give uncoupled displacements (neglecting interaction effect). Left column: Spectral amplitude of displacement in $mm - \mu sec$. Right column: Time histories in mm.

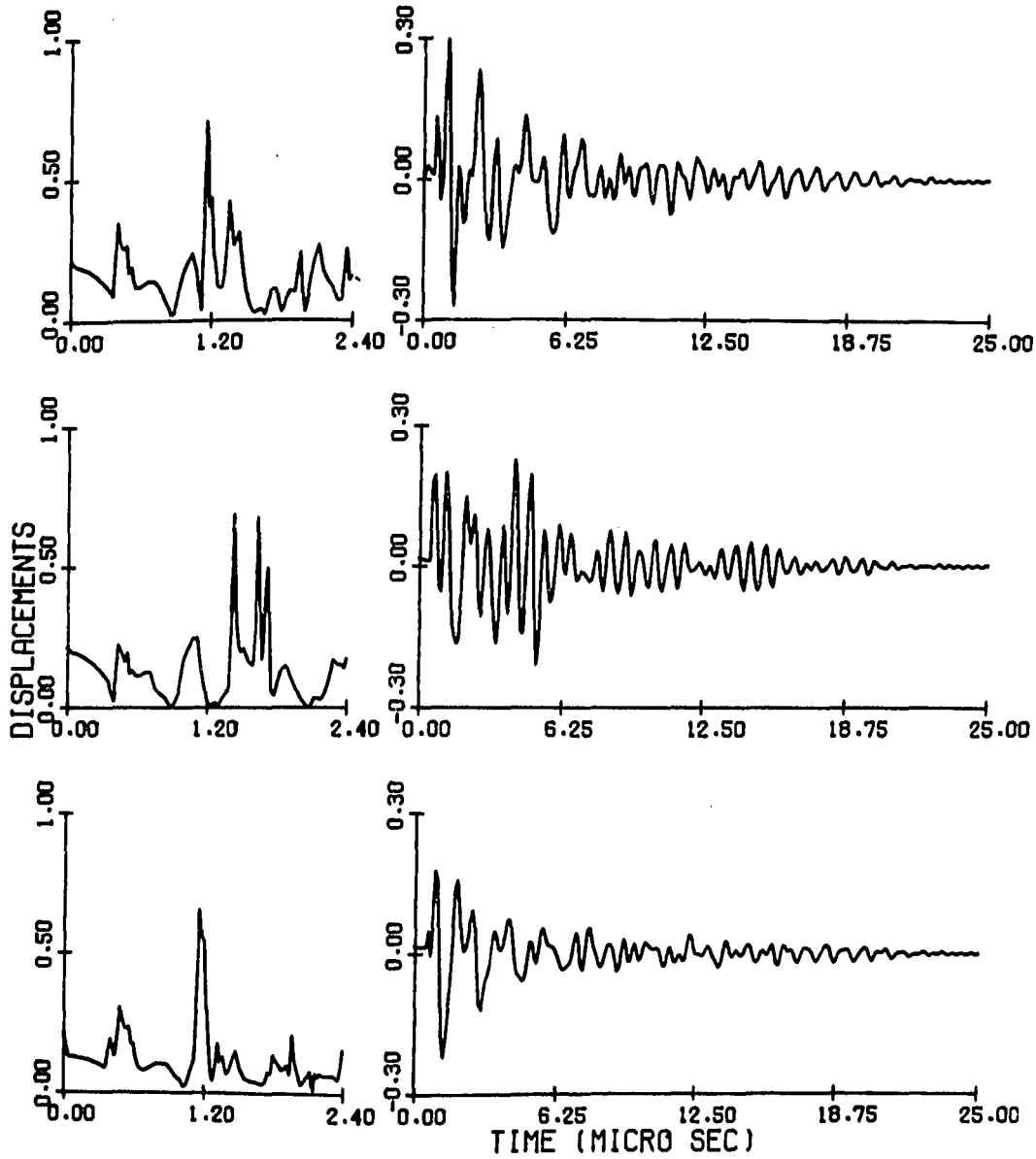

Fig. 3.12: Spectral amplitudes (left column) and time histories (right column) of displacement at A(3,0). Top row is for isotropic layers ($C_{44} = C_{55} = \mu$). Middle row is for anisotropic layers with ($C_{55} = 1.5C_{44} = 1.5\mu$) and the bottom row is for anisotropic layers with ($C_{44} = 1.5C_{55} = 1.5\mu$).

CHAPTER–4

RESPONSE OF AN ORTHOTROPIC HALF-SPACE WITH A SUBSURFACE CRACK: IN–PLANE CASE

Scattering of elastic waves by a subsurface crack in an orthotropic half space subjected to a surface line load with an arbitrary angle of inclination is analyzed in this chapter. Green's functions are developed and used along with the representation theorem to reduce the problem to a set of simultaneous singular integral equations in the Fourier transformed domain. Solution of these equations is then obtained by expanding the unknown crack opening displacement (COD) in terms of Chebychev polynomials. Numerical results are given for specific examples involving orthotropic materials.

4.1 PROBLEM FORMULATION

A homogeneous, orthotropic, linearly elastic solid, which occupies the half-plane $y > 0$, contains a subsurface crack parallel to the free surface as shown in Fig. 4.1. The crack with traction free surfaces having a length of $2a$ is located at a depth h. The incident line load, $T = \delta(x)f(t)$ is applied at the origin at an angle of inclination θ as shown in the figure.

To solve this problem we need to solve two fundamental problems–1) a flawless half-space subjected to a line load at the boundary and 2) the Green's functions corresponding to two unit loads in x and y-directions respectively. Representation theorem is then used along with the Green's functions to obtain the scattered displacement field.

4.1.1 Flawless Half-Space Subjected to a Line Load at the Boundary

The geometry of this problem is similar to that shown in Fig. 4.1, the only difference

is that there is no crack. The time harmonic inplane stress field of time dependence $e^{-i\omega t}$ acts as a line load at an angle of inclination θ at the origin.

Constitutive equations of the material can be written in the tensorial notation as

$$\sigma_k = C_{kj}\epsilon_j \qquad (k,j = 1,2,6) \tag{4.1}$$

where repeated subscript indicate summation and C_{kj} is the stiffness tensor. For orthotropic materials C_{16}, C_{26}, C_{61} and C_{62} are equal to zero. The engineering strains, ϵ_j, in equation (4.1) are defined by

$$\epsilon_1 = u_{,x}\,, \quad \epsilon_2 = v_{,y}\,, \quad \epsilon_6 = u_{,y} + v_{,x} \tag{4.2}$$

where u and v are displacement components in x and y directions respectively and comma (,) indicates partial derivative. Equations of motion of the problem are given by

$$C_{11}u_{,xx} + C_{66}u_{,yy} + (C_{12} + C_{66})v_{,xy} = \rho u_{,tt} \tag{4.3a}$$

$$C_{22}v_{,yy} + C_{66}v_{,xx} + (C_{12} + C_{66})u_{,xy} = \rho v_{,tt} \tag{4.3b}$$

where ρ is the density of the elastic material.

Solutions of these coupled equations in the Fourier transformed domain (ω) can be written as

$$U(x,y) = \frac{1}{2\pi}\int_{-\infty}^{\infty} A_j e^{p_j y + ikx} dk \qquad (j = 1,2) \tag{4.4a}$$

$$V(x,y) = \frac{1}{2\pi}\int_{-\infty}^{\infty} A_j S_j e^{p_j y + ikx} dk \qquad (j = 1,2) \tag{4.4b}$$

where p_j is the j-th root with negative real part and/or positive imaginary part of the following equation

$$\begin{aligned} C_{22}C_{66}p^4 + p^2(k^2C_{12}^2 + 2C_{12}C_{66}k^2 + C_{22}\rho\omega^2 - k^2C_{11}C_{22} + C_{66}\rho\omega^2) \\ + (\rho^2\omega^4 - k^2C_{66}\rho\omega^2 - k^2C_{11}\rho\omega^2 + k^4C_{11}C_{66}) = 0 \end{aligned} \tag{4.5}$$

Roots with positive real part and/or negative imaginary part are ruled out by the radiation conditions. This gurantees that stress field will decay as one moves away from the source and there will not be a upward propagating wave since there is no reflecting boundary below $y = 0$ line. A_j are the unknown functions of k and ω to be determined by using boundary conditions and are given in the Appendix-D, and

$$S_j = \frac{k^2 C_{11} - p_j^2 C_{66} - \rho\omega^2}{ikp_j(C_{12} + C_{66})} \quad \text{(no summation on j)} \tag{4.6}$$

Equations (4.5) and (4.6) are obtained by taking Fourier transform of equation (4.4) with respect to x and substituting in equation (4.3) after taking Fourier transform of it with respect to x and t.

4.1.2 Green's Function: A Line Load in a Flawless Half-Space

A number of Green's functions are available in literature [Xu and Mal (1988) and references there in] for isotropic materials, in terms of displacement potentials. But none of these can be used for orthotropic materials directly. So in this section two new Green's functions are developed, for unit loads in the x and y-directions.

The geometry of this problem is shown in Fig. 4.2. A time harmonic line load is acting at a point $P(x_p, y_p)$ as shown in the figure. Unit loads along x and y-directions can be considered as a body force that can be written in terms of a delta functions, $\delta(x - x_p, y - y_p, t)$. The equations of motion for this problem should be same as equations (4.3), with the additional body force term in equation (4.3a) for a unit load in the x-direction and in (4.3b) for a unit load in the y-direction. These equations of motion can be interpreted as having the same form as equation (4.3) for $y \neq y_p$ and an additional unit stress jump across the $y = y_p$ plane. The

solution of these equation can be obtained by modifying the displacement field in equation (4.4) to satisfy the stress jump condition and can be written as

$$U_\alpha^G(x,y) = \frac{1}{2\pi}\int_{-\infty}^{\infty}\left\{B_\alpha^{\pm}e^{p_1|y-y_p|} + C_\alpha^{\pm}e^{p_2|y-y_p|} + D_j^\alpha e^{p_j y}\right\}e^{ik(x-x_p)}dk \quad (4.7a)$$

$$\alpha, j = 1,2$$

$$V_\alpha^G(x,y) = \frac{1}{2\pi}\int_{-\infty}^{\infty}\left\{B_\alpha^{\pm}S_1^{\pm}e^{p_1|y-y_p|} + C_\alpha^{\pm}S_2^{\pm}e^{p_2|y-y_p|} + D_j^\alpha S_j e^{p_j y}\right\}e^{ik(x-x_p)}dk \quad (4.7b)$$

where $\alpha = 1$ for a unit load in the x-direction and 2 for a unit load in the y-direction and

$$\begin{aligned} S_j^{\pm} &= \pm S_j \quad j = 1,2 \\ B_1^{\pm} &= -\frac{p_1 p_2 a_1 (C_{12}+C_{66})}{2C_{66}(a_1 a_6 - a_2 a_5)} \\ C_1^{\pm} &= \frac{p_1 p_2 a_2 (C_{12}+C_{66})}{2C_{66}(a_1 a_6 - a_2 a_5)} \\ B_2^{\pm} &= C_2^{\mp} = \mp\frac{a_4}{2a_3} \end{aligned} \quad (4.8)$$

with "+" for $y > y_p$ and "−" for $y < y_p$. Expressions for a_1 through a_6 are given in the Appendix-D. $B_\alpha^{\pm}$, $C_\alpha^{\pm}$ are obtained by using the fact that for a unit load in the x-direction there will be a unit jump in σ_6^G while U^G, V^G and σ_2^G are continuous across $y = y_p$ plane, similarly, for a unit load in the y-direction there will be a jump in σ_2^G while U^G, V^G and σ_6^G are continuous. These conditions give rise to two sets of equations, each having four unknowns, which are then solved to obtain $B_\alpha^{\pm}$, $C_\alpha^{\pm}$. Constants D_j^α $(\alpha, j = 1,2)$ can be obtained from the boundary conditions and are given in the Appendix-D. Superscript G in U, V and σ indicates that displacements and stresses correspond to the Green's functions.

4.2 APPLICATION OF REPRESENTATION THEOREM

The displacement field due to a dislocation along a fault plane is given by the representation theorem (Knopoff, 1956; de Hoop, 1958; Mal, 1972)

$$U_k(x,y) = \int_S [U_i(\xi,\eta)]^+_- T^k_{ij}(\xi,\eta;x,y) n_j dS(\xi,\eta) \tag{4.9}$$

where,

$U_k(x,y)$ = displacement in k-direction at position (x,y)

$[U_i(\xi,\eta)]^+_-$ = displacement jump across the fault plane at (ξ,η)

$T^k_{ij}(\xi,\eta;x,y)$ = ij-component of stress at (ξ,η) due to a unit force applied in the k-direction at (x,y)

n_j = j-component of the unit normal vector to the fault plane at (ξ,η)

$dS(\xi,\eta)$ = elemental fault area

Starting with equation (4.9), after some simplifications, one can obtain the scattered displacement field, $U^s_\alpha(x_p,y_p)$, in the form

$$U^s_\alpha(x_p,y_p) = \int_{d-a}^{d+a} [\phi(x-d)\sigma^\alpha_6 \mid_{y=h} + \psi(x-d)\sigma^\alpha_2 \mid_{y=h}] dx \quad (\alpha = 1,2) \tag{4.10}$$

where σ^α_2, σ^α_6 are the stress fields corresponding to a unit load acting in the α-direction; in other words they are stress fields corresponding to the Green's functions obtained from (4.7a) and (4.7b). $\phi(x-d)$ and $\psi(x-d)$ are crack opening displacements (COD) along x and y-directions respectively and are defined as

$$\begin{aligned} \phi(x-d) &= U(x-d,h^+) - U(x-d,h^-) \\ \psi(x-d) &= V(x-d,h^+) - V(x-d,h^-) \end{aligned} \tag{4.11}$$

Taking Fourier transform of equation (4.1) with respect to t one can express the stress fields due to unit loads as the following

$$\begin{aligned} \sigma^\alpha_2 &= C_{21} U^G_{\alpha,x} + C_{22} V^G_{\alpha,y} \\ \sigma^\alpha_6 &= C_{66} U^G_{\alpha,y} + C_{66} V^G_{\alpha,x} \end{aligned} \tag{4.12}$$

Substituting the values of U_α^G and V_α^G from equation (4.7) we get

$$\begin{aligned}
\sigma_6^1 &= \frac{1}{2\pi}\int_{-\infty}^{\infty} F_1(k)e^{ik(x-x_p)}dk \\
\sigma_2^1 &= \frac{1}{2\pi}\int_{-\infty}^{\infty} F_2(k)e^{ik(x-x_p)}dk \\
\sigma_6^2 &= \frac{1}{2\pi}\int_{-\infty}^{\infty} F_3(k)e^{ik(x-x_p)}dk \\
\sigma_2^2 &= \frac{1}{2\pi}\int_{-\infty}^{\infty} F_4(k)e^{ik(x-x_p)}dk
\end{aligned} \tag{4.13}$$

where the functions $F_j(k)$ $(j = 1, 2, 3, 4)$, are given in the Appendix-D.

Combining equations (4.13) and (4.10), after some simplifications one can write

$$\begin{aligned}
U^s(x_p, y_p) = &\frac{1}{2\pi}\int_{d-a}^{d+a}\phi(x-d)\int_{-\infty}^{\infty} F_1(k)|_{y=h}e^{ik(x-x_p)}dkdx \\
&+\frac{1}{2\pi}\int_{d-a}^{d+a}\psi(x-d)\int_{-\infty}^{\infty} F_2(k)|_{y=h}e^{ik(x-x_p)}dkdx
\end{aligned} \tag{4.14a}$$

$$\begin{aligned}
V^s(x_p, y_p) = &\frac{1}{2\pi}\int_{d-a}^{d+a}\phi(x-d)\int_{-\infty}^{\infty} F_3(k)|_{y=h}e^{ik(x-x_p)}dkdx \\
&+\frac{1}{2\pi}\int_{d-a}^{d+a}\psi(x-d)\int_{-\infty}^{\infty} F_4(k)|_{y=h}e^{ik(x-x_p)}dkdx
\end{aligned} \tag{4.14b}$$

The scattered stress field can be obtained from the displacement field of equation (4.14). To satisfy the stress free boundary conditions this stress field should be equal to the negative of the incident stress field that can be obtained from equation

(4.4), hence

$$
\begin{aligned}
&-iC_{21}\int_{-\infty}^{\infty} kF_1(k)|_{y=y_p=h}\int_{-a}^{a}\phi(x)e^{ik(x-x_p)+ikd}dxdk\\
&-iC_{21}\int_{-\infty}^{\infty} kF_2(k)|_{y=y_p=h}\int_{-a}^{a}\psi(x)e^{ik(x-x_p)+ikd}dxdk\\
&+C_{22}\int_{-\infty}^{\infty} \frac{\partial F_3(k)}{\partial y_p}|_{y=y_p=h}\int_{-a}^{a}\phi(x)e^{ik(x-x_p)+ikd}dxdk\\
&+C_{22}\int_{-\infty}^{\infty} \frac{\partial F_4(k)}{\partial y_p}|_{y=y_p=h}\int_{-a}^{a}\psi(x)e^{ik(x-x_p)+ikd}dxdk\\
&=-\int_{-\infty}^{\infty}\{A_1(ikC_{21}+C_{22}S_1p_1)e^{p_1h}\\
&\qquad +A_2(ikC_{21}+C_{22}S_2p_2)e^{p_2h}\}e^{kx_p}dk
\end{aligned}
\tag{4.15a}
$$

$$
\begin{aligned}
&C_{66}\int_{-\infty}^{\infty} \frac{\partial F_1(k)}{\partial y_p}|_{y=y_p=h}\int_{-a}^{a}\phi(x)e^{ik(x-x_p)+ikd}dxdk\\
&+C_{66}\int_{-\infty}^{\infty} \frac{\partial F_2(k)}{\partial y_p}|_{y=y_p=h}\int_{-a}^{a}\psi(x)e^{ik(x-x_p)+ikd}dxdk\\
&-iC_{66}\int_{-\infty}^{\infty} kF_3(k)|_{y=y_p=h}\int_{-a}^{a}\phi(x)e^{ik(x-x_p)+ikd}dxdk\\
&-iC_{66}\int_{-\infty}^{\infty} kF_4(k)|_{y=y_p=h}\int_{-a}^{a}\psi(x)e^{ik(x-x_p)+ikd}dxdk\\
&=-\int_{-\infty}^{\infty}\{A_1C_{66}(p_1+ikS_1)e^{p_1h}\\
&\qquad +A_2C_{66}(p_2+ikS_2)e^{p_2h}\}e^{kx_p}dk
\end{aligned}
\tag{4.15b}
$$

In the above equations the only unknowns are the crack opening displacements ϕ and ψ, which are obtained in the next section.

4.2.1 Computation of the Crack Opening Displacement Functions

In order to evaluate the crack opening displacements, $\phi(x)$ and $\psi(x)$ are expanded in a complete set of Chebyshev polynomials, as in equation (2.16) with $a_1 = a_2 = a$. To obtain the unknown coefficients α_n and γ_n, both sides of equation (4.15a) are multiplied by $\phi_m(x_p)$, then integrated from $x_p = -a$ to $x_p = a$ and both

sides of equation (4.15b) are multiplied by $\psi_m(x_p)$, then integrated from $x_p = -a$ to $x_p = a$. After some algebraic manipulation an infinite set of linear equations is obtained to be solved for α_n and γ_n,

$$\begin{aligned} \sum_{n=1}^{\infty}(K_{mn}\alpha_n + L_{mn}\gamma_n) &= f_1(k) \\ \sum_{n=1}^{\infty}(M_{mn}\alpha_n + N_{mn}\gamma_n) &= f_2(k) \end{aligned} \tag{4.18}$$

where

$$\begin{aligned} f_1(k) &= l_m \int_{-\infty}^{\infty} \{A_1(ikC_{21} + C_{22}S_1p_1)e^{p_1h} \\ &\qquad + A_2(ikC_{21} + C_{22}S_2p_2)e^{p_2h}\}\frac{J_m(ka)}{k}e^{ikd}dk \\ f_2(k) &= l_m \int_{-\infty}^{\infty} \{A_1C_{66}(p_1 + ikS_1)e^{p_1h} \\ &\qquad + A_2C_{66}(p_2 + ikS_2)e^{p_2h}\}\frac{J_m(ka)}{k}e^{ikd}dk \end{aligned} \tag{4.19}$$

$$\begin{aligned} K_{mn} &= \int_{-\infty}^{\infty}\left[-C_{21}i\pi\frac{F_1(k)}{k}|_{y=y_p=h} + \frac{\pi}{k^2}C_{22}\frac{\partial F_3(k)}{\partial y_p}|_{y=y_p=h}\right]J_m(ka)J_n(ka)dk \\ L_{mn} &= \int_{-\infty}^{\infty}\left[-C_{21}i\pi\frac{F_2(k)}{k}|_{y=y_p=h} + \frac{\pi}{k^2}C_{22}\frac{\partial F_4(k)}{\partial y_p}|_{y=y_p=h}\right]J_m(ka)J_n(ka)dk \\ M_{mn} &= \int_{-\infty}^{\infty}\left[C_{66}\frac{\pi}{k^2}\frac{\partial F_1(k)}{\partial y_p}|_{y=y_p=h} - C_{66}i\pi\frac{F_3(k)}{k}|_{y=y_p=h}\right]J_m(ka)J_n(ka)dk \\ N_{mn} &= \int_{-\infty}^{\infty}\left[C_{66}\frac{\pi}{k^2}\frac{\partial F_2(k)}{\partial y_p}|_{y=y_p=h} - C_{66}i\pi\frac{F_4(k)}{k}|_{y=y_p=h}\right]J_m(ka)J_n(ka)dk \end{aligned} \tag{4.20}$$

and J_m is the Bessel function of first kind of order m, and

$$l_m = \begin{cases} \mathrm{i} & \texttt{for odd } m \\ -\mathrm{i} & \texttt{for even } m \end{cases}$$

Matrices K, L, M and N are all symmetric. In addition when $(m+n)$ is even $K_{mn} = N_{mn} = 0$ and when $(m+n)$ is odd $L_{mn} = M_{mn} = 0$.

Equations (4.18) have infinite series in their expressions, however, they can be terminated after a finite number of terms without introducing any significant

error [Kundu (1985)]. Then α_n, γ_n can be obtained from a finite set of linear equations.

4.2.2 Computation of Surface Displacement

The total displacement U_α is given by

$$U_\alpha = U_\alpha^i + U_\alpha^s \quad (\alpha = 1, 2) \tag{4.21}$$

in which U_α^i is the total field, in absence of any crack, given by equation (4.4), where as the scattered field U_α^s, represents the change in U_α^i due to the presence of the crack. U_α^s is given by equation (4.14). After some mathematical simplification one can write the displacement components U and V of any surface point $P(x_p, 0)$ in the following manner

$$U^i(x_p, 0) = \frac{1}{2\pi} \int_{-\infty}^{\infty} (A_1 + A_2) e^{ikx_p} dk \tag{4.22a}$$

$$V^i(x_p, 0) = \frac{1}{2\pi} \int_{-\infty}^{\infty} A_j S_j e^{ikx_p} dk \qquad (j = 1, 2) \tag{4.22b}$$

and

$$\begin{aligned} U^s(x_p, 0) = i &\int_0^\infty \frac{F_1(k)}{k} \cos(kd - kx_p) \sum_{n=odd}^{\infty} \{\alpha_n J_n(ka)\}\, dk \\ &- \int_0^\infty \frac{F_1(k)}{k} \sin(kd - kx_p) \sum_{n=even}^{\infty} \{\alpha_n J_n(ka)\}\, dk \\ &- \int_0^\infty \frac{F_2(k)}{k} \sin(kd - kx_p) \sum_{n=odd}^{\infty} \{\gamma_n J_n(ka)\}\, dk \\ &+ i \int_0^\infty \frac{F_2(k)}{k} \cos(kd - kx_p) \sum_{n=even}^{\infty} \{\gamma_n J_n(ka)\}\, dk \end{aligned} \tag{4.23a}$$

$$
\begin{aligned}
V^s(x_p,0) = &-\int_0^\infty \frac{F_3(k)}{k}\sin(kd-kx_p)\sum_{n=odd}^{\infty}\{\alpha_n J_n(ka)\}\,dk \\
&+i\int_0^\infty \frac{F_3(k)}{k}\cos(kd-kx_p)\sum_{n=even}^{\infty}\{\alpha_n J_n(ka)\}\,dk \\
&+i\int_0^\infty \frac{F_4(k)}{k}\cos(kd-kx_p)\sum_{n=odd}^{\infty}\{\gamma_n J_n(ka)\}\,dk \\
&-\int_0^\infty \frac{F_4(k)}{k}\sin(kd-kx_p)\sum_{n=even}^{\infty}\{\gamma_n J_n(ka)\}\,dk
\end{aligned}
\tag{4.23b}
$$

then equations (4.22) and (4.23) are added to obtain the total surface displacement.

4.3 RESULTS

The method discussed above has been implemented in a FORTRAN program. Results are given for a Graphite-Epoxy composite specimen which is used widely in the aircraft industry. Response of the cracked half-space to different impact loadings are shown in Figs. 4.3 through 4.8. The time dependence of the applied load is given in chapter 2 (see equation 2.40). Results are given for $\tau = 2$ micro second and P equal to 10. The following material properties of the Graphite-Epoxy composite [Kuo (1984a)] are used for all subsequent analyses.

$$
\begin{aligned}
C_{11} &= 138.4408 \text{ GPa} \\
C_{22} &= 14.5365 \text{ GPa} \\
C_{12} &= 3.0530 \text{ GPa} \\
C_{66} &= 5.8565 \text{ GPa} \\
\rho &= 7.44 \text{ gm/cm}^3
\end{aligned}
\tag{4.24}
$$

For the sample problem considered here, the half crack length is taken as 1 mm, depth of crack h is taken as 0.5 mm and distance of crack center from the point of application of load is taken as 2 mm. Fig. 4.3 shows the variation of the integrands of K_{12} and L_{11} as a function of k. The left column shows the variation of imaginary

part of K_{12} (real part being zero) while the right column shows the variation of the real part of L_{11} (imaginary part being zero). It should be noted that depending on the material properties, elements of the K, L, M and N matrices can either be real or imaginary. The top row is for a frequency of 0.04 MHz and the bottom row is for a frequency of 1.20 MHz. Similar characteristics would have been observed if the integrands of N and M were plotted instead of K and L. From the figure it is evident that as the frequency increases, the decay rate of the integrand decreases thus increasing the cost of integration. Fig. 4.4 shows the variation of crack opening displacements (COD) along the crack length at 0.04 MHz for $F(\omega)$ equal to 10. The left column shows the variation of displacement along the x-direction (U) while the right column shows the same in the y-direction (V). Three rows correspond to three angles of inclination (θ), which are 0^0 (top row), 45^0 (middle row) and 90^0 (bottom row). In each plot two curves are drawn, the thick curve shows the COD of the sample problem described above and the thin curve is for a similar problem where the load is shifted horizontally just above the center of the crack ($d = 0\ mm$). From the problem geometry and the direction of applied load it is obvious that for $d = 0$, the problem is symmetric for $\theta = 0^0$ and antisymmetric for $\theta = 90^0$. Hence for $\theta = 0^0$ one should expect symmetric V and antisymmetric U where as for $\theta = 90^0$, V and U should be antisymmetric and symmetric respectively. This is what we get in our computation also. However in the COD plots (thin curves of Fig. 4.4) both U and V appear to be symmetric for $\theta = 0^0$ (top row) and $\theta = 90^0$ (bottom row). This is because COD amplitudes are plotted in these figures, hence both symmetric and antisymmetric curves appear to be symmetric in the figure. For 45^0 inclination (middle row) COD plots are neither symmetric nor antisymmetric. Variation of U and V are also neither symmetric nor antisymmetric for the sample problem at any

angle of inclination, however deviation of COD amplitudes from symmetry appears to be very small.

In Figs. 4.5 through 4.8 thick and thin curves indicate the surface response of the orthotropic half-space with and without the cracks respectively. Angle of inclination (θ) for the applied load is taken as 45^0. Left and right columns give spectral amplitudes and time histories respectively. In Figs. 4.5 and 4.6 variations of u and v on the surface of the half space are shown. Top and bottom rows indicate the displacement at x_p equal to 5 and 15 mm respectively (see Fig. 4.1). It should be noted here that for both Figs. 4.5 and 4.6 the difference between surface displacements with and without the subsurface crack is more at $x_p = 5$ mm than that at $x_p = 15$ mm. Intuitively also one should expect it, since the effect of crack decays as the distance from the crack increases.

Horizontal (u) and vertical (v) displacements at $x_p = 5$ mm are plotted in Figs. 4.7 and 4.8 for three different angles of inclination θ, which are 0^0 (top row), 45^0 (middle row) and 90^0 (bottom row). It can be seen in these two figures that as the external load changes its orientation from vertical ($\theta = 0^0$, top row) to horizontal position ($\theta = 90^0$, bottom row) u increases and v decreases. Qualitatively we can justify these results since a horizontal force should produce more horizontal displacement, where as a vertical force should produce more vertical displacement as long as Poisson's ratio is less than 1.

It should also be noted that the peak displacement increases with the presence of the crack. This is because a cracked half-space is more flexible than an uncracked half-space, hence cracked half-space gives larger displacement.

The nature of computed results qualitatively agrees with the expected form. However, these results could not be compared with any other published result since

no analytical or numerical results are available in the literature for any problem with geometry and loading similar to this one.

In this analysis traction free crack surfaces are considered; in other words it is assumed that the crack surfaces do not come in contact with each other. However under dynamic loading the crack surfaces could come in contact with each other and introduce nonlinearity in the problem. Under certain situations these crack surface tractions may significantly alter the surface displacements computed here. However under some other real situation, such as a subsurface crack of nonzero width being excited dynamically by an ultrasonic signal, the crack surfaces may vibrate and yet may not come in contact with each other. The assumption of stress free crack surfaces is justified under such situations. Then the response computed with this simplifying assumption should be close to the actual response.

In all the results presented in this chapter the difference between the cracked and uncracked half-space response is found to be very small. However, this difference should significantly increase if the crack length is increased or the frequency content in the spectral plot is increased by subjecting the half-space to a sharper impact excitation (see chapter 2). Since the main emphasis in this dissertation is devoted to the development of the method to solve the specific problem, an elaborate parametric study is beyond the scope of current study and is not attempted here.

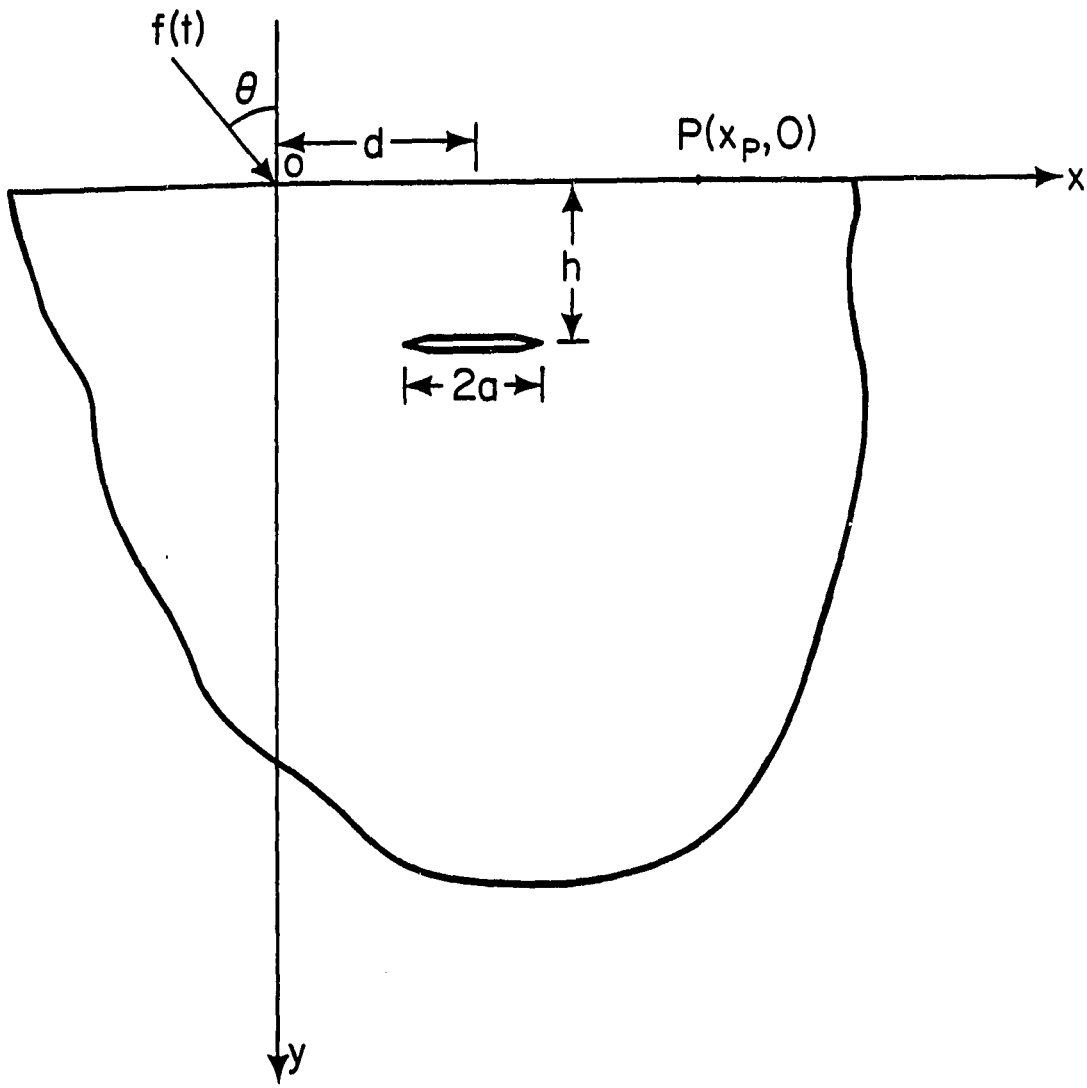

Fig. 4.1: Geometry of the problem. An orthotropic half-space containing a subsurface crack.

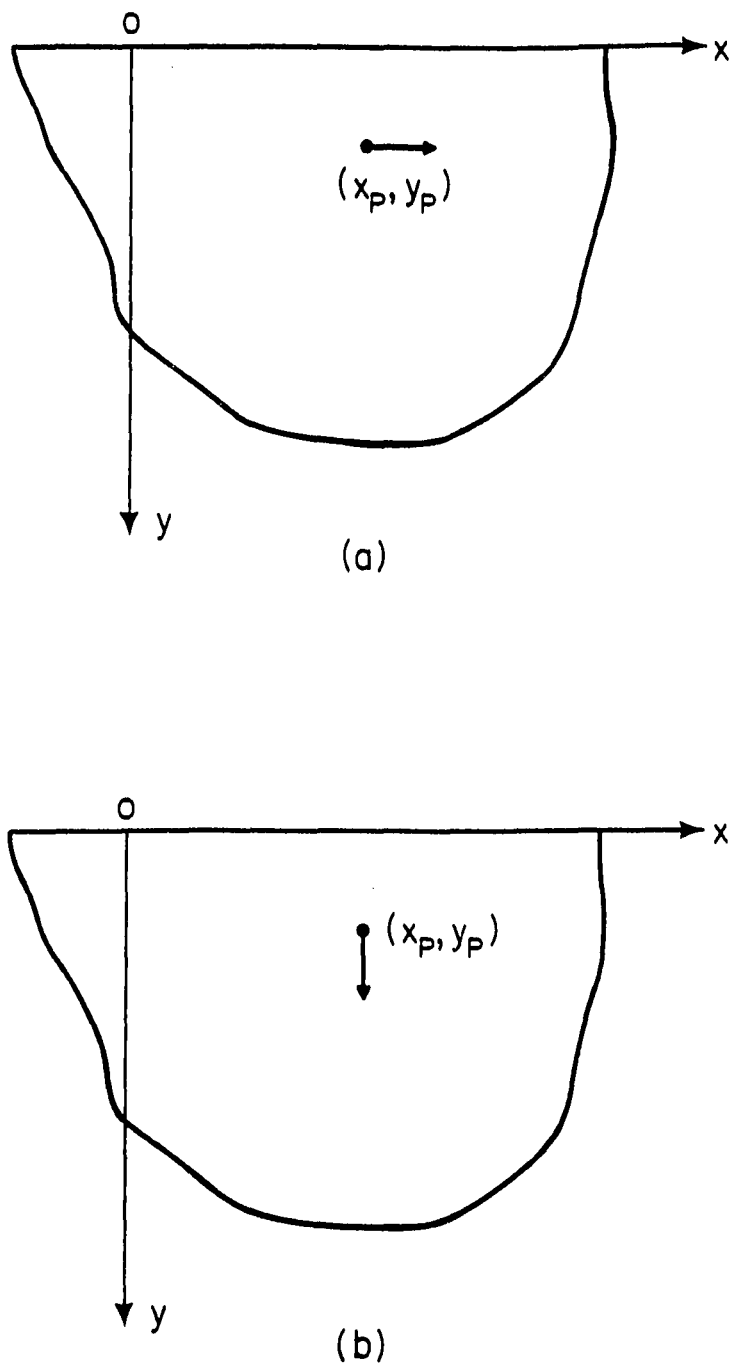

Fig. 4.2: A line load in a half-space: a) line load in horizontal direction, b) line load in vertical direction.

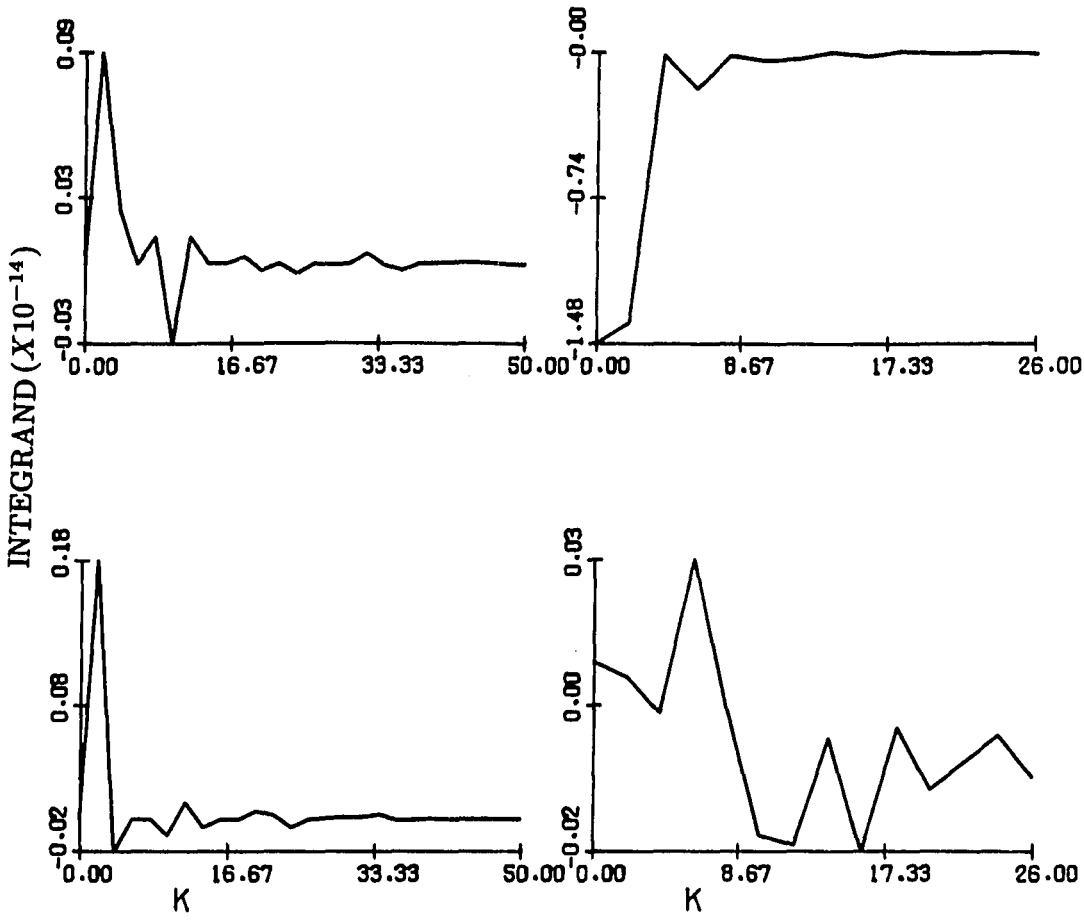

Fig. 4.3: Variation of imaginary part of $K(1,2)$ (real part being zero) and real part of $L(1,1)$ (imaginary part being zero) with k. Left column shows $K(1,2)$ and right column shows $L(1,1)$. Top and bottom rows are at frequencies 0.04 MHz and 1.20 MHz respectively.

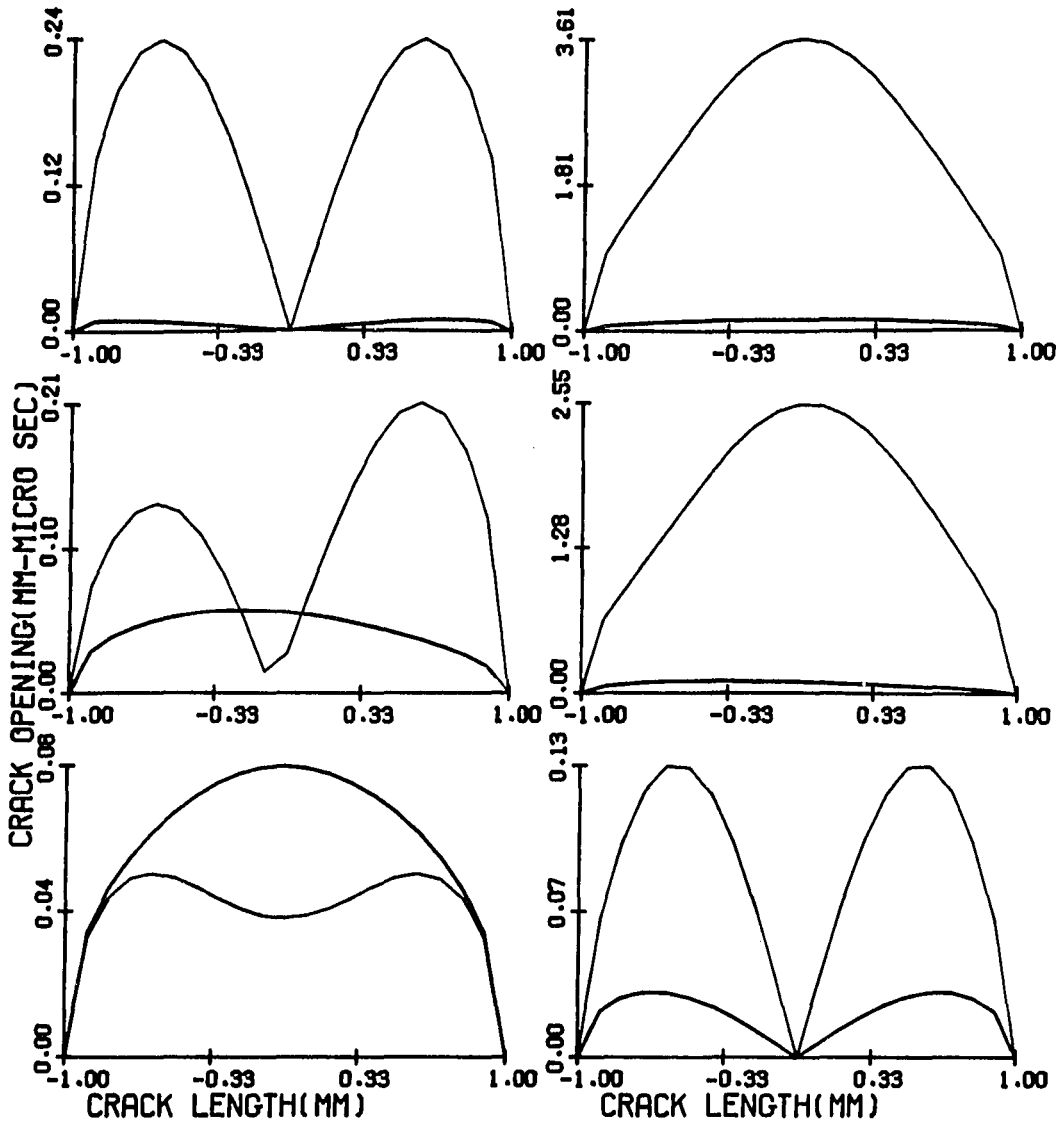

Fig. 4.4: Spectral amplitude (in mm-μsec) of crack opening displacements at a frequency 0.04 MHz for $F(\omega)$ equal to 10. Left and right columns show the displacements along x and y-directions respectively. Thin and thick curves are for $d = 0$ mm and 2 mm respectively (see Fig. 1).

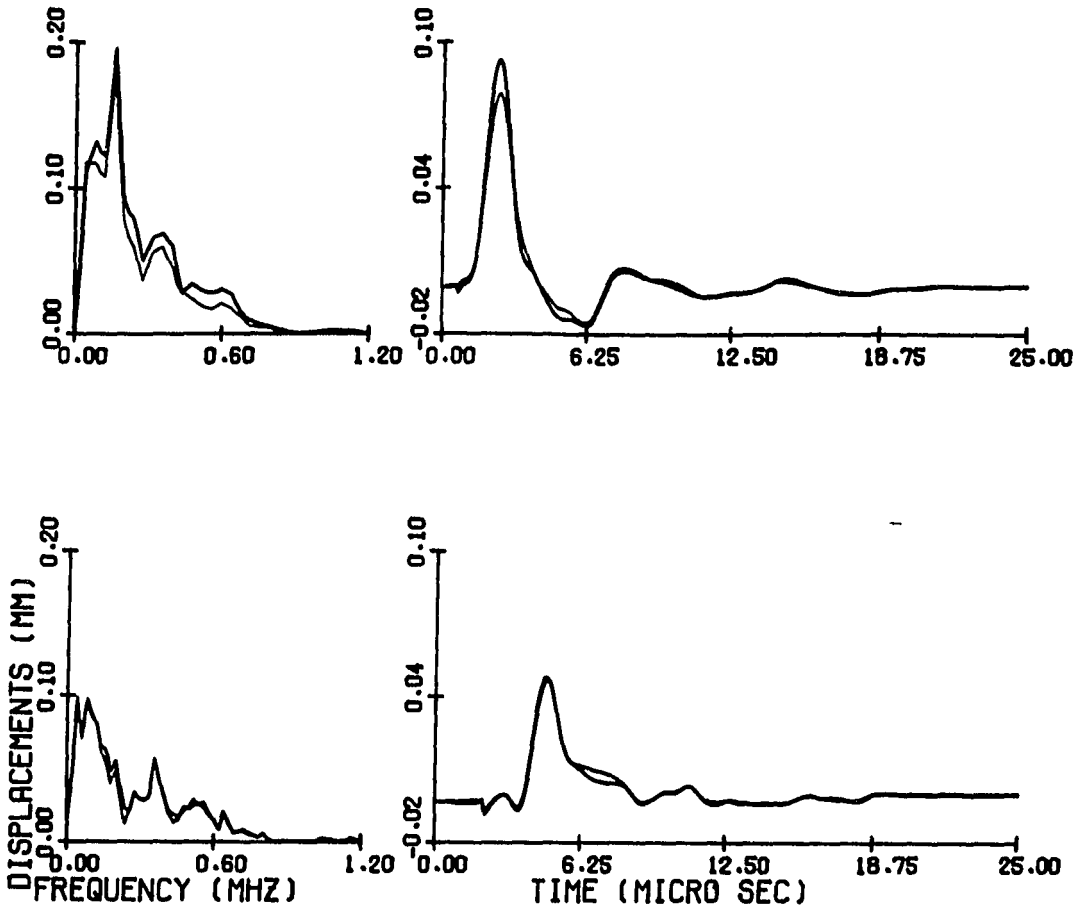

Fig. 4.5: Surface displacements along the x-direction in an orthotropic half-space. The half-space is excited by a line load at $d = 2$ mm with an angle of inclination, $\theta = 45^0$ and pulse duration time $\tau = 2$ μsec. The top and bottom rows show the surface displacements at $x = 5$ and 15 mm respectively (see Fig. 4.1). Left and right columns give spectra and time histories respectively. Thick curves show the displacement in presence of the crack while thin curves are for a flawless half-space.

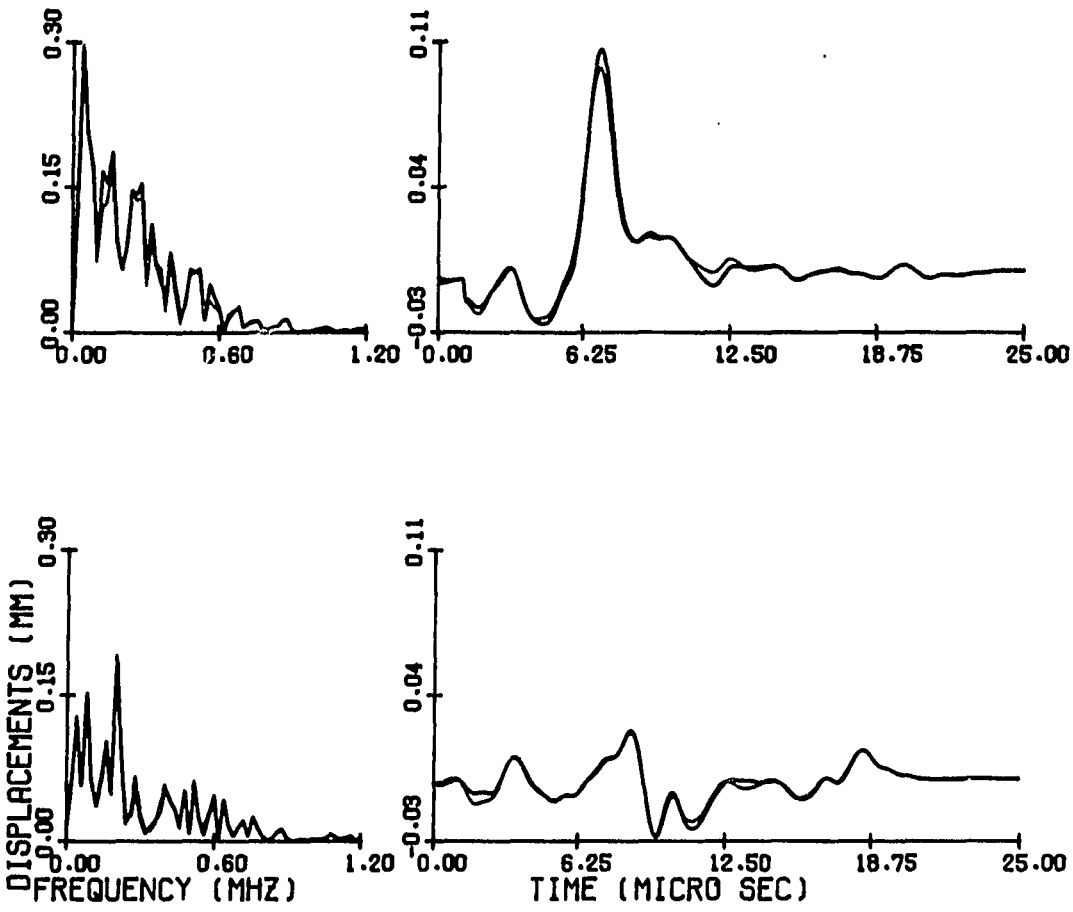

Fig. 4.6: Same as Fig. 4.5 but computed displacements are along the y-direction.

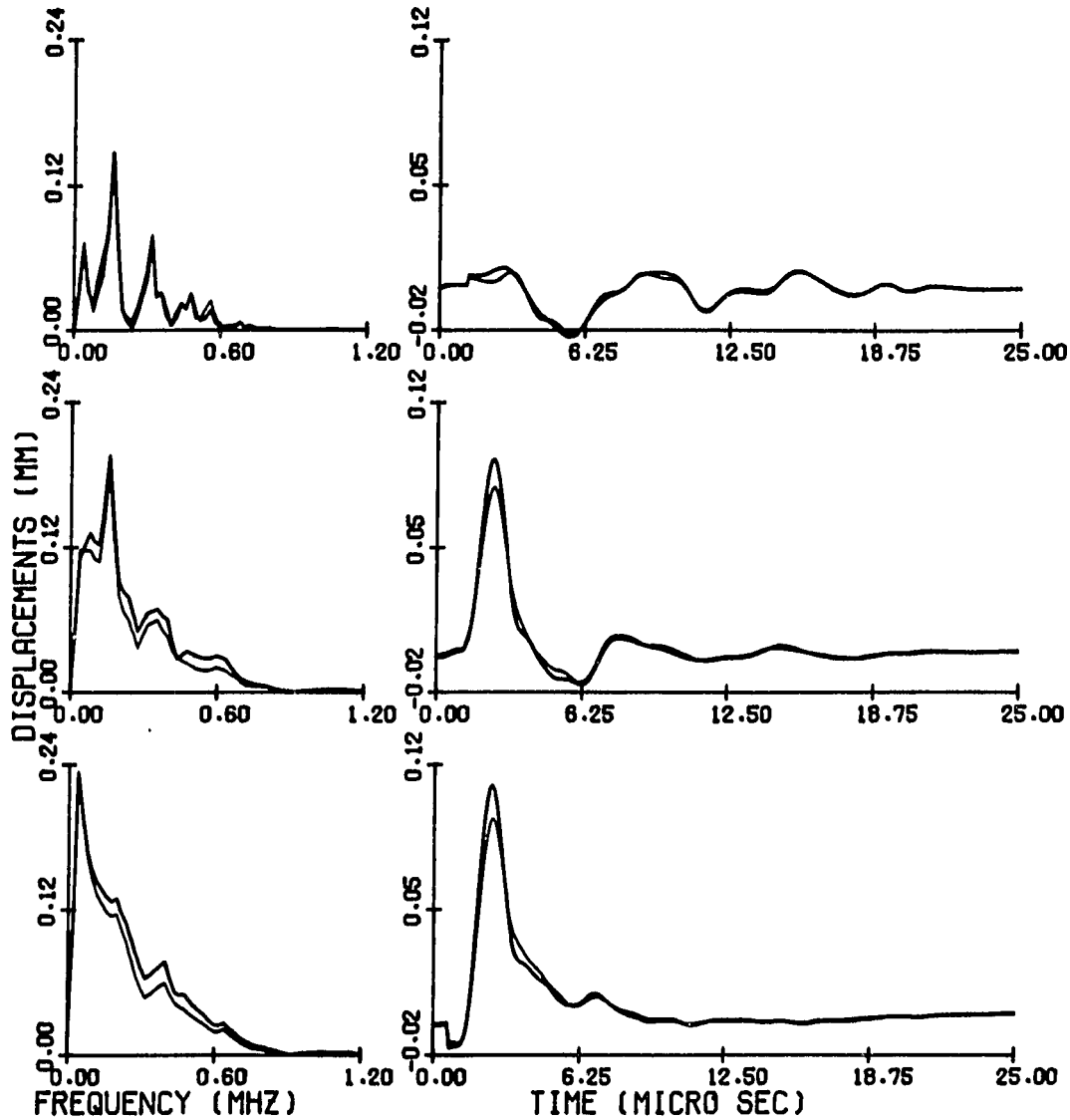

Fig. 4.7: Surface displacements along the x-direction for a load applied at $d = 2\ mm$, with the pulse duration time $\tau = 2\ \mu$sec. Top, middle and bottom rows are for angles of inclination equal to 0^0, 45^0 and 90^0 respectively. Left and right columns give spectral amplitudes and time histories respectively. Thick curves are for the cracked half-space and thin curves are for the flawless half-space.

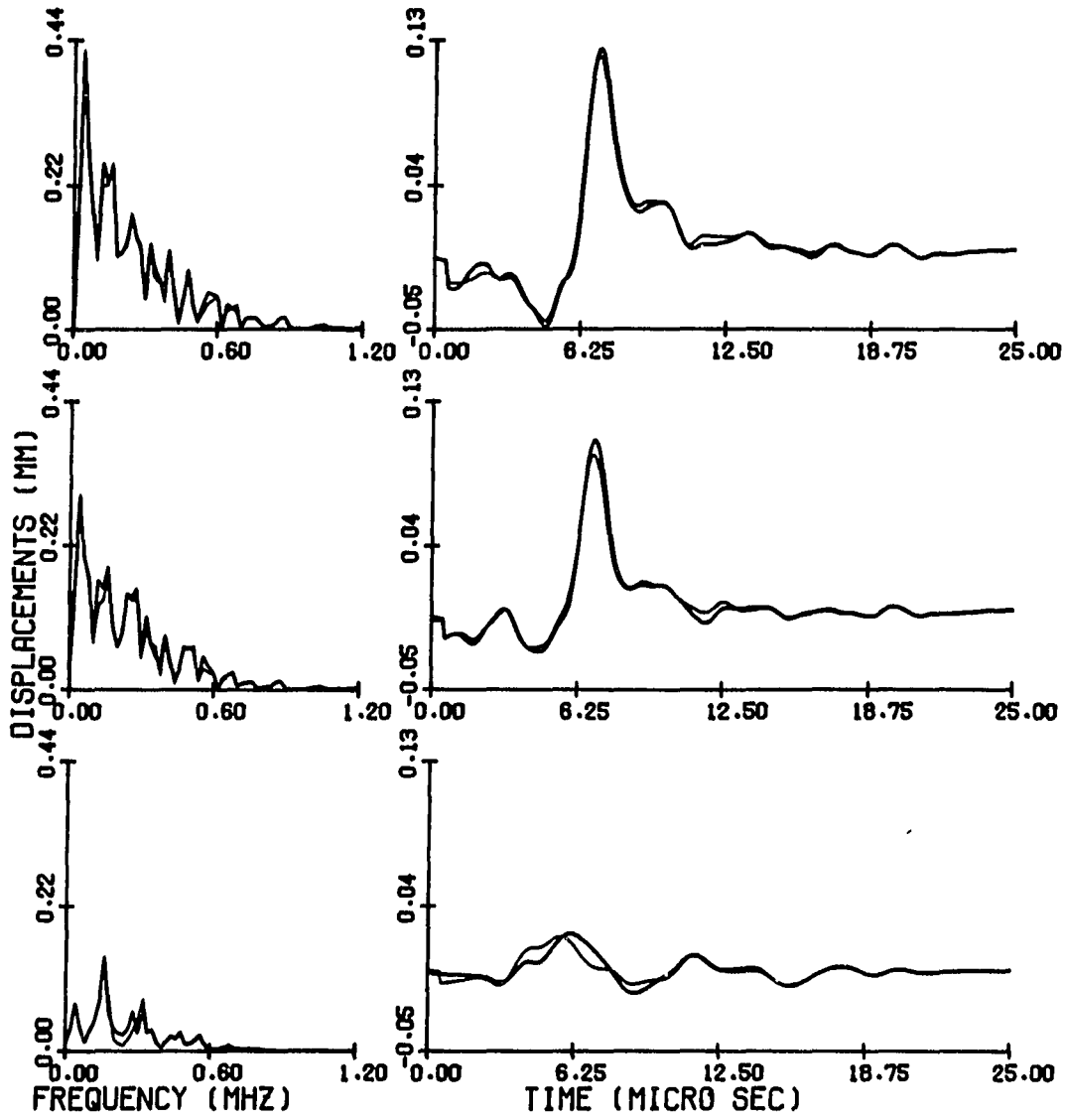

Fig. 4.8: Same as Fig. 4.7 but computed displacements are along the y-direction.

CHAPTER–5

CONCLUSIONS AND RECOMMENDATIONS FOR FURTHER RESEARCH

5.1 CONCLUSIONS

Analytical study of subsurface cracks subjected to dynamic loads in isotropic materials can be performed by using boundary integral equation (BIE) methods. Two most popular techniques for formulating boundary integral equations in isotropic materials for dynamic crack problems are Neerhoff's (Neerhoff, 1979) method and frequency domain representation theorem (Knopoff, 1956). In this dissertation, these techniques have been extended to orthotropic materials. Most difficult part for solving these problems is the evaluation of the singular integrals. Techniques of Kundu (Kundu, 1983) to obtain such integrals have been modified to obtain the integrals involved.

Both techniques mentioned above require Green's functions. For antiplane problems Green's functions available for isotropic materials are modified to include anisotropic materials. For in-plane problems involving orthotropic materials, no Green's functions are available in literature. So two new Green's functions are developed for line load in horizontal and vertical directions in a semi-infinite medium.

In this dissertation, solutions are given for line loads. From these solutions one can obtain solution to a more complex loading situation by suitable integration.

In a real situation, sometimes there is not just a single crack, but rather a configuration of multiple cracks, for example, when a body is hit by a projectile a number of cracks are generated. The question which has motivated part of the work in this dissertation is to what extent the response of one crack can be affected by the presence of a neighboring crack. When the faces of the crack are in contact and the crack is actually partially closed or when there are more than one neighboring

cracks, the analysis will be more involved. The simplified analysis of this dissertation can account for a partially closed crack if it can be represented by a configuration of two neighboring cracks. Solutions of such problems are obtained by formulating the problem as a coupled set of integral equations, thus the interaction between two cracks is properly accounted for.

Parametric studies involving loading, crack geometries and material properties are performed to study the effect of cracks on the structural response. The following conclusions are drawn from these studies for the range of problems analysed in this dissertation:

1) It is observed that the interaction between the cracks significantly affect the surface motion and crack opening displacements if the crack lies on the path of propagation of waves.

2) For the same excitation and crack geometries, motion in anisotropic materials decays faster than that in isotropic materials.

3) It is observed that fiber orientation has a strong influence on the crack opening displacements.

4) For the antiplane problem, a change of shear moduli associated with the crack surface stresses affects the results more than a change in shear moduli which are not directly associated with the crack surface stresses.

5) For the same problem geometry, material properties, and peak load; an increased load duration gives a larger COD and surface displacements.

5.2 RECOMMENDATIONS FOR FURTHER RESEARCH

A crack with closed and rough crack faces may be a poor reflector of ultrasonic waves, and thus difficult to detect and characterize. Attempts should be made to to develop a dynamic model that will incorporate absorption of waves at

the crack surface. It is also mandatory to incorporate contact and slip between the crack surfaces where they can significantly affect the scattering pattern of waves by the cracks.

Although, in the present study attention is restricted to a layered half-space and a three-layered plate, composites are usually made of several layers. Attempts should be made to develop a realistic model of analysis for multilayered composites with interface cracks.

In order to verify the analytical results, controlled laboratory tests are imperative. Through comparison of predicted crack responses and extensive test measurement under controlled conditions, the predictive capabilities of the anlytical results can be assessed beyond question.

APPENDIX-A

Expressions of A_1, B_1, A_2,B_2 and C_1, D_1, C_2 of equations (2.2) and (2.6) are given here.

$$A_1 = \frac{p_1^2 \cos(\eta_1 h) + ip_1 \sin(\eta_1 h)}{p_1^2 \cos^2(\eta_1 h) + \sin^2(\eta_1 h)}$$

$$B_1 = A_1$$

$$A_2 = 1$$

$$B_2 = \frac{ip_1 - \tan(\eta_1 h)}{ip_1 + \tan(\eta_1 h)}$$

$$C_1 = \frac{pQ_1(\mu_x^1\eta_1 - \mu_x^2\eta_2) + P(\mu_x^1\eta_1 + \mu_x^2\eta_2)}{\eta_1[\mu_x^2\eta_2(Q_1^2+1) - \mu_x^1\eta_1(Q_1^2-1)]}$$

$$D_1 = \frac{Q_1(PQ_1 + p)(\mu_x^1\eta_1 - \mu_x^2\eta_2)}{\eta_1[\mu_x^2\eta_2(Q_1^2+1) - \mu_x^1\eta_1(Q_1^2-1)]}$$

$$C_2 = \frac{2\mu_x^2(PQ_1 + p)}{\mu_x^2\eta_2(Q_1^2+1) - \mu_x^1\eta_1(Q_1^2-1)}$$

where

$$p_1 = \frac{\mu_x^2\eta_2}{\mu_x^1\eta_1}$$

$$Q_1 = exp(i\eta_1 h)$$

$$P = exp(i\eta_1 y_p)$$

$$p = Q_1/P$$

η_1, η_2, μ_x^1 and μ_x^2 are defined in equation (2.2) and (2.6).

APPENDIX-B

Equations (2.4), (2.5) and (2.25) are derived here. Equation of equlibrium for antiplane strain is given as

$$\frac{\partial \sigma_4}{\partial y} + \frac{\partial \sigma_5}{\partial x} = \rho \frac{\partial^2 u}{\partial^2 t} \tag{B.1}$$

where σ_4 and σ_5 are the shear stresses related to yz and zx-directions. Constitutive equations of the anisotropic materials considered here can be written as

$$\begin{aligned} \sigma_4 &= C_{44}\epsilon_4 \\ \sigma_5 &= C_{55}\epsilon_5 \end{aligned} \tag{B.2}$$

where the engineering strain ϵ_4 and ϵ_5 for antiplane strain are defined as

$$\epsilon_4 = \frac{\partial u}{\partial y} \quad \epsilon_5 = \frac{\partial u}{\partial x} \tag{B.3}$$

Substitution of equations (B.2) and (B.3) into equation (B.1) gives the equation of equilibrium in time domain as

$$C_{44}\frac{\partial^2 u}{\partial^2 y} + C_{55}\frac{\partial^2 u}{\partial^2 x} = \rho \frac{\partial^2 u}{\partial^2 t} \tag{B.4}$$

Fourier transform of this equation gives equation (2.4).

Let the solution of equation (2.4) be

$$U = e^{ikx+i\eta y} \tag{B.5}$$

Substituting this in equation (2.4) and after some simlification one can write

$$\eta = \pm \left\{ \frac{\rho\omega^2 - C_{55}k^2}{C_{44}} \right\}^{\frac{1}{2}} \tag{B.6}$$

In time domain displacement function for a plane wave front can be written by adding $e^{-i\omega t}$ factor in equation (B.5), i. e.

$$\begin{aligned} u &= e^{ikx+i\eta y-i\omega t} \\ &= e^{\{k^2+\eta^2\}^{\frac{1}{2}}i(x\sin\theta+y\cos\theta-ct)} \end{aligned} \tag{B.7}$$

where θ is the angle of incidence of the plane wave front and c is the shear wave velocity in the material and is given by

$$c = \frac{\omega}{\{k^2+\eta^2\}^{\frac{1}{2}}} \tag{B.8}$$

From geometric interpretation of equation (B.7) one can write

$$k^2 = (k^2+\eta^2)\sin^2\theta \tag{B.9}$$

Substitution of equation (B.6) in (B.9) after some simlification gives rise to equation (2.5).

Now equation (2.25) is derived. By changing limits in equation (2.23) we can write

$$\begin{aligned} U^s(x_p,0) = &-\frac{1}{4\pi}\int_{-a_1}^{a_1}\phi(x)\int_{-\infty}^{\infty}f(k)e^{ik(x-x_p)}dkdx \\ &-\frac{1}{4\pi}\int_{-a_2}^{a_2}\psi(x)\int_{-\infty}^{\infty}f(k)e^{ik(x+d-x_p)}dkdx \end{aligned} \tag{B.10}$$

The integration with respect to x in the equation (B.10) can be obtained analytically (Neerhoff, 1979) as

$$\begin{aligned} \int_{-a_1}^{a_1}\phi(x)e^{ikx}dx &= \sum_{n=1}^{\infty}\alpha_n\frac{i\pi}{k}J_n(ka_1) \\ \int_{-a_2}^{a_2}\psi(x)e^{ikx}dx &= \sum_{n=1}^{\infty}\gamma_n\frac{i\pi}{k}J_n(ka_1) \end{aligned} \tag{B.11}$$

If we substitute equation (B.11) into equation (B.10) we obtain equation (2.25).

APPENDIX-C

Expressions of A_j, B_j, C_j^α and D_j^α (j = 1,2,3) of equations (3.1) and (3.3) are given here. Partial derivatives of C_2^2 and D_2^2 with respect to y_p (see equaiton 3.11) are also defined here.

$$\begin{aligned}
A_2 &= \frac{2iF(\omega)(F_3+F_4)}{M} \\
B_2 &= \frac{2iF(\omega)Q_1Q_2^2(F_3+F_4)}{M} \\
A_1 &= \frac{(A_2+B_2)Q_1+R}{1+Q_1^2} \\
B_1 &= A_1 - R \\
A_3 &= \frac{A_2+B_2Q_2^{-1}}{1+Q_3^2} \\
B_3 &= A_3Q_3^2
\end{aligned} \tag{C.1}$$

where M, F_1, F_2, F_3, F_4 and Q_j are defined in (3.21) and R is defined in (C.2)

$$R = -\frac{iF(\omega)}{\mu_x^1\eta_1} \tag{C.2}$$

η_j are defined in equation (3.1) and (3.2). $F(\omega)$ is the Fourier Transform of the applied stress field on the plate boundary, ω is the frequency.

Now C_j^α and D_j^α of equation (3.3) are defined,

$$
\begin{aligned}
C_2^2 &= \frac{F_1 - F_2}{\eta_2 M}\{(F_3 - F_4)p_2 Q_2 - (F_3 + F_4)P_2\} \\
D_2^2 &= Q_2\frac{F_3 - F_4}{\eta_2 M}\{(F_1 - F_2)P_2 Q_2 - (F_1 + F_2)p_2\} \\
C_1^2 &= D_1^2 = \frac{\eta_2 Q_1}{\eta_1(Q_1^2 - 1)}(C_2^2 - D_2^2 - \frac{P_2}{\eta_2}) \\
C_3^2 &= D_3^2 Q_3^{-2} = \frac{\eta_2}{\eta_3(1 - Q_3^2)}(C_2^2 Q_2 - D_2^2 Q_2^{-1} + \frac{p_2}{\eta_2}) \\
C_2^1 &= \frac{E(F_1 + F_2)F_3}{M} \\
D_2^1 &= -\frac{EQ_2 F_1(F_3 - F_4)}{M} \\
C_1^1 &= D_1^1 + \frac{P_1}{\eta_1} = \frac{\frac{\mu_x^1}{\mu_x^2}Q_1(C_2^1 + D_2^1) + \frac{P_1}{\eta_1} - \frac{p_1 Q_1}{\eta_1}}{(1 + Q_1^2)} \\
C_3^1 &= D_3^1 Q_3^{-2} = \frac{\eta_2(C_2^1 Q_2 - D_2^1 Q_2^{-1})}{\eta_3(1 - Q_3^2)}
\end{aligned}
\tag{C.3}
$$

where

$$
\begin{aligned}
P_2 &= e^{i\eta_2(y_p - y_1)} \\
p_2 &= e^{i\eta_2(y_2 - y_p)} \\
P_1 &= e^{i\eta_1 y_p} \\
p_1 &= e^{i\eta_1(y_1 - y_p)} \\
E &= \frac{(2P_1 + 2p_1 Q_1)F_2}{\eta_2(1 + Q_1^2)Q_1 F_1}
\end{aligned}
\tag{C.4}
$$

Partial derivatives of C_2 and D_2 with respect to y_p have the following forms

$$
\begin{aligned}
\frac{\partial C_2^2}{\partial y_p} &= -\frac{i}{M}(F_1 - F_2)\{p_2 Q_2(F_3 - F_4) + P_2(F_3 + F_4)\} \\
\frac{\partial D_2^2}{\partial y_p} &= \frac{i}{M}(F_3 - F_4)\{P_2 Q_2(F_1 - F_2) + p_2(F_1 + F_2)\}
\end{aligned}
\tag{C.5}
$$

where M, F_1, F_2, F_3, F_4, Q_2, P_2 and p_2 are defined in (3.21), (C.2) and (C.4). Clearly if $y_p = y_1$ then $P_2 = 1$, $p_2 = Q_2$ and if $y_p = y_2$ then $P_2 = Q_2$, $p_2 = 1$.

APPENDIX-D

Expressions of A_j, D_j^{α}, (α, j =1 , 2), a_j, (j = 1 to 6) in equations (4.4), (4.7) and (4.8) are given in this section. Value of Functions $F_j(k)$, (k = 1 to 4) in equation (4.13) are also defined hare.

$$A_1 = \frac{-a_{22}F(\omega)\cos\theta + a_{12}F(\omega)\sin\theta}{a_{11}a_{22} - a_{12}a_{21}}$$
$$A_2 = \frac{+a_{21}F(\omega)\cos\theta - a_{11}F(\omega)\sin\theta}{a_{11}a_{22} - a_{12}a_{21}} \qquad (D.1)$$

where

$$a_{11} = ikC_{21} + C_{22}S_1p_1$$
$$a_{12} = ikC_{21} + C_{22}S_2p_2$$
$$a_{21} = C_{66}(p_1 + ikS_1) \qquad (D.2)$$
$$a_{22} = C_{66}(p_2 + ikS_2)$$

and

$$D_1^1 = \frac{a_{22}R_1 - a_{12}R_2}{a_{11}a_{22} - a_{12}a_{21}}$$
$$D_2^1 = \frac{-a_{21}R_1 + a_{11}R_2}{a_{11}a_{22} - a_{12}a_{21}}$$
$$D_1^2 = \frac{a_{22}R_3 - a_{12}R_4}{a_{11}a_{22} - a_{12}a_{21}} \qquad (D.3)$$
$$D_2^2 = \frac{-a_{21}R_3 + a_{11}R_4}{a_{11}a_{22} - a_{12}a_{21}}$$

where

$$R_1 = -B_1^- e^{p_1 y_p} a_{11} - C_1^- e^{p_2 y_p} a_{12}$$
$$R_2 = B_1^- e^{p_1 y_p} a_{21} + C_1^- e^{p_2 y_p} a_{22}$$
$$R_3 = -B_2^- e^{p_1 y_p} a_{11} - C_2^- e^{p_2 y_p} a_{12} \qquad (D.4)$$
$$R_4 = B_2^- e^{p_1 y_p} a_{21} + C_2^- e^{p_2 y_p} a_{22}$$

$$
\begin{aligned}
a_1 &= p_1(k^2C_{11} - C_{66}p_2^2 - \rho\omega^2) \\
a_2 &= p_2(k^2C_{11} - C_{66}p_1^2 - \rho\omega^2) \\
a_3 &= C_{22}C_{66}(p_1^2 - p_2^2) \\
a_4 &= -ik(C_{12} + C_{66}) \\
a_5 &= p_1(p_2^2C_{12} + k^2C_{11} - \rho\omega^2) \\
a_6 &= p_2(p_1^2C_{12} + k^2C_{11} - \rho\omega^2)
\end{aligned}
\tag{D.5}
$$

$$
\begin{aligned}
F_1(k) &= C_{66}(B_1^+ p_1 e^{p_1|y-y_p|} + p_2 C_1^+ e^{p_2|y-y_p|} + D_1^1 p_1 e^{p_1 y} + D_2^1 p_2 e^{p_2 y}) \\
&\quad + ikC_{66}(B_1^+ S_1 e^{p_1|y-y_p|} + C_1^+ S_2 e^{p_2|y-y_p|} + D_1^1 S_1 e^{p_1 y} + D_2^1 S_2 e^{p_2 y}) \\
F_2(k) &= ikC_{21}(B_1^+ e^{p_1|y-y_p|} + C_1^+ e^{p_2|y-y_p|} + D_1^1 e^{p_1 y} + D_2^1 e^{p_2 y}) \\
&\quad + C_{22}(B_1^+ S_1 p_1 e^{p_1|y-y_p|} + C_1^+ S_2 p_2 e^{p_2|y-y_p|} + D_1^1 S_1 p_1 e^{p_1 y} + D_2^1 S_2 p_2 e^{p_2 y}) \\
F_3(k) &= C_{66}(B_2^+ p_1 e^{p_1|y-y_p|} + p_2 C_2^+ e^{p_2|y-y_p|} + D_1^2 p_1 e^{p_1 y} + D_2^2 p_2 e^{p_2 y}) \\
&\quad + ikC_{66}(B_2^+ S_1 e^{p_1|y-y_p|} + C_2^+ S_2 e^{p_2|y-y_p|} + D_1^2 S_1 e^{p_1 y} + D_2^2 S_2 e^{p_2 y}) \\
F_4(k) &= ikC_{21}(B_2^+ e^{p_1|y-y_p|} + C_2^+ e^{p_2|y-y_p|} + D_1^2 e^{p_1 y} + D_2^2 e^{p_2 y}) \\
&\quad + C_{22}(B_2^+ S_1 p_1 e^{p_1|y-y_p|} + C_2^+ S_2 p_2 e^{p_2|y-y_p|} + D_1^2 S_1 p_1 e^{p_1 y} + D_2^2 S_2 p_2 e^{p_2 y})
\end{aligned}
\tag{D.6}
$$

ASSOCIATED PUBLICATIONS

[1] Karim, M. R. and Kundu, T.: Transient Surface Response of Layered Isotropic and Anisotropic Half-spaces with Interface Cracks: SH Case, International Journal of Fracture, 37, 245–262 (1988).

[2] Karim, M. R. and Kundu, T.: Transient Response of a Three Layered Composites with Two Interface Cracks Due to a Line Load, Acta Mechanica, (1988), in press.

[3] Karim, M. R., Kundu, T., Desai, C. S.: Detection of Delamination Cracks in Layered Fiber Reinforced Composite Plates, ASME Journal of Pressure Vessel Technology, (1988), in Press.

[4] Karim, M. R. and Kundu, T.: Dynamic Response of an Orthotropic Halfspace with a Subsurface Crack: In–Plane Case, Submitted to ASME Journal of Applied Mechanics (1988).

[5] Kundu, T. and Karim, M. R.: Interface Crack in an Orthotropic Half–Space Under Impact loading, Submitted to the 12th Canadian Congress of Applied Mechanics, Ottowa, Canada (1989).

[6] Karim, M. R. and Kundu, T.: Acoustic Microscopy in Characterizing Fiber Reinforced Composites, Submitted to the ASME Pressure Vessels and Piping Conference, Hawaii, USA (1989).

LIST OF REFERENCES

[1] Abramowitz, M. and Stegun, I.A.: *Hand Book of Mathematical Functions*, New York, U. S. A., Dover Publications (1970).

[2] Achenbach, J. D. and Gautensen, A. K.: A Ray Theory for Elastodynamic Sress Intensity Factors, ASME Journal of Applied Mechanics, 44, 123–129 (1978).

[3] Achenbach, J. D. and Brind, R. J.: Elastodynamic Stress Intensity Factor for a Crack Near a Free Surface, ASME Journal of Applied Mechanics, 48, 539–542 (1981a).

[4] Achenbach, J. D. and Brind, R. J.: Scattering of Surface Waves by a Subsurface Crack, J. of Sound and Vibrations, 76,43–56 (1981b).

[5] Achenbach, J. D. and Norris, A. N.: Loss of Specular Reflection Due to Nonlinear Crack-Face Interaction, Journal of Nondestructive Evaluation, 3, 229–239 (1982).

[6] Achenbach, J. D., Lin, W. and Keer, L. M.,: Surface Waves Due to Scattering by a Near–surface Parallel Crack, IEEE Trans. Sonics and Ultrasonics, SU–30(4), 270–276, (1983).

[7] Ang, D. and Knopoff, L: Diffraction of Scalar Elastic Waves by a Finite Crack, Proc. Nat. Acad. Sci., 51, 593–598 (1964).

[8] Ang, W. T.: A Crack in an Anisotropic Layered Material Under the Action of Impact Loading, ASME Journal of Applied Mechanics, 55, 120–125 (1988).

[9] Angel, Y. C. and Achenbach, J. D.: Reflection and Transmission of Elastic Waves by a Periodic Array of Cracks, ASME Journal of Applied Mechanics, 52, 33–41 (1985).

[10] Arin, K. and Erdogan, F.: Penny Shaped Interface Crack Bonded to Dissimilar Half Spaces, International Journal of Engng. Science, 9, 213–232 (1971).

[11] Arin, K.: A Note on the Fracture of Laminated Composites, Letters Appl. Engng. Sciences, 3, 81–85 (1975).

[12] Barenblatt, G. I.: The Mathematical Theory of Equilibrium Cracks in Brittle Fracture, Advances in Applied Mechanics, 7, 55-128 (1962).

[13] Boström, A.: Elastic Wave Scattering from an Interface Crack: Antiplane Strain, ASME Journal of Applied Mechanics, 54, 503–508, (1987).

[14] Bogy, D. B.: The Plane Elastostatic Solution for a Symmetrically Loaded Crack in a Strip Composite, International Journal of Engng. Science, 11, 985–996 (1973).

[15] Copson, E. T.: On Certain Dual Integral Equations, Proceedings, Glasgow Mathematical Association, 5, 19–24 (1961).

[16] Chen, Y.: General Case of Multiple Crack Problems in an Infinite Plate, Engng. Fracture Mech., 20, 591–597 (1984).

[17] Chudnovosky, A. and Kachanov, M.: Interaction of a Crack with a Field of Micro-cracks, International Journal of Engineering Sci., 21, 1009–1018 (1983).

[18] Chudnovosky, A., Dolgoposky, A. and Kachanov, M.: Elastic Interaction of a Crack with a Microcrack Array, Part I and II, International Journal of Solids and Structures, 23, 1–10, 11–21, (1987a, b).

[19] Comninou, M.: The Interface Crack, ASME Journal of Applied Mechanics, 44, 631–636 (1977a).

[20] Comninou, M. (1977b): Interface Crack with Friction in the Contact Zone, ASME Journal of Applied Mechanics, 44, 780–781.

[21] Comninou, M. and Dunders, J.: Reflection and Refraction of Elastic Waves with a Unilateral Interface, Proceedings, Royal Society, London, Series A, 356, 509–528 (1977).

[22] Comninou, M. and Dunders, J.: Interaction of Elastic Waves with a Unilateral Interface, Proceedings, Royal Society, London, Series A, 368, 141–154 (1979).

[23] Comninou, M. and Schmueser, D.: Interface Crack in a Combined Tension Compression Shear Field, ASME Journal of Applied Mechanics, 46, 345–348 (1979).

[24] Cook, T. S. and Erdogan, F.: Stresses in Bonded Materials with a Crack Perpendicular to the Interface, International Journal of Engng. Sciences, 10, 677–697 (1972).

[25] Datta, S. K.:Diffraction of SH-wave by an Edge Crack, ASME Journal of Applied Mechanics, 46, 101–106 (1979).

[26] Delale, F. and Erdogan, F.: Bonded Orthotropic Strips with Cracks, International Journal of Fracture, 15, 343–364, (1979).

[27] de Hoop, A. T.: Representation Theorems for Displacement in an Elastic Solid and Their Application to Elastodynamic Diffraction Theory, D. Sc. Thesis, Technische Hogeschool, Delft (1958).

[28] Dugdale, D. S.: Yielding of Steel Sheets Containing Slots, J. Mech. Phys. Solids, 8, 100–104 (1960).

[29] Erdogan, F. and Gupta, G. D.: The Stress Analysis of Multilayered Composites with Flaws, International Journal of Solids and Structures, 7, 39–61 (1971).

[30] Erdogan, F. and Gupta, G. D.: Layered Composites with an Interface Flaw, International Journal of Solids and Structures, 7, 1089–1107 (1971).

[31] Erdogan, F. and Arin, K.: Penny-Shaped Interface Crack in an Elastic Layer and a Half-Space, International Journal of Engng. Science, 10, 115–125 (1972).

[32] Erdogan, F. and Gupta, G. D.: On the Numerical Solution of Singular Integral Equations, Quarterly of Applied Mathematics, 30, 525–534 (1972).

[33] Erdogan, F. and Biricikoglu, V.: Two Bonded Half Plane with a Crack Going Through the Interface, International Journal of Engng, Science, 11, 745–766 (1973).

[34] Erdogan, F. and Gupta, G. D.: The Problem of Edge Cracks in an Infinite Strip, ASME Journal of Applied Mechanics, 41, 1001–1006 (1974).

[35] Erdogan, F. and Bakioglu, M.: Fracture of Plates Which Consists of Periodic Dissimilar Strips, Internatonal Journal of Fracture,12, 71–84 (1976).

[36] Erdogan, F. and Bakioglu, M.: Stress-free End Problem in Layered Materials, Internatonal Journal of Fracture, 13, 739–749 (1977).

[37] Eshelby, J. D.: The Continuum Theory of Lattice Defects, Solid State Physics, 3, Academic Press (1956).

[38] Flitman, L. M.: On the Motion of a Rigid Strip-mass Lying on an Elastic Half-space and Excited by a Seismic Wave , Journal of Applied Mathematics and Mechanics, 28, 1582–1604 (1964).

[39] Georgiadis, H. G. and Papadopoulos, G. A.: Determination of SIF in a Cracked Plane Orthotropic Strip by the Wiener-Hopf Technique, International Journal of Fracture, 34, 57–64 (1987).

[40] Goree, J. D. and Venezia, W. A.: Bonded Elastic Half Planes with an Interface Crack and a Perpendicular Intersecting Crack that Extends into the Adjacent Materials, International Journal of Engng. Science,15, 1–27 (1977).

[41] Gracewski, S. M. and Bogy, D. B.: Elastic Wave Scattering from an Interface Crack in a Layered Half Space Submerged in Water: Part 1: Applied Traction at the Liquid–Solid Interface, ASME Journal of Applied Mechanics, 53, 326–332 (1986a).

[42] Gracewski, S. M. and Bogy, D. B.: Elastic Wave Scattering from an Interface Crack in a Layered Half Space Submerged in Water: Part 2: Incident Plane Waves and Bounded Beams, ASME Journal of Applied Mechanics, 53, 323–338 (1986b).

[43] Griffith, A. A.: The Phenomenon of Flow and Rupture in Solids, Phil. Tran. Royal Soc. London, 21, 163–198 (1921).

[44] Griffith, A. A.: The Theory of Rupture, Proceedings of the First International Congress of Applied Mechanics, Delft, 55–63 (1924).

[45] Gross, D. and Zhang, Ch.: Diffraction of SH-waves by a System of Cracks: Solution by an Integral Equation Method, International Journal of Solids and Structures, 24, 41–49 (1988).

[46] Gupta, G. D.: A Layered Composite with a Broken Laminate, International Journal of Solids and Structures, 9, 1141–1154 (1973).

[47] Hassan, T.: Numerical Study of Transient Response of an Interface-Crack in a Two Layered Plate, M. S. Thesis, University of Arizona (1985).

[48] Horii, H. and Nemat-Nasser, S.: Elastic Field of Interacting Inhomogeneities, International Journal of Solids and Structures, 21, 731–745 (1985).

[49] Hoagland, R., Hahn, G. and Rosenfield, A.: Influence of Microstructure on the Fracture Propagation in Rock, Rock Mech., 5, 77–106 (1973).

[50] Irwin, G. R.: Analysis of Stress and Strains Near the End of a Crack Traversing a Plate, ASME Journal of Applied Mechanics, 24, 361–364 (1957).

[51] Irwin, G. R.:*Fracture Mechanics, Structural Mechanics*, Pergamon press, New York, 557–592 (1960).

[52] Itou, S.: Three-Dimensional Wave Propagation in a Cracked Elastic Solid, ASME Journal of Applied Mechanics, 45, 807–811 (1978).

[53] Itou, S.: Diffraction of an Anti-plane Shear Wave by Two Coplaner Griffith Cracks in an Infinite Elastic Medium, International Journal of Solids and Structures, 16, 1147–1153 (1980).

[54] Jain, D. L. and Kanwal, R. P.: Diffraction of Elastic Waves by Two Coplaner Griffith Cracks in an Infinite Elastic Medium, International Journal of Solids and Structures, 8, 961–975 (1972).

[55] Joshi, S.P., and Sun, C.T.: Impact Induced Fracture in a Laminated Composite, J. Composite Materials, 19, 51–56, (1985).

[56] Kachanov, M.: A Simple Technique of Stress Analysis in Elastic Solids With Many Cracks, International Journal of fracture, 28, R11-R19 (1985).

[57] Kachanov, M. and Montagut, E.: Interaction of Crack With Certain Microcrack Arrays, Engineering Fracture Mechanics, 25, 625–636 (1986).

[58] Kachanov, M.: Elastic Solids with Many Cracks: a Simple Method of Analysis, Internationational Journal of Solids and Structures,23, 23–43 (1987).

[57] Kassir, M. K. and Bandyopadhyay, K. K.: Impact Response of a Cracked Orthotropic Medium, ASME Journal of Applied Mechanics, 50, 630–636 (1983).

[58] Keer, L. M. , Lin, W. and Achenbach, J.D.: Resonance Effect for a Crack Near a Free Surface, ASME Journal of Applied Mechanics, 51, 65–70 (1984a).

[59] Knopoff, L.: Diffraction of Elastic Waves, Journal of Acoustic Society of America, 28, 217–219 (1956).

[60] Kostrov, B. V.: Motion of a Rigid-strip Mass Soldered into an Elastic Medium Excited by a Plane Wave, Journal of Applied Mathematics and Mechanics, 28, 113–126 (1964).

[61] Kundu, T. and Mal, A. K.: Diffraction of Elastic Waves by a Surface Crack on a Plate, ASME Journal of Applied Mechanics, 48, 507–576, (1981).

[62] Kundu, T.: Computation of Surface Motion in a Stratified Half-Space, Ph. D. Dessertation, UCLA (1983).

[63] Kundu, T. and Mal, A.K.: Elastic Waves in a Multilayered Solid Due to a Dislocation Source, Wave Motion, 7, 459–471 (1985).

[64] Kundu, T.: Transient Response of an Interface-Crack in a Layered Plate, ASME Journal of Applied Mechanics, 53, 579–586 (1986).

[65] Kundu, T. and Hassan, T.: A Numerical Study of the Transient Behavior of an Interfacial Crack in a Layered Plate, International Journal of Fracture, 35, 55–69 (1987).

[66] Kundu, T.: Dynamic Interaction Between Two Interface Cracks in a Three Layered Plate, International Journal of Solids and Structures, 24, 27–39(1987a).

[67] Kundu, T.: The Transient Response of Two Cracks at the Interface of a Layered Half-Space, International Journal of Engineering Science 25, 1427–1439 (1987b).

[68] Kuo, A.-Y.: Transient Stress Intensity Factors of an Interfacial Crack Between Two Dissimilar Anisotropic Half-Spaces: Part 1 Orthotropic Materials, ASME Journal of Applied Mechanics, 51, 71–76 (1984a).

[69] Kuo, A.-Y.: Transient Stress Intensity Factors of an Interfacial Crack Between Two Dissimilar Anisotropic Half-Spaces: Part 2 Fully Anisotropic Materials, ASME Journal of Applied Mechanics, 51, 780–786 (1984b).

[70] Lin, W., Keer, L. M. and Achenbach, J. D.: Dynamic Stress Intensity Factor for an Inclined Sub–surface Crack, ASME Journal of Applied Mechanics, 51, 773–779 (1984b).

[71] Loeber, J. F. and Sih, G. C.: Transmission of Anti-Plane Shear Waves Past an Interface Crack in Dissimilar Media, Engineering Fracture Mechanics, 5, 699–725 (1973).

[72] Love, A. E. H.: *Mathematical Theory of Elasticity*, Dover Publications, New York, (1944).

[73] Lu, M. C. and Erdogan, F.: Stress Intensity Factors in Two Bonded Elastic Layers Containing Cracks Perpendicular to and on the Interface-I. Analysis, Engineering Fracture Mechanics, 18, 491–506 (1983).

[74] Luong, W. C., Keer, L. M. and Achenbach, J. D.: Elastodynamic Stress Intensity Factors of a Crack Near an Interface, International Journal of Solids and Structures, 11, 919–925 (1975).

[75] Mal, A. K.: Interaction of Elastic Waves with a Griffith Crack, International Journal of Engg. Sci., 8, 763–776 (1970).

[76] Mal, A. K.: Rayleigh Waves from a Moving Thrust Fault, Bulletin of the Seismological Society of America, 62, 751–762 (1972).

[77] Marcinkowski, M. J.: *Unified Theory of the Mechanical Behaviour of Matter*, John Wiley, New York, (1979a).

[78] Marcinkowski, M. J.: Burgers Circuits Associated with Distortions, Acta Mechanica, 33, 207–228 (1979b).

[79] Mendelson, D. A., Achenbach, J. D. and Keer, L. M.: Scattering of Elastic Waves by a Surface–Breaking Crack, Wave Motion, 2, 277–292 (1980).

[80] Miles, J. W: Homogeneous Solution in Elastic Wave Propagation, Quat. Appl. Math, 18, 37–47 (1960).

[81] Miller, R. K. and Tran, H. T.: Reflection, Refraction and Absorption of Elastic Waves at a Frictional Interface: P and SV Motion, ASME Journal of Applied Mechanics, 48, 155–160 (1981).

[82] Mott, N. F.: Fracture of Metals: Theoretical Consideration, Engineering, 165, 16–18 (1948).

[83] Muskhelishvili, N. I: *Some Basic Problems of Mathematical Theory of Elasticity*, P. Noordhoff, Holland (1953).

[84] Neerhoff, F. L.: Diffraction of Love Waves by a Stress-Free Crack of Finite Width in the Plane Interface of a Layered Composite, Applied Scientific Research, 35, 265–315 (1979).

[85] Noble, B: *Methods Based on Wiener-Hopf Techniques*, Pergamon Press, New York (1958).

[86] Papadopoulus, M.: Diffraction of Plane Elastic Waves by a Crack with Application to a Problem of Brittle Fracture, Journal of Austral. Math. Soc., 3, 325–339 (1963).

[87] Pao, Y. H.: Dynamic Stress Concentration in an Elastic Plate, ASME Journal of Applied Mechanics, 29, 299–305 (1962).

[88] Pao, Y. H. and Mow, C. C.:Dynamic Stress Concentration in an Elastic Plate with Rigid Circular Inclusion, Proccedings of Fourth U.S. National Congress of Applied Mechanics, 1, 335–345 (1962).

[89] Ravera, R. J., and Sih, G. C.: Transient Analysis of Stress Waves Around Cracks Under Anti-plane Strain, Journal of Acoustic Soc. Am., 47, 875–881.

[90] Rice, J. R.: A Path Independent Integral and Approximate Analysis of Notches and Cracks, ASME Journal of Applied Mechanics, 24, 379–386 (1968).

[91] Rose, L. R. F. (1986): Microcrack Interaction with a Main Crack, International Journal of Fracture, 31, 233–242 (1986).

[92] Rubinstein, A. A.: Macrocrack Interaction with Semi-infinite Microcrack Array, International Journal of Fracture, 27, 113–119 (1985).

[93] Rubinstein, A. A.: Microcrack-Microdefect Interaction, ASME Journal of Applied Mechanics, 53, 505–510 (1986).

[94] Ryan, R. L. and Mall, S.: Scattering of Anti-plane Shear Waves by a Submerged Crack, International Journal of Solids and Structures, 18, 1145–1152 (1982).

[95] Thau, S. A. and Pao, Y. H.: Stress Intensification Near a Semi-infinite Rigid-smooth Strip Due to Diffraction of Waves, ASME Journal of Applied Mechanics, 34, 119–126 (1967).

[96] Sih, G. C: Some Elastodynamic Problems of Cracks, International Journal of Fracture, 4, 51–58 (1968).

[97] Sih, G. C., Embly, G. T. and Ravera, R. S.: Impact Response of a Finite Crack Inplane Extension, International Journal of Solids and Structures, 8, 977–993 (1972).

[98] Sih, G.C. and Loeber, J.F.: Wave Propagation in an Elastic Solid with a Line of Discontinuity or Finite Crack, Quarterly of Applied Mathematics, 27, 193–213, (1969).

[99] Sih, G. C. and Chen, E. P.: Normal and Shear Impact of Layered Composite with a Crack: Dynamic Stress Intensification, ASME Journal of Applied Mechanics, 47, 351–358 (1980).

[100] Srivastava, K. N. and Gupta, O. P. and Palaiya, R. M.: Interaction of Elastic Waves in Two Dissimilar Elastic Half-planes Having Griffith Crack at the Interface-I, International Journal of Fracture, 14, 145–154 (1978).

[101] Srivastava, K. N., Palaiya, R. M. and Gupta, O. P.: Interaction of Longitudinal Wave with a Penny Shaped Crack at the Interface of two Dissimilar Elastic Solids-II, International Journal of Fracture, 15, 591–599 (1978).

[102] Stone, M. L., Gosh, G. L. and Mal, A. K.: Diffraction of Antiplane Shear Waves by an Edge Crack, ASME Journal of Applied Mechanics, 47, 359–362 (1980).

[103] Thau, S. A. and Lu, T.: Diffraction of Transient Horizontal Shear Waves by a Finite Ribbon, International Journal of Engineering Science, 7, 857–874 (1971a).

[104] Thau, S.A. and Lu, T.: Transient Stress Intensity Factor for a Finite Crack in an Elastic Solid Caused by a Dilatational Wave, International Journal of Solids and Structures, 8, 113–126, (1971b).

[105] Thompson, R. B. and Fiedler, C. J.: The Effect of Crack Closure on Ultrasonic Measurements, Review of Progress in QNDE, 3A, Thompson, D. O. and Chimenti, D. E., eds., Plenum, New York, 207–215 (1984).

[106] Van den Hijden, J. H. M. T. and Neerhoff, F. L.: Scattering of Elatic Waves by a Plane Crack of Finite Width, ASME Journal of Applied Mechanics, 51, 646–651 (1984).

[107] Vinson, J. R. and Sierakowski,R.L.: *The Behavior of Structures Composed of Composite Materials*, 1st ed, Dordrecht, Netherland, Martinius Nijhoff Publisher, (1986).

[108] Volterra, V.: Ann. Ecole. Norm., Paris, Series-3, 24, 401–517 (1907).

[109] Williams, M. L.: On the Stress Distribution at the Base of a Stationary Crack, ASME Journal of Applied Mechanics, 24, 109–114 (1956).

[110] Williams, M. L.: The Stress Around a Fault or Crack in Dissimilar Media, Bulletin of the Seismological Society of America, 49, 199–204 (1959).

[111] Xu, P.-C. and Mal, A. K.: Calculation of the Inplane Green's Functions for a Layered Viscoelastic Solid, Bulletin of the Seismological Society of America, (1988), in press.

[112] Yang, H. J. and Bogy, D. B.: Elastic Wave Scattering from an Interface Crack in a Layered Half-Space, ASME Journal of Applied Mechanics, 52, 42–50 (1985).

[113] Zhang, X. S.: A Central Crack at the Interface Between Two Different Media in a Rectangular Sheet Under Antiplane Shear, Engineering Fracture Mechanics, 19, 709–715 (1984).

[114] Zhang, Ch. and Achenbach, J. D.: Scattering by Multiple Crack Configurations, ASME Journal of Applied Mechanics, 55, 104–110 (1988).